MICROFABRICATION OF AN ORGAN-ON-A-CHIP DEVICE TO MODEL

CARDIOTOXICITY INDUCED BY CHEMOTHERAPIES FOR CANCER

NANOMEDICINE EVALUATION

by

Pooneh Soltantabar

APPROVED BY SUPERVISORY COMMITTEE:

_____

Mihaela C. Stefan, Chair

_____

Stuart F. Cogan

_____

Shalini Prasad

_____

Taylor Ware

For my family

MICROFABRICATION OF AN ORGAN-ON-A-CHIP DEVICE TO MODEL

CARDIOTOXICITY INDUCED BY CHEMOTHERAPIES FOR CANCER

NANOMEDICINE EVALUATION

by

POONEH SOLTANTABAR, BS ,MS

DISSERTATION

Presented to the Faculty of

The University of Texas at Dallas

in Partial Fulfillment

of the Requirements

for the Degree of

DOCTOR OF PHILOSOPHY IN

BIOMEDICAL ENGINEERING

THE UNIVERSITY OF TEXAS AT DALLAS

December 2020

ACKNOWLEDGMENTS

It would not have been possible to write this PhD disseration without the help and support of kind people around me, to only some of whom it is possible to give particular mention here. First and foremost, I would like to express my deepest gratitude to my supervisor, Prof. Mihaela Stefan. I will forever be grateful to you for taking a chance on me 4 years ago and offering me your mentorship, love and care. Under your guidance, I successfully overcame many difficulties and your unflinching courage has always inspired me to do more. You have taught me another aspect of life, that, "goodness is the only investment that never fails." For all this, I sincerely thank you from the bottom of my heart and will be truly indebted to you throughout my lifetime.

I would like to extend my gratitude to my committee members, Dr. Stuart Cogan, Dr. Shalini Prasad, and Dr. Taylor Ware, for their insightful comments. I am very thankful for the valuable help and advice I received from Dr. Stuart Cogan's research group for the microfabrication of my device. I would like to thank Dr. Michael Biewer for his advice and insight into my project. My sincere gratitude goes to all of the members in the Stefan and Biewer labs. Especially, my appreciation goes to Erika Calubaquib for being so wonderful to work with and being an amazing supportive friend.

Finally, I acknowledge the people who mean a lot to me, my family. My gratitude goes to a very special person, my husband, Ebi, who has always been there for me. I greatly value his contribution and deeply appreciate his belief in me. I would like to thank my mother and my best friend (Moloud) for giving me unconditional support and love throughout my life, no matter what path I

MICROFABRICATION OF AN ORGAN-ON-A-CHIP DEVICE TO MODEL

CARDIOTOXICITY INDUCED BY CHEMOTHERAPIES FOR CANCER

NANOMEDICINE EVALUATION

Pooneh Soltantabar, PhD
The University of Texas at Dallas, 2020

Supervising Professor: Mihaela C. Stefan

Cancer is the leading cause of death worldwide, and more efficient treatments and pre-clinical tests for the evaluation of novel therapies are in high demand. Chemotherapy, as the most common cancer treatment, is facing severe challenges, including low water solubility of anti-cancer drugs and the cardiotoxicity induced by them. Nanotechnology has made significant contributions to the development of drug delivery systems by reducing the toxicities, which leads to improvement in conventional chemotherapies. Chapter 2 describes a micellar drug delivery system's design using benzyl substituted poly(ε-caprolactone) as the hydrophobic block, and co-loaded doxorubicin anticancer drug and quercetin cardioprotective agent to increase the solubility of the anticancer drug in water and reduce the cardiotoxicity induced by the anticancer drug. Oligo(ethylene) glycol substituted poly(ε-caprolactone)s were used as hydrophilic blocks and make the polymer thermoresponsive. Our proposed biodegradable and thermoresponsive micellar DDS can open the door to developing a more effective platform for cancer treatment.

Although many therapeutics have been developed so far, the pharmaceutical industry is still facing challenges for drug discovery, which is mostly attributed to the lack of proper pre-clinical testing. In Chapter 3, we try to model the cardiotoxicity induced by anticancer drugs on an organ-on-a-chip device to improve conventional pre-clinical cell culture. Organ-on-a-chip devices can mimic the whole-body response to therapeutics by fluidically connecting microscale cell cultures and generating a realistic model of human organs of interest. We described a pumpless heart/liver-on-a-chip (HLC) using the HepG2 hepatocellular carcinoma cells and H9c2 rat cardiomyocytes to reproduce the cardiotoxicity induced by Doxorubicin (DOX) in vitro. Our designed HLC device represents a unique approach to assess the off-target toxicity of drugs and their metabolites, which will eventually improve current pre-clinical studies.

TABLE OF CONTENTS

LIST OF FIGURES

LIST OF TABLES

CHAPTER 1

INTRODUCTION

1.1 Cancer and drug delivery systems

Cancer diseases are uncontrolled growth and division of cells that can spread to other body organs. In 2015, an estimation by the World Health Organization revealed that cancer is the first leading cause of death before age 70 years in 91 countries, and it ranks third or fourth in an additional 22 countries.[1] Chemotherapy, surgery, and radiation therapy are the standard cancer treatments, wherein chemotherapy is mostly utilized. The mechanism of action for conventional chemotherapies is killing the fast-dividing cancer cells by blocking the DNA synthesis and mitosis of these cells. The current chemotherapy drugs are not selective, so they can affect the normal tissues and cause intense undesired adverse effects.[2]

Nanotechnology has made significant contributions to the development of drug delivery systems by reducing the toxicities, leading to an improvement in conventional chemotherapies. Some of the exciting features of nanotechnology in oncological applications are listed below:[3]

- Increasing efficiency and reducing the adverse effects that result in a higher therapeutic index;

- Improvements of pharmaceutical features of active agents by increasing their stability and circulation time;

- Enabling the sustained release of active agents;

- The possibility of combination therapy of multiple drugs to improve treatment efficiency;

- Targeted or stimuli-responsive drug delivery systems.

Drug delivery systems have the potential to bridge the gap between existing effective active agents and desired treatments that are not achievable through conventional therapies.[4] Nanocarriers can dramatically improve therapeutics by overcoming the physiological barriers and preserving the function of pharmaceutical agents. These unique biological features are attributed to their small size (diameter within 1-100 nm) and large surface area to volume ratio. These carriers can encapsulate active agents such as anti-cancer drugs, DNA and proteins, and can be bound or absorbed to specific sites with higher efficiency.[3]

Considerable improvements in therapies have been observed by developing new carriers over the years [5] (Figure 1.1). Liposomes were the first class of therapeutic nanocarriers to receive clinical approval for cancer treatment. Two liposomal formulations of Dox (Doxil and Myocet) have already been commercialized.
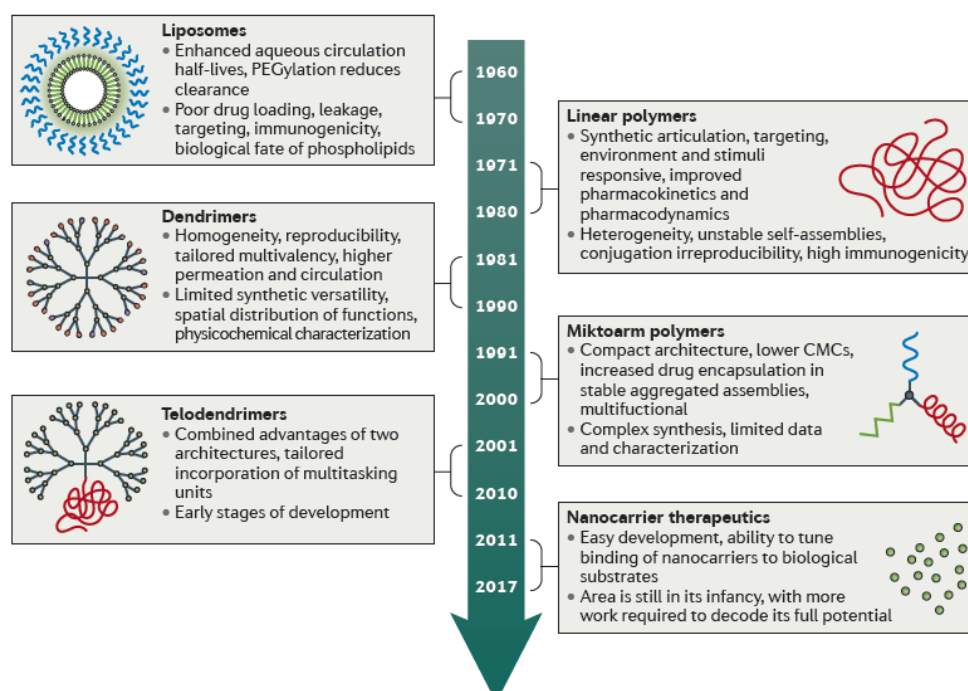
Figure 1.1. The evolution of drug delivery systems. A summary of the timeline, advantages, and disadvantages of each nanocarrier. Reused with permission. [5]

Polymeric nanocarriers have shown great potential in nanomedicine applications due to their tunable structures, which is possible through their synthesis. By this tunability, drug loading and biodistribution of these particles can be tailored to achieve higher therapeutic efficiency.[67] Active agents can be either dispersed in a polymer matrix or can be attached to the polymer backbone. Polymeric nanoparticles can be prepared from synthetic polymers, such as poly (lactic acid) (PLA) and poly(ε-caprolactone) (PCL) or from natural polymers, such as gelatin, dextran, and collagen. Natural polymers have relatively short drug release, while synthetic polymers have the advantage of the controlled release of drugs over time. Among various polymeric nanocarriers, **polymeric micelles** have gained considerable attention due to their excellent biocompatibility, physicochemical properties, drug loading and release capacities, and facile preparation methods.[8] These nanocarriers that have been developed by the synthesis of amphiphilic block copolymers can self-assemble in the form of spherical nanoscale structures in an aqueous medium resulting in a hydrophobic core and a hydrophilic shell. Anti-cancer drugs, which are most highly hydrophobic compounds, can be encapsulated in these nanocarriers, thus improving the interaction of poorly water-soluble drugs with biological medium (Figure 1.2).
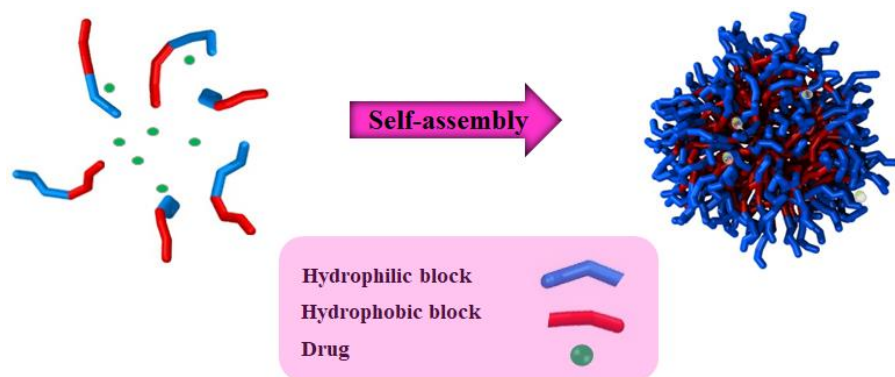
Figure 1.2. Demonstration of the self-assembly of micelles. Reproduced with permission. [9]

1.1.1 Thermoresponsive drug delivery systems

Thermoresponsive polymers change their structure in response to changes in temperature and can be classified into two groups based on the temperature dependency of their solubility in water. The first group goes through phase transition by shrinking and precipitation below a specific temperature called upper critical solution temperature (UCST).[10] The other group shrink above a specific temperature called lower critical solution temperature (LCST), which is widely used in biomedical applications.[11] The LCST of polymers can be tuned by variations of the starting monomer for polymerization.

Polymer nanocarriers are used to increase the solubility of poorly soluble drugs; however, controlling the drug release from nanocarriers is still challenging. In this regard, thermoresponsive polymers may be the key to build controlled drug delivery systems. Polymeric micelles that demonstrate a dramatic change in their structure in response to temperature can be made by incorporating thermoresponsive polymer blocks in their core-shell design. These systems can be exploited for selective drug release at the tumor site, which is possible through external temperature elevation at the site.[12] Moreover, using these systems, the duration of the drug action at the target site can be controlled.

1.1.2 Increasing the drug loading capacity by using substituted polymers

As mentioned earlier, the core of the micelles (which are mostly aliphatic polyesters) accommodates the drug through either physical encapsulation or conjugation to the polymer backbone. The micelle size, stability, and loading capacity can be tuned by hydrophobic properties of the core or attaching functional groups to it.[13,14] During recent years, aliphatic polyesters have

become promising biomaterials due to their hydrolyzable backbones; hence in some cases, they received FDA approval.[15] Among the standard aliphatic polyesters such as poly(lactic acid)s (PLAs), poly(glycolic acid)s (PLGAs), and poly(ε-caprolactone)s (PCLs). PCLs can be easily substituted with functional groups and have great synthetic versatility. Recently a lot of efforts have been focused on improving the loading capacity of micelles by developing substituted PCLs.[9] The substituents in γ position of the caprolactone monomer are more favorable for our research because the substituents at this position are far from the ester functional group and do not affect the polymerization rate.

In 2012, Chang and coworkers[16] reported that the introduction of hydroxyl groups onto the hydrophobic of micelles (Figure 1.3, **M₁**) could increase the Dox loading from 4.6 wt% in unsubstituted caprolactone, up to 7.2 wt% in hydroxyl substituted. This loading improvement was attributed to hydrogen bonding between the drug and the polymer backbone. In 2013, a series of amphiphilic copolymers with poly(ethylene glycol) PEG as hydrophilic block and poly(4-methyl-ε-caprolactone), or poly(4-phenyl-ε-caprolactone) (Figure 1.3, **M₂** and **M₃**) as hydrophobic block was synthesized by Peng et al.[15] The encapsulation efficiency of indomethacin was ∼40 wt% for substituted cores, while this value was only 29 wt% for unfunctionalized cores.[17] In a study by our group[18], the tunability of Dox drug loading of micelles by the addition of various substituents was investigated (Figure 1.3, **M₄₋₈**). It was observed that copolymers synthesized by **M₄** and **M₇** demonstrated higher drug loading. For **M₇**, the higher loading is attributed to π stacking interaction between the polymer and Dox.
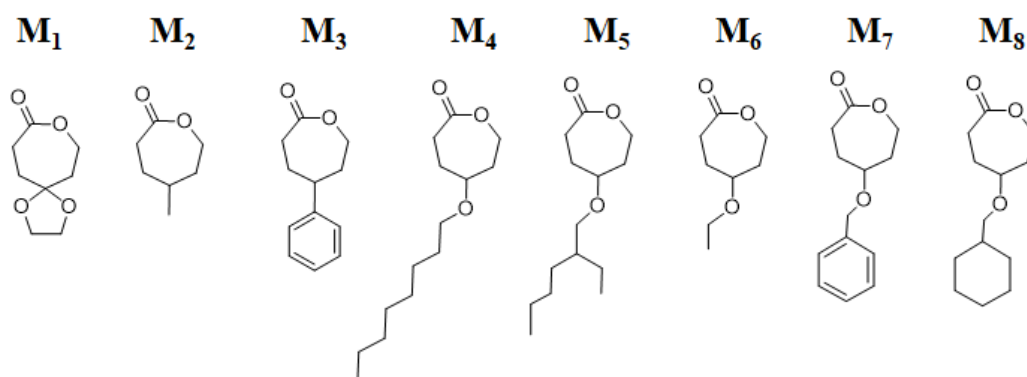
Figure 1.3. Functional caprolactone monomers. Reproduced with permission. [9]

1.1.3 Cardiotoxicity induced by chemotherapy

The heart is an organ that consumes a high amount of energy to pump blood all over the body, so it is rich in mitochondria, which has the primary role of energy generation in cells. These subcellular organelles are considered as the main target of doxorubicin-induced cardiotoxicity. Iron has pivotal roles in the process of energy production in the heart, including oxygen transport, DNA synthesis, or detoxification processes. To perform these functions, iron is in the balance between the deposition sites and metabolic use. If the iron amount exceeds the metabolic needs of the cell, it exposes the cell to potentially damaging reactions that convert normal by-products of cell respiration, like superoxide anion ($O_2^{\bullet-}$) and hydrogen peroxide (H_2O_2), into highly damaging hydroxyl radicals. Therefore, iron, which is an essential micronutrient, can also catalyze free radical reactions.[19,20] To hinder any damaging effect of iron to cells, cells have evolved a 24 sub-unit protein called ferritin, which can safely store excess iron. Anthracycline drugs (an effective class of anti-cancer drugs) such as Dox can disrupt this cycle. These anti-cancer drugs are large molecules, so they cannot enter the ferritin, but they can release the stored iron by electron

tunneling mechanisms; in fact, they can delocalize the iron through redox sites and transprotein channels of ferritin.[21]

Dox can generate complexes with iron that can react with oxygen and form reactive oxygen species (ROS). ROS can oxidize the lipids, proteins, and DNA in cells, which ultimately leads to cardiac dysfunction.[22] Detoxifying enzymes can neutralize the ROS in cells to prevent their damaging effect. Still, cardiomyocytes have a low amount of ROS detoxifying agents in comparison to other cell types that makes them the main target of ROS damages.[21]

Another proposed mechanism for Dox cardiotoxicity is the production of its primary metabolite, doxorubicinol (DOXOL). DOXOL is the primary metabolite of DOX, which is even more potent than DOX in compromising the systolic and diastolic cardiac function. [23] DOXOL involves in perturbations of Ca2+ homeostasis, which contributes to the time-dependent cardiotoxicity.[24]

1.1.4   Cardioprotective role of polyphenols

Antioxidants such as polyphenols can react with free radicals and reduce the damage to lipids, proteins, and other cell parts.[25] The protective function of antioxidants has been explained with two possible mechanisms in literature:[26,27]

H-atom transfer

The free radical ($R^\bullet$) removes a hydrogen atom from the antioxidant (ArOH):

$R^\bullet + ArOH \rightarrow RH + ArO^\bullet$
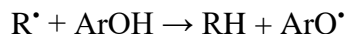
One-electron transfer

The antioxidant can give an electron to the free radical:

$R^\bullet + ArOH \rightarrow R^- + ArOH^{\bullet+}$

7
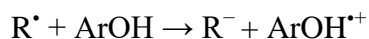
The resulting radicals (ArO$^\bullet$ and ArOH$^{\bullet+}$) are more stable, which prevent the radical chain reactions.

1.1.5   Multidrug resistance and the role of polyphenols

In addition to the cardioprotective properties, polyphenols also play multidrug resistance by acting as chemosensitizers. Multidrug resistance (MDR) in cancer is the resistance ability of cancer cells to anticancer drugs. This resistance to multiple anticancer drugs is one of the primary reasons that cause failure in cancer therapy.[28] Several mechanisms have been reported to explain MDR. The most common theory regarding this resistance is explained by the overexpression of P-glycoprotein (P-gp), which belongs to the superfamily of ATP binding cassette (ABC) transporter proteins.[29] (P-gp), is a transmembranous ATP-dependent efflux pump which behaves as an energy-dependent efflux pump of anticancer agents.[30,31]

More recently, research has been focused on finding MDR modulators to reverse the activity of P-gp. The co-administration of these MDR regulators enhance the net accumulation of drugs within the tumor cells. The mechanism of action of these chemosensitizers that regulate the MDR is complex. Chemosensitizers mostly bind to anticancer drug binding locations on P-gp, which leads to blockage of P-gp activity and preventing the undesired transport of drugs out of cells. Chemosensitizers either directly block P-gp activity by binding to chemotherapeutic drug binding sites or bind to other modulator binding sites, which cause inhibition of drug binding or transport.[29] Another method for reversing the MDR is the down-regulation of P-gp expression.[32,33] The utilization of the MDR modulators to achieve a more effective treatment increases the number of medications and consequently adds to the patient's burden. Chemosensitizers based on natural

food or beverage components could be valuable in enhancing the activity of anti-cancer drugs without side-effects, and thus improving the quality of life of patients.[34]

It has been reported that flavonoids (a subclass of polyphenols), such as flavonols (quercetin), flavanones (naringenin), isoflavones (genistein), and glycosylated flavonol derivatives (rutin), are shown to directly interact with P-gp and inhibition of their function.[35,36] Studies have reported that Que can interact with P-gp and block its activity.[37] Moreover, Que can also reduce the expression of P-gp.[38] ABC transporters have two transmembrane domains (TMDs) that form the pathways through the membrane for substrate efflux and two nucleotide-binding domains (NBDs), which contribute to ATP binding and are considered as " engines"[39,40]. Que can interact with either ATP-binding sites or substrate binding sites and cause impairment in these transporters' function, which prevents the undesired efflux of drugs.[35] In other words, Que may competitively or noncompetitively interact with other anticancer drugs (which are also substrates of these transporters) for substrate-binding sites.[41]

To sum up, the co-administration of the polyphenols with anticancer drugs and their cardioprotective and chemosensitizing role has been proved and reported.[35,36] However, the co-encapsulation of these agents with Dox using drug delivery systems is scarce. Our primary approach in Chapter 2 is to co-encapsulate Dox and Que in a micelle for improved therapeutic efficacy. This goal is achieved by co-encapsulating the drugs in a thermoresponsive polymeric micelles. These micellar systems offer some advantages over the currently FDA approved thermoresponsive carriers, ThermoDox®. ThermoDox® is a liposomal formulation of Dox that facilitates targeted delivery to site of action at temperatures exceeding 40°C. However, liposomal formulations often suffer from the possibility of drug leakage from these carriers as well as low

drug loading. Our polymeric micelles not only addresses the issue of the low drug loading, but also provides the opportunity of tuning the thermoresponsivity of these carriers in a broader range of temperatutes (rather that one fixed temperature) through changing in structure of polymers.

1.2 Microfluidic devices for drug discovery

The study and treatment of cancer are very complex due to the dynamic nature of cancer.[42] The pharmaceutical industry is now facing several challenges for drug discovery. First, there are high research and development costs, which can be over 10 billion dollars for each drug to get into the market. Second, long development times, which can take up to 10 years. Third, serious side effects happen during the clinical test of drugs or even when the drug is commercialized in many cases. These problems are due to the lack of proper and efficient pre-clinical tests.[43-44]

1.2.1   Current pre-clinical tests

Animal models are a widespread pre-clinical test currently. Historically, it has been shown that animal models such as rodents and non-human primates cannot predict the human response to drugs, so that these tests may yield misleading results. Unfortunately, only 11% of drugs that pass the animal study tests successfully are effective for a human.[45] It has been proposed that this problem can be attributed to the non-efficient methodology of testing animals. Nevertheless, there is another argument that even the improvement of protocols cannot be helpful because animals and humans have very complicated bodies with different evolutionary trajectories, so it is not safe to generalize that animals will have a similar response to humans[46]. Moreover, many countries have restricted animal studies due to ethical issues.[43]

Another approach for pre-clinical testing of drugs that have been engineered is *in vitro* models. Conventional **two-dimensional (2D) cell cultures** were established about one hundred years ago.[47] 2D cell cultures are valuable tools at the early stages of drug discovery to identify the potential drugs for cancer treatments. However, it has been demonstrated that conventional 2D culture models are not efficient enough to recapitulate many important characteristics of tumors because they fail to predict tissue functions and drug activities *in vivo.*[48,49]

In contrast to what is assumed in 2D cell culture models, tumor cells *in vivo* grow in a 3D extracellular matrix (ECM).[50] It has been reported that cells show different behaviors in 3D compared to 2D. To better resemble the tumor microenvironment, **3D cultures**, which better represent the spatial and chemical complexity of living tissues, were proposed to understand cancer biology better.[51] 3D cell cultures were developed about 50 years ago and are based on incorporating cells in the hydrogels, which are either natural and synthetic polymers. These polymers induce cells to polarize and interact with adjacent cells[48].

Although 3D cell cultures are useful tools to study the molecular basis of tissue function and capturing the responsiveness of drugs, they still have some limitations. For instance, these systems lack normal mechanical cues that affect organ function and development, such as shear stress, tension, and compression induced by fluid flow.[52] Moreover, assessing the interactions between different organs through these 3D systems is not possible because there are no fluid circulations throughout the system.[48] Having said that, developing better tools to improve the efficiency of research and development for drug screening is necessary.[53]

1.2.2 Organ-on-a-chip

To address all the limitations of current pre-clinical tests, a new class of microfluidic device was developed to replicate *in vivo* functions of organs on a microchip. This new technology, called "Organ-on-a-chip"[48],[54-55] or "Body-on-a-Chip"[56-57], can mimic human physiological conditions. The word "chip" in organ-on-a-chip originates from its fabrication process, a modified method of photolithographic etching that is used for manufacturing computer microchips. This fabrication method enables controlling the features in nm and μm scales, which is the same scale as what living cells experience *in vivo.*[48]

These devices, which hold great promise as the next generation of pre-clinical tests, were considered the "Top 10 Emerging Technologies of 2016" by the World Economic Forum's Meta-Council on Emerging Technologies.[43] Organ-on-a-chip devices are used for culturing living cells in a continuously perfused chamber to mimic the tissue and organ level physiology, which are not possible through conventional 2D and 3D cell culture systems. Moreover, high-resolution imaging of the metabolic activity of cells is possible by using these devices.

A simple example of an organ-on-a-chip device is a single perfused chamber that accommodates one single cell line. However, more complicated systems with multiple cell lines have been fabricated that recreates the organ interactions through connected microchannels. The main goal of these systems may not be creating a whole living body but to play minimal functions of organs and their interactions and study drug distribution *in vitro* through these fluidically linked chambers.[48]

1.2.3 Evaluation of nanomedicine by using microfluidic

As mentioned earlier, nanomedicines should be biodegradable with low toxicity and high drug loading and stability *in vivo*. As conventional nanomedicine evaluation methods neglect physiological features such as 3D growth and flow, alternative drug evaluation methods are needed to pace the clinical translation of nanomedicine. Microfluidic technologies enable the design of highly biomimetic models, which are valuable tools for the pre-screening of drugs.

Several approaches have been reported in specific organ-on-a-chip technologies. They contributed to evaluating drug delivery systems to different organs such as blood vessel[58], lung[59], liver[60], and tumor[60–63](Figure 1.4). However, these platforms for assessing nanomedicine, although not new, have not been intensively implemented.[64]
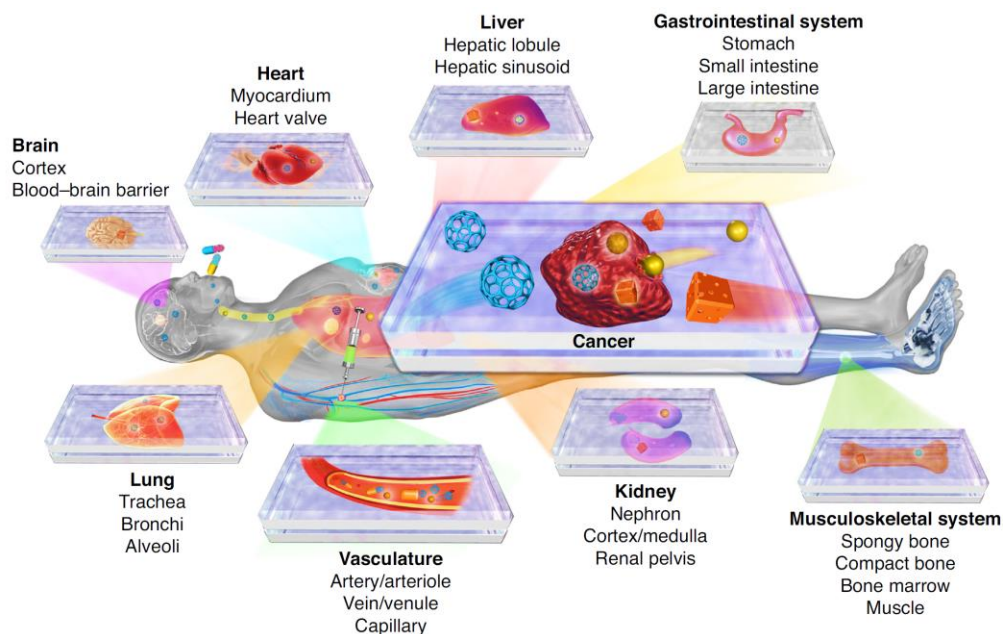
Figure 1.4.Organ-on-a-chip platforms for evaluation of nanomedicine. Reused with permission.[64]

1.2.4 Heart-on-a-chip models

Toxicity of drugs that have already passed the pre-clinical and clinical tests may also cause death. For example, Vioxx that has cost Merck over $5 billion in criminal and civil settlements, caused more than 27,000 deaths.[65] Heart, as a susceptible organ to adverse drug interactions, is considered the primary reason for drug recalls; so, *in vitro* cardio models are necessary for high throughput drug screening before commercialization.

To better mimic the human cardiac system's physiology, some researchers have cultured induced pluripotent stem cells (iPSC) differentiated cardiomyocytes in a microfluidic device for drug testing.[65] These tools are developed in various drug screening applications. In 2015, Mathur et al. designed a human iPSC-derived cardiac system and applied their designed system to test pharmacological agents with established clinical responses. The results indicated a good concordance between the results from the tissue-engineered device and clinical observations.

In another study, Bergström et al.,[66] seeded stem cell-derived human cardiac bodies (CB) in niches within a perfusion channel in the device (Figure 1.5). Beating frequency of CBs in response to various drugs such as Dox, Verapamil, and Quinidine was monitored with video imaging. A dose-dependent decrease in the beating rate of cardiomyocytes was confirmed (Figure 1.6), which was most consistent with results from the literature.
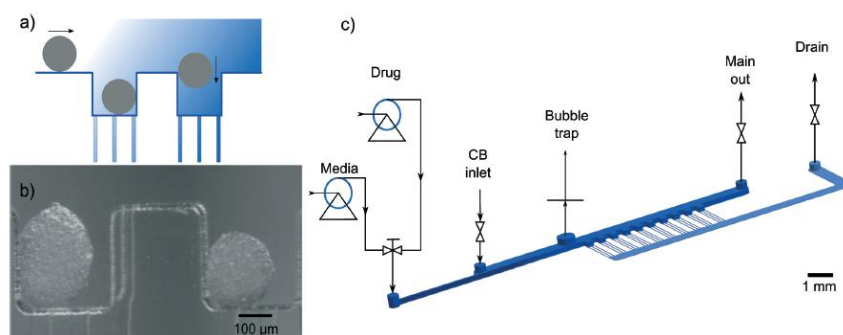
Figure 1.5.The demonstration of the microfluidic device. a) A schematic of CB seeding in the device, b) A micrograph of CBs residing in the niches, c) Schematic of the channels and niches in the device. Reproduced with permission. [66]
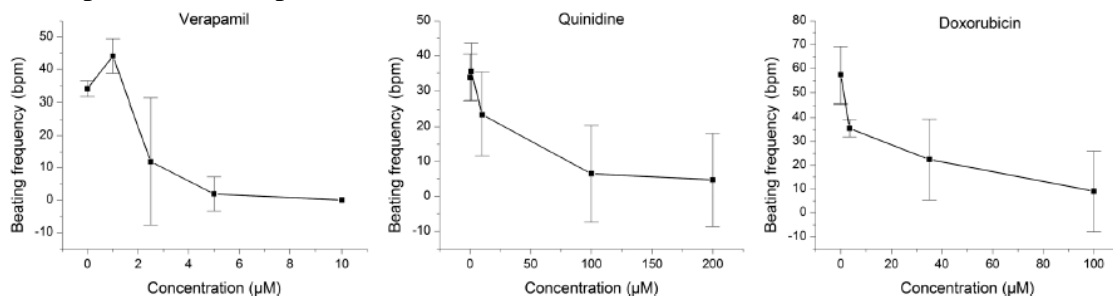
Figure 1.6. Dose-dependent beating frequency of CB in response to Verapamil, Quinidine, and Dox (a significant decrease in beating rate was observed after treatment with drugs). Adapted with permission. [66]

In 2018, a heart-on-a-chip model was developed by Ahn et al. .[67] using 3D fiber scaffolds. Cardiomyocytes were seeded on the nanofiber scaffolds and formed functional heart tissues. The *in vitro* 3D myocardium was exposed to various dosages of titanium dioxide (TiO2) nanoparticles. A calcium-sensitive dye investigated the electrophysiological effect of nanoparticles. A non-synchronous calcium transient was observed in high dosage exposure of nanoparticles attributed to a disruption in sarcomere architecture. This observation was further confirmed by the structural analysis of samples by immunostaining against sarcomeric α-actinin. The results indicated that the designed heart-on-a-chip device is a trustable tool to assess the cytotoxic effects of nanoparticles.

15

1.2.5 Liver on a chip

The liver plays a critical role in drug metabolism, which highlights the need for developing in vitro models. It has been reported that the hepatic model that is based on conventional 2D cultures cannot fully represent the complex 3D microenvironment. [68–70] These hepatic models fail to adequately respond to the drugs due to loss of functionality in monolayers. Therefore, the efforts have been focused on the encapsulation of hepatocytes in various hydrogels for better representation of hepatic functionality.[71–73] Moreover, studies show that providing a physiologically relevant dynamic environment for cells is essential for drug metabolism as many static models lack the necessary physiological cues. [74] All these limitations in current in vitro models necessitate approaches that incorporate 3D constructs of the cells in a dynamic environment achievable through microfluidics liver-on-a-chip devices.[75] Some microfluidic chips for non-cell based screening of the drugs in vitro[76] have been developed. However, the presence of cells in the model are crucial for drug testing. Specially liver-on-a-chip devices that accommodate primary human hepatocytes can better predict the drug response in the human body even better than the animal in vivo models because these cells contain metabolizing enzymes and hepatic transporters that have a pivotal role in liver functionality.[77]

1.2.6 Models for cardiotoxicity induced by anti-cancer drugs on a chip

The cardiotoxicity induced by either anti-cancer drugs or their metabolites generated from cancer tissue is the primary concern in the chemotherapy approach for cancer treatment[78] (Figure 1.7). In some studies, the attempts were focused on modeling this damage using organ-on-a-chip devices.

16
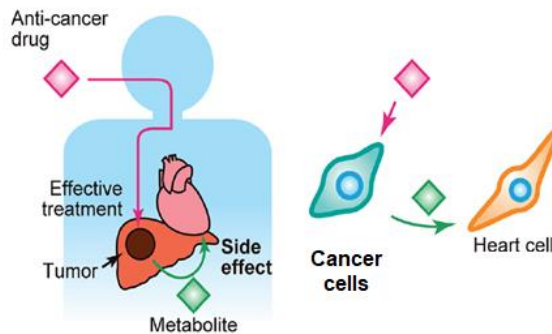
Figure 1.7. Communication between cancer cells and healthy heart cells via the exchange of metabolites and the side effects of anticancer drugs. Adapted with permission. [79]

In 2017, Kamei et al.[79] designed an integrated heart-cancer on a chip (iHCC) to recapitulate the cardiotoxicity induced by the common anti-cancer drug, Dox. Human primary cardiomyocytes and hepatocellular carcinoma (HepG$_2$) cells were cultured on a PDMS chip with an artificial blood circulatory system that connects the two-issue chambers (Figure 1.8) and enable the drug and metabolites transfer from one chamber to another. After the operation and cell culture in the system, the Dox was introduced to the system for 24 hrs. The biological assays were performed to evaluate the viability and proliferating of cells. The results demonstrated that after adding the drug, the toxicity of cardiomyocytes cultured in iHCC increased significantly compared to the static control, which there was no connection between cell lines. The higher cardiotoxicity in the device was attributed to Dox metabolites released from cancer cells and reached the heart cells through the media circulation in the device.
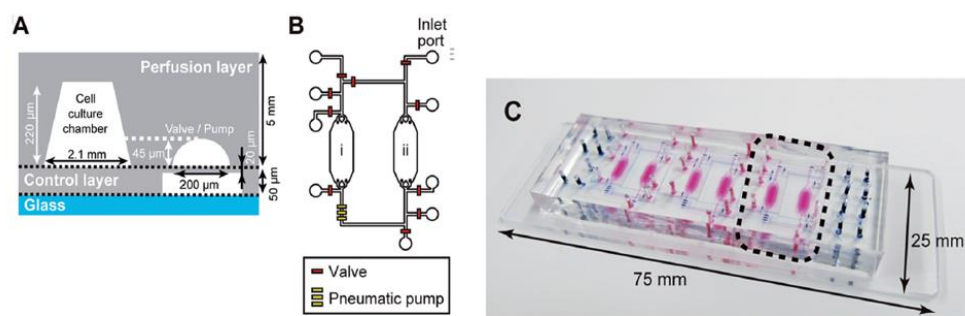
Figure 1.8. Illustration of the side view of iHCC. Including a "perfusion layer" and "control layer" B) Cell culture chambers with a medium circulation system C) Photograph of fabricated iHCC. Adopted with permission. [79]

In another study, the effect of off-target cardiotoxicity was investigated using a human *in vitro* microfluidic system.[80] A cantilever array chip and a customized multielectrode array were incorporated to the system for measuring cardiac mechanical function and electrical activity, respectively (Figure 1.9). Two model drugs Cyclophosphamide (CP) (a non-cardiotoxic parent drug that generates a cardiotoxic metabolite upon liver metabolism) and Terfenadine (TER) (a cardiotoxic parent drug that produces a non-cardiotoxic metabolite after the liver metabolism) were used for system validation. The results indicated that CP significantly affected the cardiac function when the metabolizing component(liver) was present in the system, which confirms the toxicity of CP upon hepatic metabolism. Moreover, they observed cardioprotection effects after the introduction of TER into the system in the presence of the liver, which was not observed in the absence of the liver in the system. Therefore, using this integrated heart-liver system, they were able to predict human cardiac toxicity upon compound transformation through hepatic metabolism.
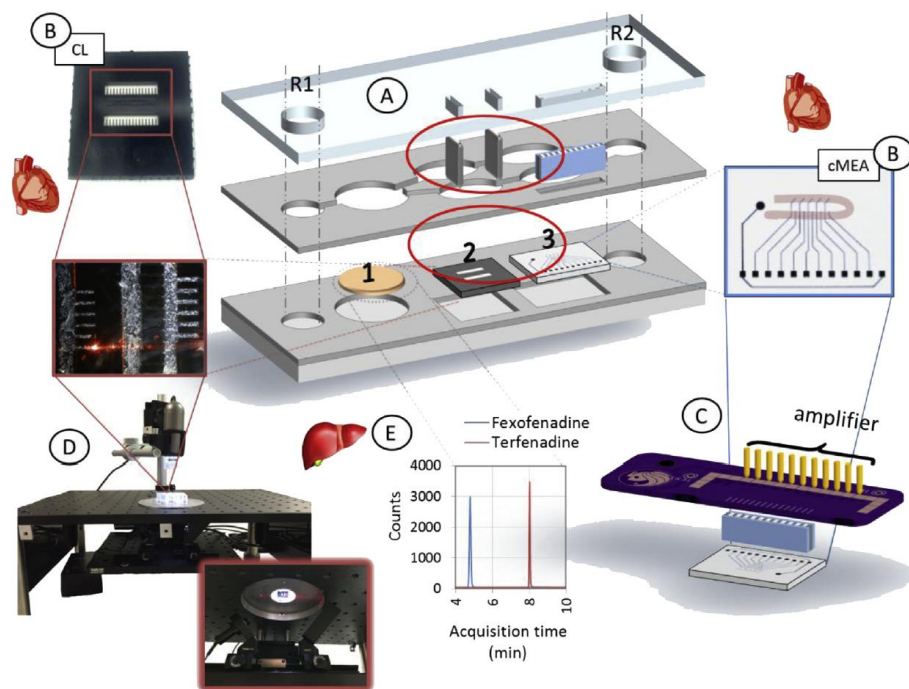
Figure 1.9. Cardiac and liver co-culture in a pumpless microfluidic system. Reused with permission. [80]

In another study by Oleaga et al.[81] an organ-on-a-chip device was designed to integrate four different organs (heart, liver, skeletal muscle, and neural component) for toxicity studies (Figure 1.10).
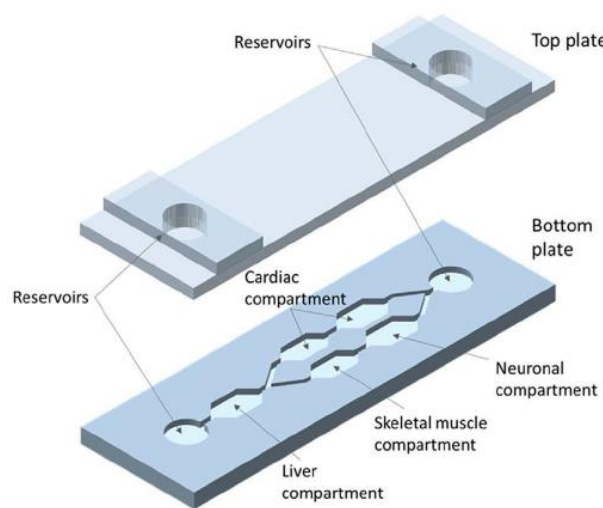
Figure 1.10. Schematic view of the microfluidic device fabricated for four different cell compartments. Reused with permission. [81]

The toxicity effect of several drugs, including Dox, was evaluated using this two-layer gravity-induced flow device. Both viability and functionality of cardiomyocytes were affected by Dox treatment, which was consistent with previous results from the literature. The obtained data demonstrated a 65% decrease in cell viability of cardiomyocytes. The toxic effect of Dox on the function of cardiomyocytes was further demonstrated by a 47% decrease in heart beating rate (Figure 1.11).
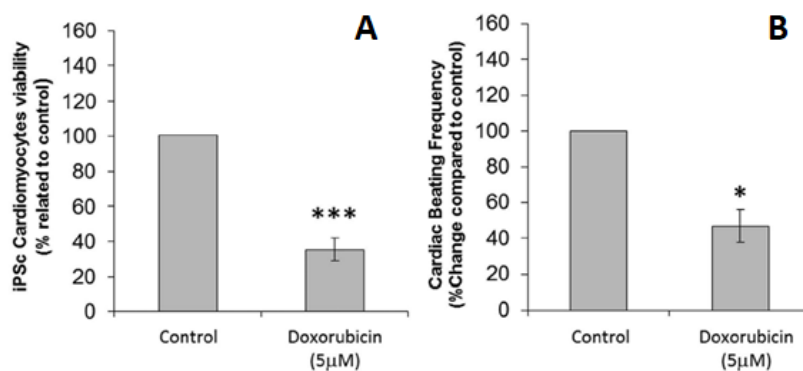
Figure 1.11. Cytotoxic effect of Dox on heart cells A) Viability of cardiomyocytes B) Beating the frequency of cardiomyocytes. Reused with permission. [81]

To sum up, the cardiotoxicity induced by anticancer drugs (which is one of the major reasons for chemotherapy failure) was rarely investigated and modelled on a microfluidic chip. In Chapter 3 of these dissertation, we try to model this damage using organ-on-a-chip technology. Our design offers a few advantages over already developed devices. It is a pumpless device wich will make it more cost-effective and easier to perform compared to traditional designs that required pumps. The removal of pump and tubing connections not only eliminates the possibility of leakage from these connections and bubble formation, but also will remove the need for excessive fluid circulation in the device. Therefore, a more physiologically relevant ratio of media to cell (compared to body) is observed in these systems.

CHAPTER 2

ENHANCEMENT OF LOADING EFFICIENCY BY CO-LOADING OF DOXORUBICIN AND QUERCETIN IN THERMORESPONSIVE POLYMERIC MICELLES[1]

Authors - Pooneh Soltantabar, Erika L. Calubaquib, Ebrahim Mostafavi, Michael C. Biewer, and Mihaela C. Stefan

The Department of Bioengineering, BSB 11

The University of Texas at Dallas

800 West Campbell Road

Richardson, Texas 75080-3021

Author contribution:

MCS conceived the idea, acquired funding, and supervised the authors in this project. ELC synthesized all the hydrophilic monomers(ME2CL, ME3CL, and ME4CL). PS and ELC synthesized the hydrophobic monomer (BnCL) and conducted polymerization reactions for all the polymers (PME2CL-b-PBnCL, PME3CL-b-PBnCL, and PME3CL-b-PBnCL). ELC analyzed the ^{1}H NMR and ^{13}C NMR spectrum of all monomers and final polymers to confirm the structures. PS prepared the micelles and performed a full characterization of micelles, including CMC determination, loading capacity, DLC for size determination, and drug release studies. ELC investigated the thermoresponsivity of polymers through LCST study and conducted TEM for size measurement. The ESI-MS spectra of samples were acquired and analyzed by ELC. All biological studies, including the cytotoxicity of the empty and drug-loaded micelles, was performed by PS with inputs from EM. The manuscript was written by PS and ELC with inputs from MCS, MCB, and EM. Both PS and ELC discussed the results and revised the final manuscript.

2.1 Abstract

Chemotherapy faces challenges, including poor aqueous solubility of the drugs, and cardiotoxicity. Micellar drug delivery systems (DDS) are used to encapsulate anticancer drugs for better therapeutic effects, however, with poor loading content. Herein, we synthesized a micellar DDS using γ-benzyloxy substituted poly(ε-caprolactone) as the hydrophobic block, and co-loaded anticancer doxorubicin (Dox) and antioxidant quercetin (Que). γ-Substituted oligo(ethylene) glycol (OEG) poly(ε-caprolactone)s were used as hydrophilic blocks to make the polymers thermoresponsive. Variation of the OEG chain allowed the tunability of the LCST. Moreover, drug

loading and release were studied. Thermodynamic stability, size, and morphology were determined by fluorescence measurements, dynamic light scattering, and transmission electron microscopy. Combination loading demonstrated improved loading of Dox and Que. Biological studies were performed using HepG2 human liver cancer and H9c2 rat heart cells. The use of biodegradable, biocompatible, and thermoresponsive polymers and the co-loading approach is a good strategy in developing DDSs.

2.2 Introduction

In 2015, the World Health Organization estimated that cancer is the first leading cause of death before age 70 years in 91 countries, and it ranks third or fourth in an additional 22 countries.[4] The current chemotherapeutic drugs are not selective. They can be uptaken by both healthy and cancerous cells, leading to undesired side effects.[4] Nanotechnology has made significant contributions to the development of drug delivery systems by improving the selectivity and controlling the release, which has led to improvements in conventional chemotherapies. Drug delivery systems (DDS) have the potential to bridge the gap between existing effective active agents and desired treatments that are not achievable through conventional therapies.[4]

Among the various DDS, polymeric micelles have gained attention due to their excellent biocompatibility, physicochemical properties, drug loading and release capacities, and facile preparation methods.[8] These micelles that are developed from amphiphilic block copolymers polymers can self-assemble to form spherical micelles in an aqueous medium resulting in a hydrophobic core and a hydrophilic shell. The majority of anticancer drugs are highly hydrophobic, and these compounds can be encapsulated into the hydrophobic core of the micelles.

Despite the useful properties of the nanocarriers, they still can pose toxicity to healthy tissues due to the premature release of drugs. To mitigate this, stimuli-responsive carriers have been developed for more selective therapies. The carriers can release the loaded drug by taking advantage of the differences in the physiological environment between the normal and tumor tissues, as well as exposure to external stimuli such as temperature. Thermoresponsive DDS exhibiting LCST will undergo a phase transition at elevated temperature and release the drug cargo.[82–84] Our group previously reported the synthesis of thermoresponsive poly(γ-2-[2-(2-methoxyethoxy)-ethoxy]ethoxy-ε-caprolactone) as hydrophilic blocks for several amphiphilic block copolymers.[85–87]

Anthracycline drugs such as doxorubicin (Dox) and epirubicin represent an effective class of anticancer drugs that can generate complexes that have the potential to react with oxygen and form reactive oxygen species (ROS). ROS can oxidize the lipids, proteins, and DNA in cells, which ultimately leads to cardiac dysfunction.[88] Detoxifying enzymes can neutralize the ROS in cells to prevent their damaging effects. However, cardiomyocytes have a low amount of ROS detoxifying agents in comparison to other cell types that makes them the main target of Dox-induced damages.[89] Antioxidants such as polyphenols can react with free radicals and reduce the damage to lipids, proteins, and other cell parts.[27,90,91]

In addition to the cardioprotective properties, polyphenols also have a role in overcoming multi-drug resistance (MDR) by acting as chemosensitizers.[92] The most common theory regarding this resistance is explained by the overexpression of P-glycoprotein (P-gp) in cancer cells.[29] Studies have reported that polyphenols such as quercetin (Que) can interact with P-gps and block their activity or reduce their expression.[37,38] Hence, co-administration of Dox and Que will mitigate

the toxic side effects of Dox. Alani et al. .[93] demonstrated the mitigation of Dox-induced cardiotoxicity and simultaneously chemosensitizing effect of polyphenols *in vivo* in combination with Dox. However, in their micellar DDS, only different formulations of natural polyphenols were loaded in micelles and were combined with Dox in free form (unencapsulated), which may not address the poor solubility issue of Dox. Zhang et al.[94] co-loaded Que with Dox in biotin-modified, PEGylated liposomes to investigate the chemosensitizing effect of Que. Their results indicated that Que could downregulate the expression of P-gp efflux pump on cancer cells which is the main cause of MDR. Moreover, it is claimed that the biotin-modified surface of these liposomes can facilitate the endocytosis of these particles into the cells, which may not be a very selective method as these receptors are present on the surface of both cancer and healthy cells. In another study, a stimuli micelle formed by conjugation of Que to chitosan was used for the encapsulation of Dox. In this study, they targeted the acidic pH of tumor tissue and endo/environment, which is distinct from healthy cells. The micelles demonstrated pH responsivity to an acidic environment and were capable of P-gp inhibition in cancer cells to reverse MDR.[95] On the other hand, combination loading is an effective strategy to increase drug loading. This has been demonstrated when Dox was co-loaded with resveratrol,[96] which showed an increased loading in the nanocarrier through hydrogen bonding and π-stacking interactions.

Herein, we report and study the novel thermoresponsive poly(γ-oligo(ethylene glycol)-ε-caprolactone-*b*-poly(γ-benzyloxy-ε-caprolactone) (PME$_x$CL-*b*-PBnCL, x=2 and 4) polymers, as well as the previously reported PME$_3$CL-*b*-PBnCL.[97] The overview of this work is shown in Figure 2.1. All polymers are thermodynamically stable and exhibit phase transitions at elevated temperature, allowing the temperature-dependent release of cargo. PME$_3$CL-*b*-PBnCL had the

26

closest LCST to the physiological temperature, and hence it was used for biological studies using HepG2 liver cancer cells along with H9c2 heart cells.
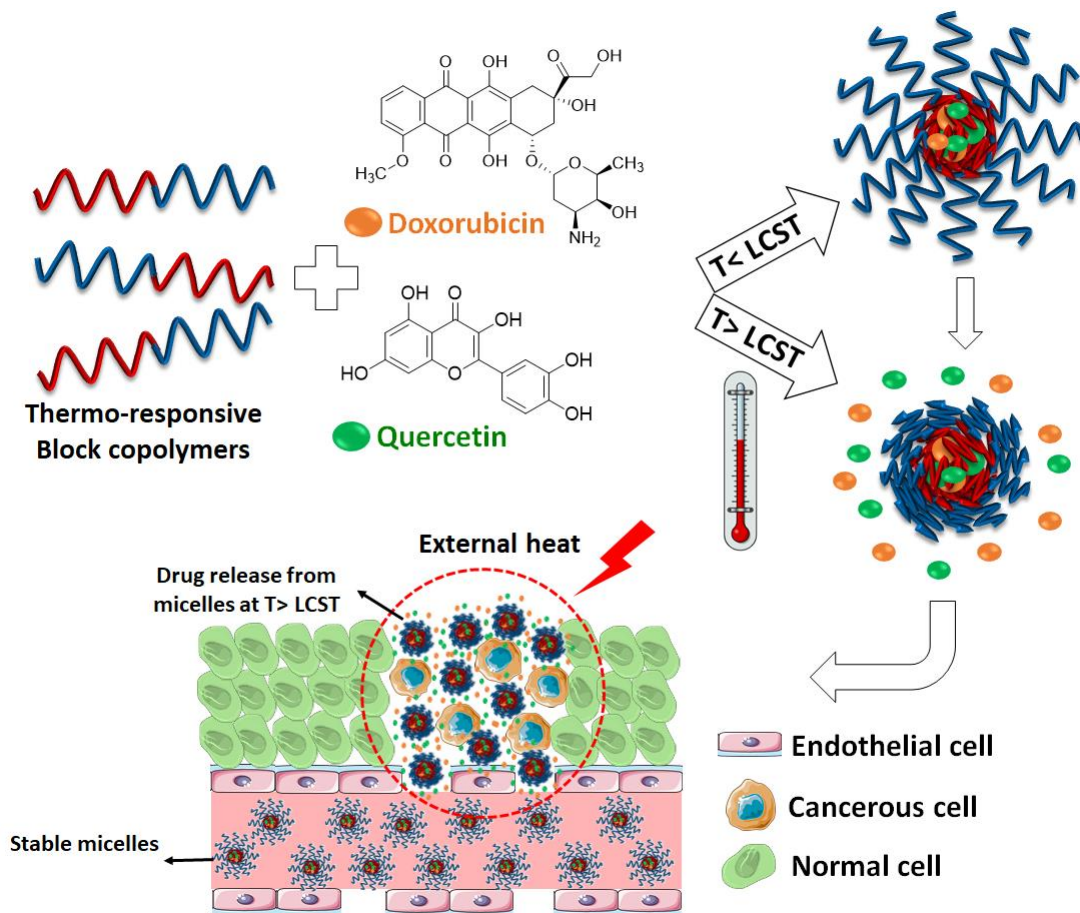
Figure 2.1. Schematic illustration of the preparation and loading of DOX and Que loaded micelles and drug release studies.

2.3 Materials and Methods

2.3.1 Materials

All commercially available chemicals were purchased from either Fisher Scientific or Sigma-Aldrich. Tin (II) 2-ethylhexanoate $(Sn(Oct)_2)$ and benzyl alcohol (BnOH) were purified by vacuum distillation. 4-Hydroxycyclohexanone and tosylated oligo(ethylene glycol) were

27

synthesized according to the previously reported procedure.[97,98] All glassware used for polymerization were kept at 120 ˚C for 24 hours then cooled down in a desiccator to remove moisture. Polymerization reactions were performed under nitrogen.

2.3.2   Analysis

A Bruker AVANCE III (500 MHz) nuclear magnetic resonance (NMR) instrument was used to collect the ^{1}H and ^{13}C NMR spectra of the monomers and polymers using CDCl$_3$ as the solvent. ESI-MS were acquired using a Waters ACQUITY UPLC M-Class with a BEH C4 column for separation and Water Synapt G2-Si Q-TOF for detection. The molecular weight and polydispersity index of the synthesized polymers were measured on a Tosoh EcoSEC HLC-8320 system equipped with a refractive index detector and with a series of four columns (TSK gel guard Super HZ-L, Super HZM-M, Super HZM-N, and Super HZ2000) using polystyrene standard calibration and HPLC grade tetrahydrofuran (THF) as the eluent. The size and distribution of particles were tested through dynamic light scattering (DLS) using the Malvern Zetasizer Nano ZS instrument equipped with a He−Ne laser (633 nm) and 173˚ backscatter detector. The morphological characterization of the synthesized polymers was performed using a JEM-1400+ TEM (JEOL USA Inc., MA). The LCST of the synthesized polymers were evaluated using a temperature-controlled Cary5000 UV-vis spectrometer. Fluorescence spectroscopy of the samples was performed using a PerkinElmer LS 50 BL luminescence spectrometer. A Biotek Cytation 3 imaging reader was used to quantify the cytotoxicity and perform cellular uptake measurements of loaded micelles. A Thermo Fisher Scientific MaxQ 4450 Incubating Shaker was used for drug release study.

2.3.3 Synthesis of Monomers

The synthesis of ME$_3$CL (or referred to as MEEECL) and BnCL has been previously reported by our group.[97] The proton and carbon NMR spectra of the new monomers are demonstrated in Figure 2.2 to Figure 2.9.
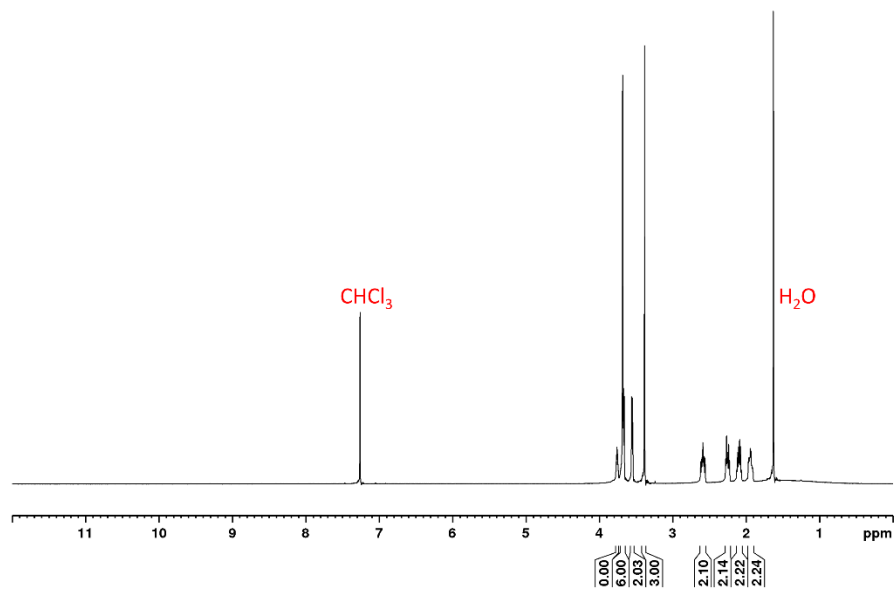
Figure 2.2. ^{1}H NMR spectrum of 4-ME2cyclohexanone.
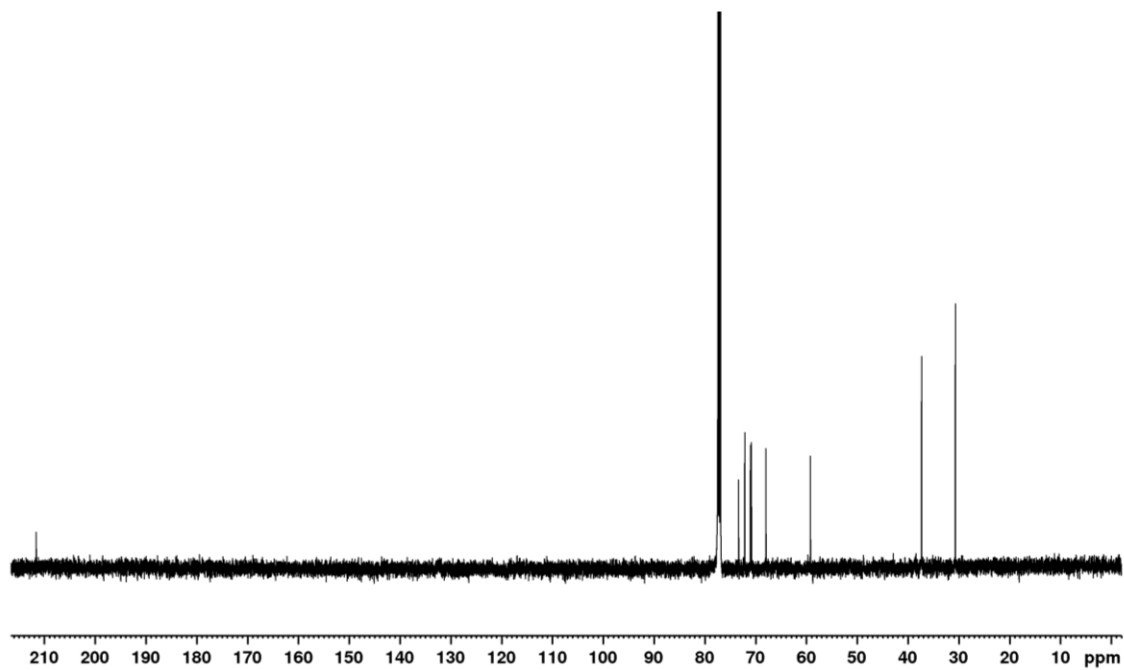
Figure 2.3. ^{13}C NMR spectrum of 4-ME2cyclohexanone.
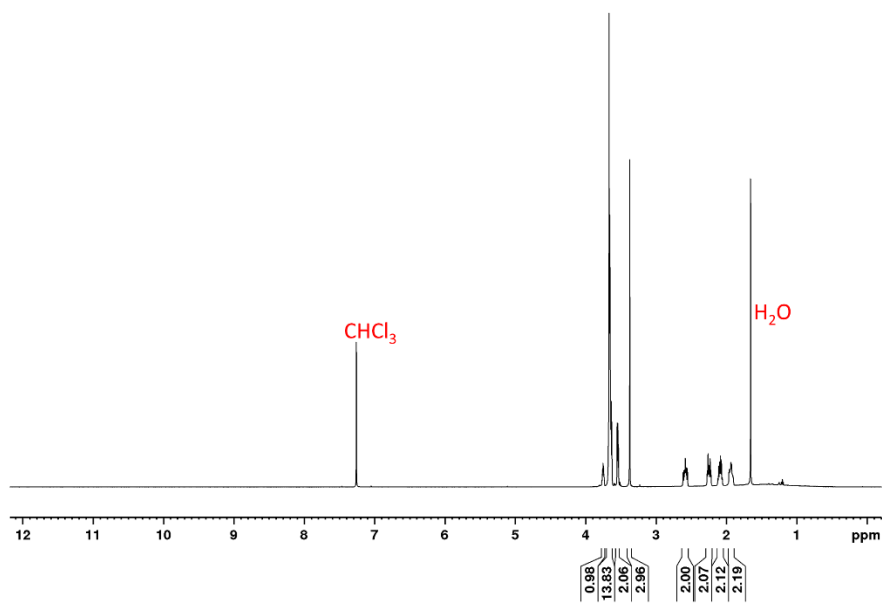
Figure 2.4. ^{1}H NMR spectrum of 4-ME4cyclohexanone.
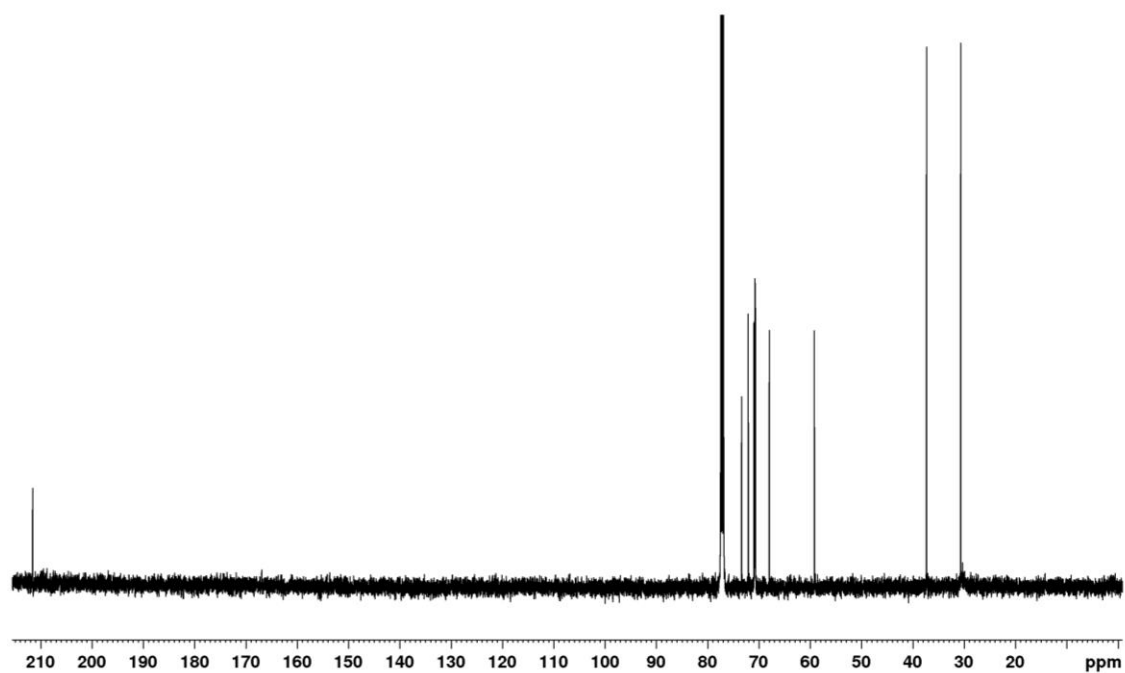
Figure 2.5. ^{13}C NMR spectrum of 4-ME4cyclohexanone.
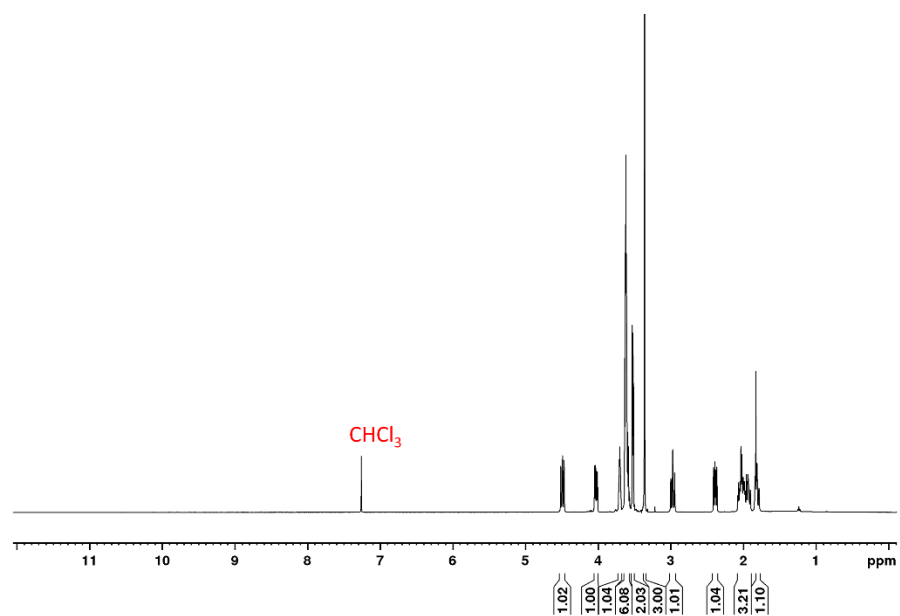
Figure 2.6. ^{1}H NMR spectrum of ME2CL.
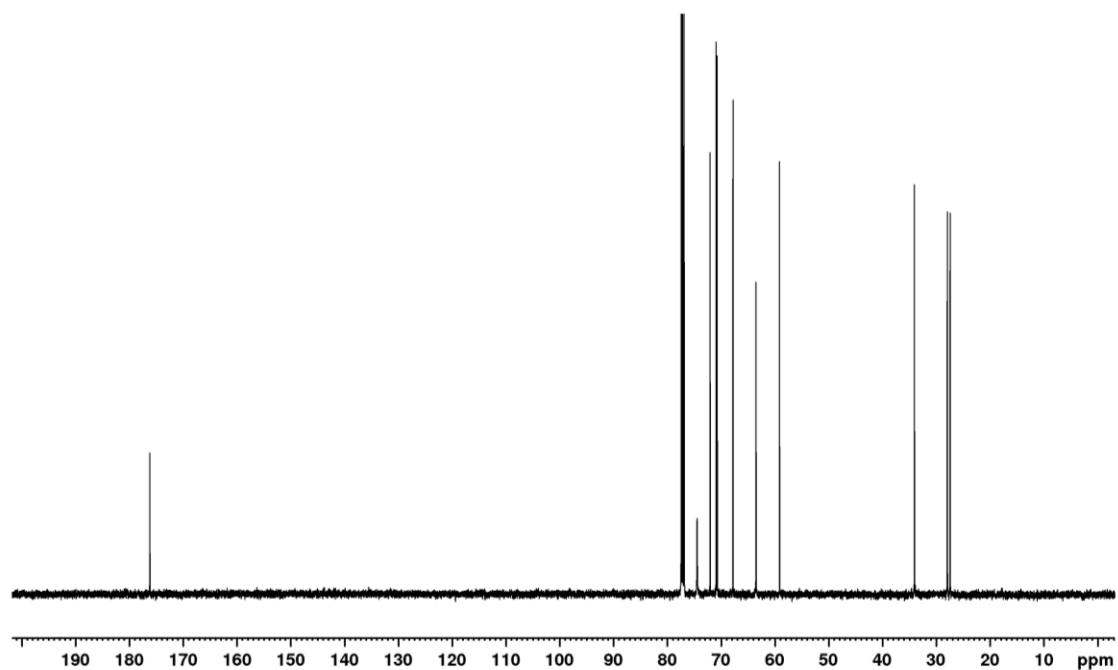
Figure 2.7. ^{13}C NMR spectrum of ME2CL.

CHCl$_3$
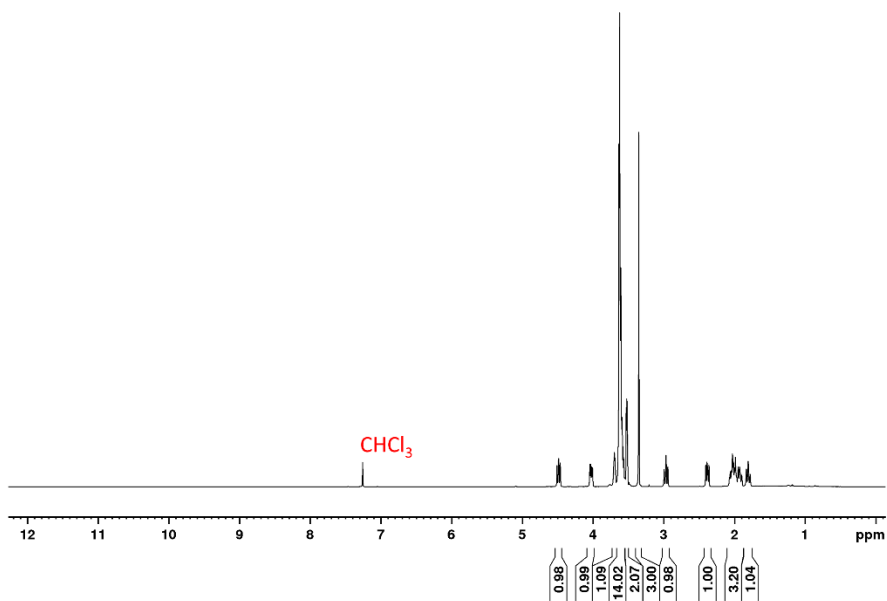
Figure 2.8. ^{1}H NMR spectrum of ME4CL.

32
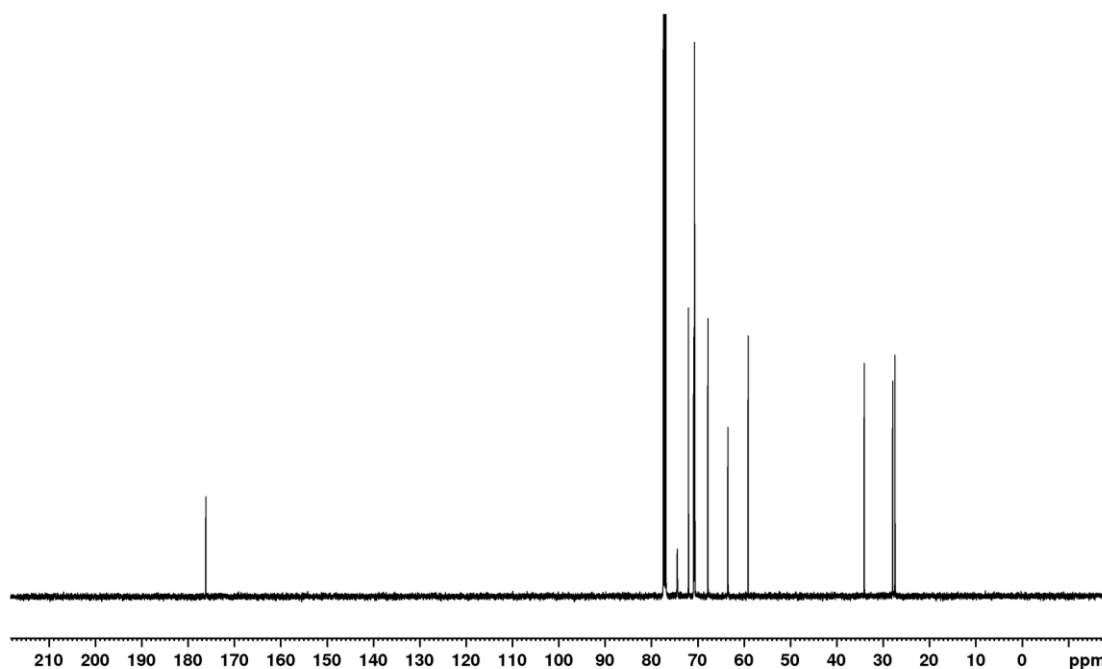
Figure 2.9. ^{13}C NMR spectrum of ME4CL.

i. Synthesis of 4-2-(2-methoxyethoxy)ethoxycyclohexanone: 4-ME₂cyclohexanone

A solution of 4-hydroxycyclohexanone (3.0 g, 26.1 mmol) in anhydrous THF was added with a suspension of NaH (0.69 g, 28.8 mmol) in anhydrous THF in an ice bath. After 30 min of stirring, 2-(2-methoxyethoxy)ethyl-4-methylbenzenesulfonate (7.2 g, 26.1 mmol) was added slowly. The mixture was stirred for 24 h at room temperature. THF was evaporated followed by extraction with ethyl acetate. The organic extract was concentrated *in vacuo*, and the product was isolated using gradient elution with 7:3 to 1:1 hexane/ethyl acetate (2.0 g, 35% yield). The same procedure was followed for the synthesis of 4-ME₃cyclohexanone and 4-ME₄cyclohexanone. 4-ME₂cyclohexanone: ^{1}H NMR δ: 1.90 - 1.97 (m, 2H), 2.06 - 2.12 (m, 2H), 2.22 - 2.28 (m, 2H), 2.56 - 2.62 (m, 2H), 3.38 (s, 3H), 3.54 - 3.56 (m, 2H), 3.66 - 3.68 (m, 6 H), 3.75 - 3.77 (m, 1 H). ^{13}C NMR δ: 211.5, 73.2, 72.0, 70.9, 70.7, 67.8, 59.1, 37.2, 30.5. 4-ME₄cyclohexanone: ^{1}H NMR δ:

33

1.90 - 1.97 (m, 2H), 2.06 - 2.12 (m, 2H), 2.22 - 2.27 (m, 2H), 2.55 - 2.62 (m, 2H), 3.38 (s, 3H), 3.54 - 3.55 (m, 2H), 3.63 - 3.67 (m, 14 H), 3.74 - 3.77 (m, 1 H). ^{13}C NMR δ: 211.6, 73.4, 72.1, 71.0, 70.9, 70.8, 70.7, 68.0, 59.2, 37.3, 30.7.

ii.   Synthesis of γ-2-(2-methoxyethoxy)ethoxy-ε-caprolactone: ME2CL

A solution of 4-ME$_2$cyclohexanone (2.0 g, 9.2 mmol) in dichloromethane was added with a solution of 77% m-chloroperoxybenzoic acid (3.5 g, 15.6 mmol) in dichloromethane in ice bath. The reaction was stirred for 24 h then the solvents were evaporated *in vacuo*. The product was isolated by flash chromatography using hexane/ethyl acetate (2.0 g, 93% yield). The same procedure was followed for the synthesis of ME$_3$CL and ME$_4$CL. ME$_2$CL: ^{1}H NMR δ: 1.79 - 2.08 (m, 4H), 2.36 - 2.41 (dd, 1H), 2.96 - 3.00 (t, 1H), 3.36 (s, 3H), 3.51 - 3.53 (m, 2H), 3.58 - 3.63 (m, 6H), 3.69 - 3.71 (m, 1H), 4.01 - 4.05 (dd, 1H), 4.47 - 4.51 (dd, 1H). ^{13}C NMR δ: 176.2, 74.5, 72.0, 70.9, 70.7, 67.8, 63.5, 59.2, 34.1, 27.9, 27.4. ME$_4$CL: ^{1}H NMR δ: 1.78 - 2.07 (m, 4H), 2.36 - 2.41 (dd, 1H), 2.95 - 2.99 (t, 1H), 3.35 (s, 3H), 3.51 - 3.53 (m, 2H), 3.56 - 3.63 (m, 14H), 3.67 - 3.70 (m, 1H), 4.01 - 4.05 (dd, 1H), 4.46 - 4.51 (dd, 1H). ^{13}C NMR δ: 176.2, 72.0, 70.9, 70.8, 70.7, 70.7, 70.6, 67.8, 63.5, 59.1, 34.1, 27.9, 27.4. The m/z obtained from ESI-MS are 233.14, 277.16, and 321.20, while the calculated m/z ([M+H]$^+$) are 233.13, 277.16, and 321.19 for ME$_2$CL (C$_{11}$H$_{20}$O$_5$), ME$_3$CL (C$_{13}$H$_{24}$O$_6$), and ME$_4$CL (C$_{15}$H$_{28}$O$_7$), respectively. The ESI-MS spectra are shown in the Figure 2.10 to Figure 2.12.
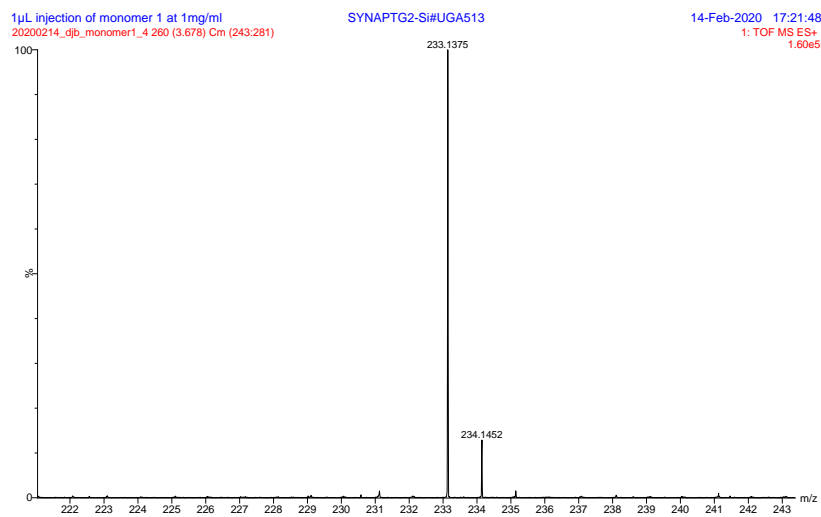
Figure 2.10. ESI-MS spectrum of ME2CL.
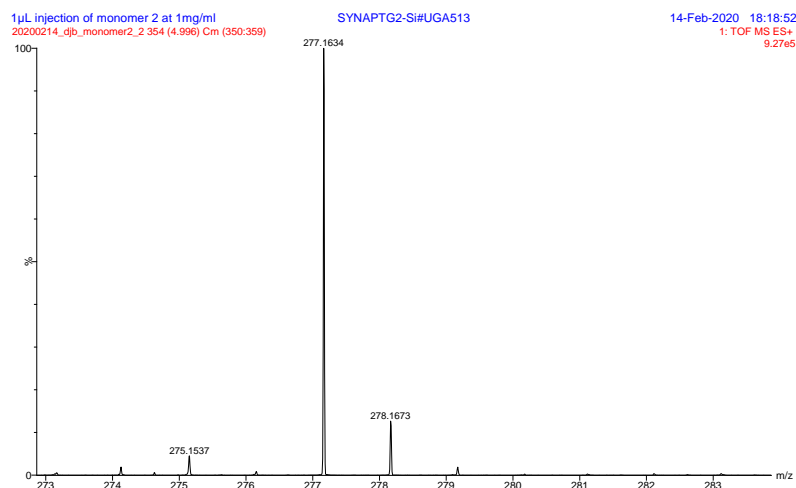
Figure 2.11. ESI-MS spectrum of ME3CL.
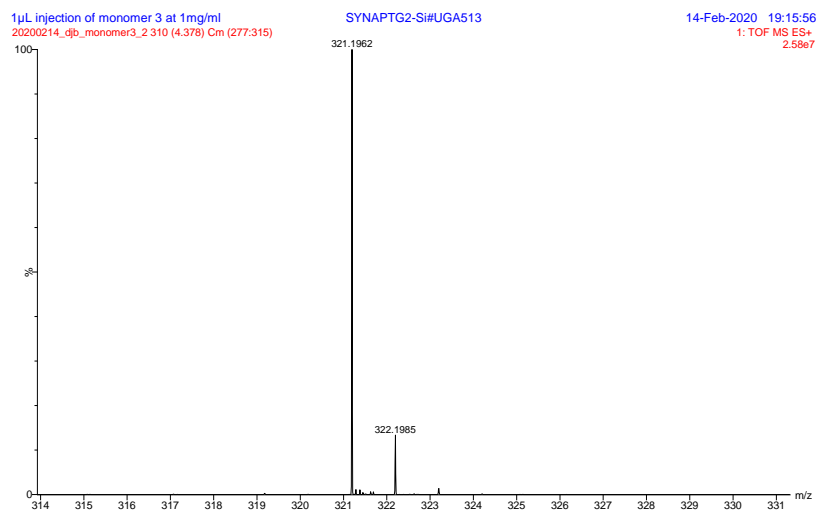
Figure 2.12. ESI-MS spectrum of ME4CL.

2.3.4 Polymerization

Synthesis of poly(γ-2-(2-methoxyethoxy)ethoxy-ε-caprolactone)-*b*-poly(γ-benzyloxy-ε-caprolactone): PME$_2$CL-*b*-PBnCL

ME$_2$CL monomer (0.93 g, 4.0 mmol)), was dried first with calcium hydride then weighed into a flame-dried Schlenk flask inside the glove box. Sn(Oct)$_2$ (32 mg, 0.08 mmol) and benzyl alcohol (8.66 mg, 0.08 mmol) both in dry toluene were added to the flask under nitrogen atmosphere. The reaction flask was purged with nitrogen before placing in an oil bath heated at 110 ˚C. Samples were periodically withdrawn to follow the conversion using ^{1}H NMR. After 100% conversion of monomer (6 h), BnCL (0.88 g, 4.0 mmol) monomer was added. The polymers were obtained by precipitation in hexane then in methanol (yield: 1.5 g). The same procedure was followed for the synthesis of PME$_3$CL-*b*-PBnCL (yield 1.2 g) and PME$_4$CL-*b*-PBnCL (yield 1.3 g) with a feed mole ratio of 50:50:1:1 for the hydrophilic monomer : hydrophobic monomer : catalyst : initiator. PME$_2$CL-b-PBnCL: ^{1}H NMR δ: 1.79 - 1.93 (m, 8H), 2.34 - 2.40 (m, 4H), 3.37 (s, 3H), 3.47 - 3.63 (m, 10H), 4.14 - 4.16 (m, 4H), 4.43 - 4.50 (m, 2H), 7.30 (b, 5H). PME$_3$CL-b-

PBnCL: ^{1}H NMR δ: 1.79-1.92 (m, 8H), 2.35 - 2.38 (m, 4H), 3.38 (s, 3H), 3.46 - 3.64 (m, 14H), 4.14 - 4.16 (m, 4H), 4.43 - 4.47 (m, 2H), 7.30 (b, 5H). PME$_4$CL-b-PBnCL: ^{1}H NMR δ: 1.79 - 1.92 (m, 8H), 2.35 - 2.38 (m, 4H), 3.37 (s, 3H), 3.37 - 3.65 (m, 18H), 4.14 - 4.16 (m, 4H), 4.43 - 4.49 (m, 2H), 7.30 (b, 5H).

2.3.5 Determination of LCST

For LCST determination, 25 mg of the polymer was dissolved in 10 mL of water to make a 0.25 wt% solution. The solution was left to equilibrate at room temperature for 24 hours before measurement. The transmittance (%) at 600 nm was measured by elevating the temperature from 5 to 70 ˚C with a heating rate of 0.5 ˚C/min. The LCST was taken at the point of a 50% drop in transmittance.

2.3.6 Preparation of Micelles

Micelles were prepared by the solvent evaporation method. Five milligrams of the polymer was dissolved in 5 mL of THF, then added dropwise to 5 mL of deionized (DI) water under constant homogenization. The final concentration of polymer in DI water was 1 mg/mL. A homogenous polymer solution was formed over 30 min of homogenization, and then the polymer solution was placed on a shaker with gentle agitation for complete evaporation of the organic solvent. The drug-loaded micelles were prepared through a similar method by dissolving both the polymer and drug in THF. The micelle solution was then filtered using a 0.45 µm nylon syringe filter then dialyzed (MW cut-off: 3500 Da) against water or PBS (for cell studies) for 24 hours to remove any unencapsulated drug.

2.3.7   Preparation of Loaded Micelles with Dox and Que

Single and combination loaded drugs were prepared through a similar method with the empty micelles. Dox·HCl was first neutralized by adding three equivalents of triethylamine in THF. In the case of combination loading, to investigate the effect of feeding ratio on final loading, three different ratios of polymer:Dox: Que (10:1:1, 10:1:5 and 10:1:10) were tested. To investigate the effect of single versus combination loading on the final loading of each drug, the ratio of 10:1:5 for polymer: Dox: Que was selected, and the micelles were loaded with both single and in combination to compare the final loadings. The final drug solutions were diluted with DMSO to collapse the micelles. By using a pre-established calibration curve for each drug (wavelengths of 480 nm for Dox and 370 nm for Que), the actual concentration of the drug in the final solution was determined. The drug loading capacity (DLC) and encapsulation efficiency (EE) were calculated using the following equations:

$$\% \text{ DLC} = \frac{\text{Weight of drug loaded(mg)}}{\text{Weight of the polymer (mg)}} \times 100 \qquad (1)$$

$$\% \text{ EE} = \frac{\text{Weight of drug loaded(mg)}}{\text{Weight of the total drug(mg)}} \times 100 \qquad (2)$$

2.3.8   Determination of Critical Micelle Concentration (CMC)

The CMC of each polymer in water was determined by using pyrene as a probe. After the formation of micelles, this hydrophobic fluorescent molecule migrates into the hydrophobic core of the micelle, which will induce a shift in the excitation spectrum of pyrene.[99,100] Various concentrations of polymer in water were prepared, and a constant volume of pyrene solution in

THF (final concentration in the solution = 3.3×10^{-7} M) was added to each solution. After evaporating the organic solvent through constant agitation, the samples were subjected to fluorescence spectroscopy at room temperature to identify the CMC. The abrupt change in the ratio of peak intensity at 337.5 nm to that at 334.5 nm ($I_{337.5}/I_{334.5}$) from the excitation spectra of pyrene versus log(c) plot indicates the onset of micellization.

2.3.9 Size and Morphology Analysis

The sizes of the empty and co-loaded micelles were measured by DLS. After the formation of micelles with a concentration of 1 mg/mL of polymer in water, samples were equilibrated at 25 ˚C in a Malvern Zetasizer Nano ZS instrument to measure the hydrodynamic diameters (Dh) of micelles. Morphological studies of the micelle solution were carried out by TEM. 40-µL of the sample and 2 wt% phosphotungstic acid were separately dropped on parafilm. A copper mesh, which was first glow-discharged, was dropped horizontally on the sample for 2 mins, then with the stain for 30s, with the dark side facing the solution. In between the sample and stain incubation, the edge of the grid was dapped with filter paper to remove excess liquid. The grid was kept on the petri dish on a filter paper with the dark side facing up.

2.3.10 Determination of *In Vitro* Drug Release

Three freshly prepared co-loaded micelles with the ratio of 10:1:5 for polymer: Dox: Que were used to determining the release profile of each polymeric micelle at various temperatures. The loaded micelle solution (4 mL), with a constant concentration of polymer at 1 mg/mL, was transferred to a dialysis bag with an MW cut-off of 3500 Da and was dialyzed against 10 mL PBS

supplemented with 10% fetal bovine serum (FBS) at pH of 7.4 for 48 hours. At specific time intervals, 1 mL of the release media was removed and was replenished with fresh PBS. Each sample was diluted with DMSO and was subjected to UV-Vis spectroscopy to quantify the amount of Dox released based on the pre-established calibration curve.

2.3.11 Cytotoxicity Studies of Co-loaded Micelles

HepG2 liver cancer (ATCC, CRL-10741) and H9c2 rat heart (ATCC, CRL-1446) cells were cultured in Dulbecco's Modified Eagle Medium (DMEM) supplemented with 10% FBS and 1 % penicillin/streptomycin (pen/strep). Cells were detached from confluent flasks through trypsinization and were re-seeded at a density of 10,000 cells/well in 96 well plates. Cells were allowed to adhere to the bottom of the wells by incubation at 37 °C at 5% CO_2 for 24 hours. After 24 hours, the media was removed, and the cells were washed with PBS. 100 μL of empty, single, and co-loaded micelle solutions, as well as a comparable concentration of free drug solutions in PBS, was added to each well followed by an additional 100 μL of fresh media. After 24 hours of incubation at 37 ˚C and 42 ˚C, the media containing micelles and free drugs were removed, and the cells were re-washed twice using the PBS. Cell viability was assessed using CellTiter-Blue, according to the manufacturer's recommended protocol.

2.3.12 Cellular Uptake

HepG2 cells were cultured in a 35 mm glass-bottom dish with a density of 250,000 cells/dish. After 24 hours of incubation for cell attachment, the media was removed, and the cells were washed with PBS. Co-loaded micelle solution (1 mL) was added to cells, followed by the addition of 2 mL of fresh media. After 4 hours of incubation at 37 and 42 ˚C, the media containing

the micelles was removed, and cells were rewashed with PBS. The cells were fixed using 4% paraformaldehyde; and finally, the cells were stained with DAPI. Micrographs of the cells were taken to determine cellular uptake of micelles using the BioTek Cytation 3 fluorescent microscope.

2.3.13 Statistical Analysis

All data analyses were performed using GraphPad Prism Software version 8. The significant difference between 2 groups was evaluated using the F-test to compare variances followed by the student t-test. In contrast, for meaningful difference evaluation between 3 or more groups, one-way ANOVA was performed. A P-value of <0.05 was considered to be significantly different.

2.4 Results and Discussion

2.4.1 Polymer Design and Synthesis

Three amphiphilic diblock copolymers with various oligo(ethylene glycol) substituents were designed for potential use as drug carriers. γ-Benzyloxy poly(ε-caprolactone) was used as the hydrophobic block since it provides an increase in loading compared to unsubstituted CL due to its ability to interact with the loaded molecule through π-stacking.[96] The addition of tri(oligo ethylene glycol) substituent was previously shown to impart hydrophilicity as well as thermoresponsivity to the polymer.[101] To tune the thermoresponsivity of the amphiphilic diblock copolymers, different lengths of OEG units were used as a pendant group (Figure 2.13).
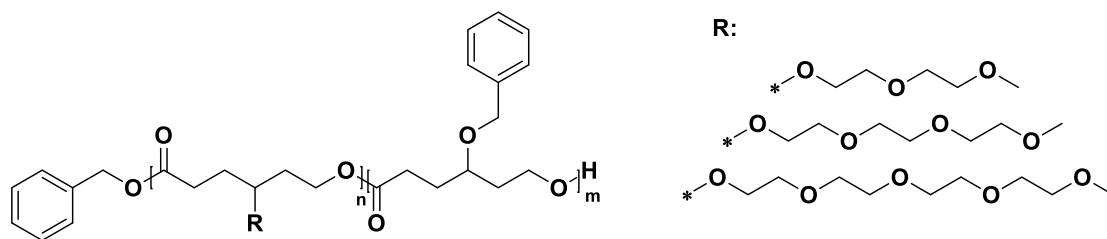
Figure 2.13. Structures of block copolymers. The block copolymers are comprised of benzyl-substituted PCL as the hydrophobic block and various OEG-substituted hydrophilic blocks.

ME_xCL monomers were first polymerized to generate the hydrophilic block until all monomers were consumed, as confirmed by ^1H NMR analysis. BnCL monomer was then added to form the hydrophobic block. A 50:50 mole ratio was targeted to obtain a comparable composition for all the amphiphilic diblock copolymers. The molecular weights, composition, and polydispersity indices are summarized in Table 2.1. The composition of the polymers was determined by the integration of the peaks of the substituents of the block copolymers, the methoxy group in the OEG substituent at ~3.37 ppm *vs.* the methylene protons of the benzyloxy substituent at ~4.5 ppm. The molecular weight was estimated by multiplying the degree of polymerization of the block copolymer with the molecular weight of the repeating unit. The degree of polymerization was estimated from the integration of the methylene benzyl protons of the initiator at ~5.1 ppm *vs.* the above-mentioned peaks. The ^1H NMR spectra and SEC traces are shown in Figure 2.14 to Figure 2.17.
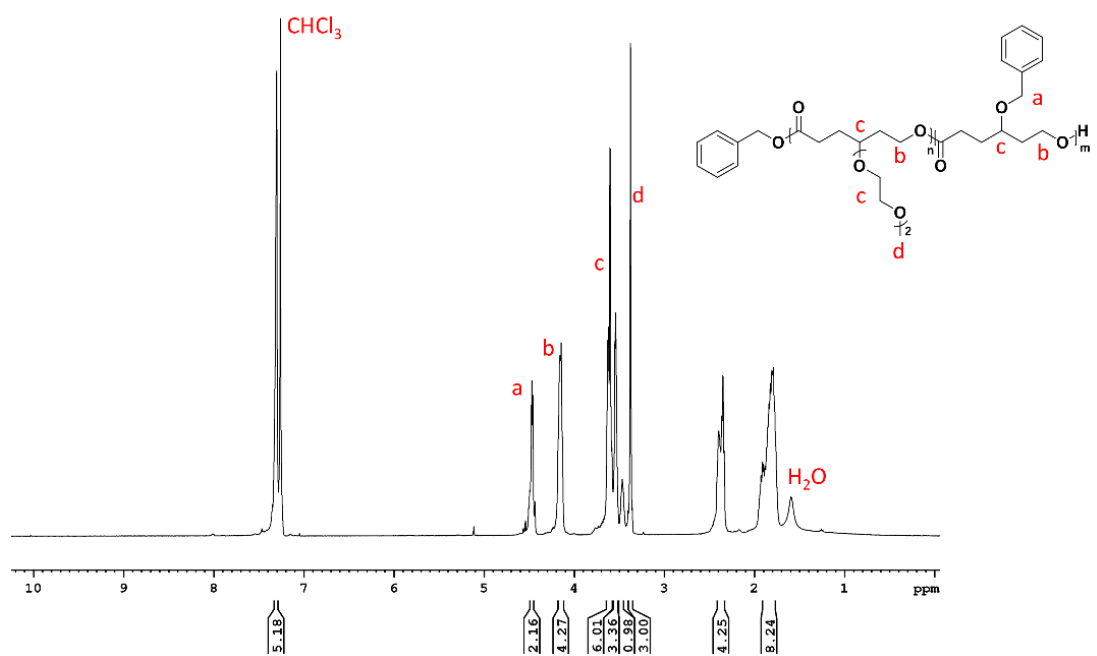
Figure 2.14. ^{1}H NMR spectrum of PME2CL-b-PBnCL.
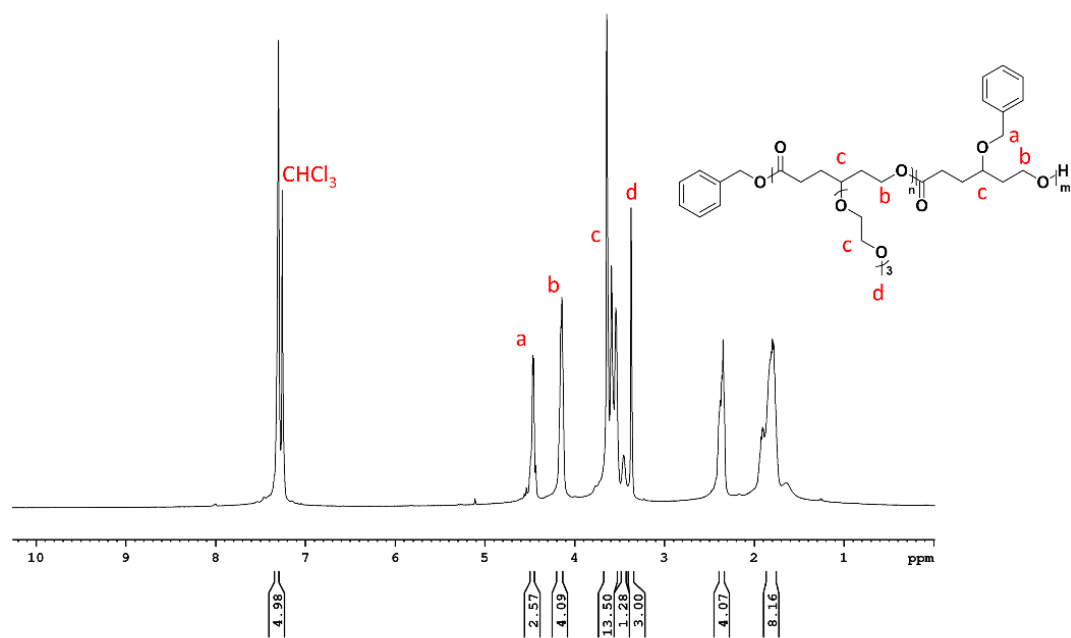
Figure 2.15. ^{1}H NMR spectrum of PME3CL-b-PBnCL.
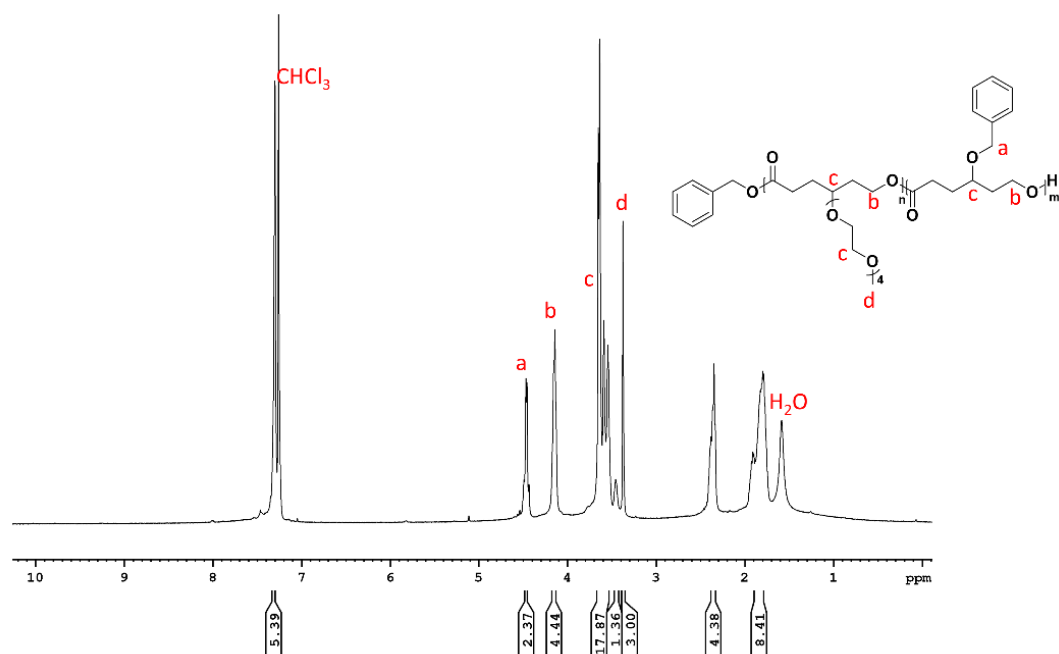
Figure 2.16. ^{1}H NMR spectrum of PME4CL-b-PBnCL.
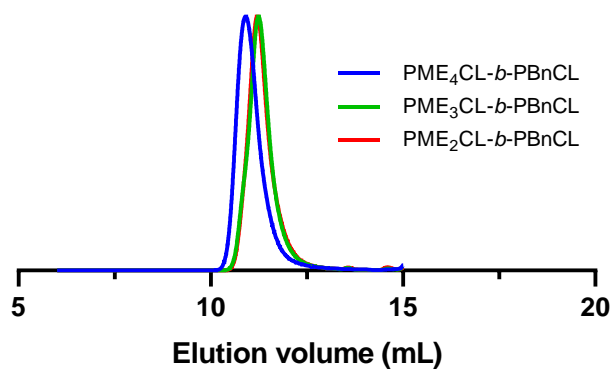
Figure 2.17. SEC traces of the diblock copolymers. The molecular weight and polydispersity index were determined through SEC equipped with a refractive index detector using a polystyrene standard.

Table 2.1. Summary of polymer compositions and molecular weight of synthesized block copolymers.

	Mol %		M_n, NMR (kg/mol)	M_n, SEC (kg/mol)	PDI SEC
	Feed ratio	Measured ratio[a]			
PME$_2$CL-*b*-PBnCL	50 : 50	49 : 51	21.2	7.2	1.31
PME$_3$CL-*b*-PBnCL	50 : 50	53 : 47	22.5	7.3	1.30
PME$_4$CL-*b*-PBnCL	50 : 50	57 : 43	25.4	10.8	1.40

[a]mol % was calculated from ^{1}H NMR analysis

2.4.2 Self-Assembly and Thermoresponsivity

The self-assembly of the micelles was investigated through CMC determination by using pyrene as a probe. The fluorescence of pyrene is solvent polarity dependent[102], which leads to its excitation peak shift from 334.5 nm in the hydrophilic environment to 337.5 nm in a hydrophobic environment. The ratio of intensities of the peaks ($I_{337.5}/I_{334.5}$) versus the log of concentration results in CMC value for each polymer. The CMC value of each polymer is presented in Figure 2.18(A-C). The CMC values of polymers were in the same order with PME$_2$CL-*b*-PBnCL, PME$_3$CL-*b*-PBnCL, and PME$_4$CL-*b*-PBnCL having the CMC values of 4.9×10^{-5}, $5.6 \times 10^{-5,}$ and 5.8×10^{-5} mg/mL, respectively. These low CMC values indicate the good thermodynamic stability of the micelles as the CMC is an important factor used to describe this property.[99]
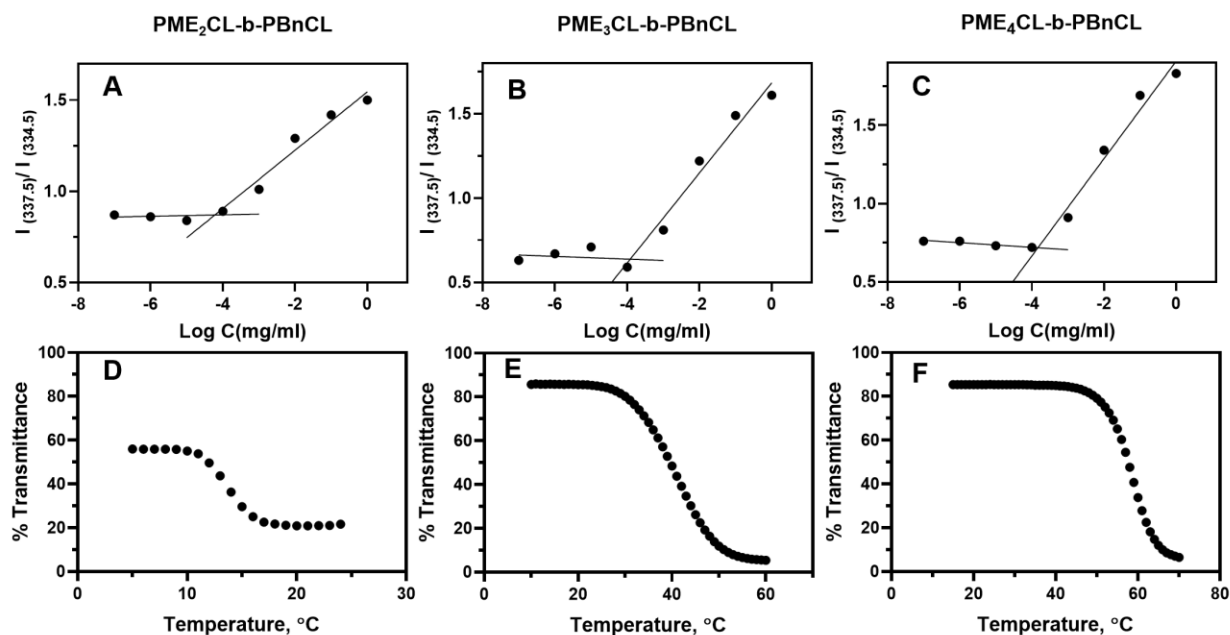
Figure 2.18. CMC (top) and transmittance (bottom) plots of synthesized polymers. CMC values measured by fluorescence spectroscopy using pyrene as a fluorescent probe. (A) PME2CL-b-PBnCL, (B) PME3CL-b-PBnCL, and (C) PME4CL-b-PBnCL blocks showed the CMC values of the order of 10^{-5}, which indicates high thermodynamic stability of the micelles. The transmittance of synthesized polymers was measured with UV-vis upon heating of the aqueous polymer solution. The LCST values for (D) PME$_2$CL-b-PBnCL, (E) PME$_3$CL-b-PBnCL and (F) PME$_4$CL-b-PBnCL blocks were 15 ˚C, 41 ˚C and 59 ˚C, respectively.

The LCST of the polymers shown in Figure 2.18(D-F) were determined using turbidimetric measurements of 0.25 wt% aqueous solutions of the polymers. The % transmittance was obtained at 600 nm with a heating rate of 0.5 ˚C min^{-1}. Transmittance decreases above the LCST due to the dehydration and precipitation of the polymer from the aqueous solution. The LCST was taken as the temperature where there is a 50% drop in the transmittance during heating. Varying the length of OEG units, we observed that as the length of the OEG chain increases, the LCST also increases. The block copolymers with di-, tri-, and tetra- OEG chains had LCST of 15 ˚C, 41 ˚C, and 59 ˚C, respectively. PME$_2$CL-b-PBnCL had the lowest LCST since it has the shortest OEG chain, thus the least hydrated.[103] This result is consistent with the LCST values of various OEG-substituted

polymethacrylates.[104]   The low transmittance of PME$_2$CL-*b*-PBnCL is due to its low aqueous solubility. The LCST for each block copolymer can be further tuned by variation in the ratio of hydrophobic to hydrophilic blocks.

2.4.3   Size and Morphology of Empty and Combination Loaded Micelles

The hydrodynamic diameters of the micelles were evaluated by performing DLS analysis (Figure 2.19(G-I)). The DLS measurement for empty micelles revealed that the PME$_2$CL-*b*-PBnCL polymer formed micelles with a larger size of 81.5 nm than PME$_3$CL-*b*-PBnCL and PME$_4$CL-*b*-PBnCL having sizes of 29.2 nm and 31.18 nm, respectively. The large size of PME$_2$CL-*b*-PBnCL micelles compared to the other blocks might be attributed to the dominance of the hydrophobic segment over hydrophilic, resulting in a higher surface area for hydrophobic segment interactions. DLS of loaded micelles showed the sizes of 93.1 nm, 39.11 nm, and 44.0 nm for PME$_2$CL-*b*-PBnCL, PME$_3$CL-*b*-PBnCL, and PME$_4$CL-*b*-PBnCL micelles, respectively. The loaded micelles showed a slight increase in hydrodynamic diameter compared to empty ones, which can be due to incorporating the hydrophobic molecules into the core of the micelles. TEM images were captured to study the morphology of empty and drug-loaded micelles. The TEM images in Figure 2.19(A-F) show the morphology of the micelles to be spherical both before and after drug loading. Similar behavior was observed in previously reported poly(ε-caprolactone) micelles.[99–101,105] The sizes measured through DLS were closed to the values obtained from TEM, however, for the latter, the micelles are in a dehydrated state resulting in size shrinkage.
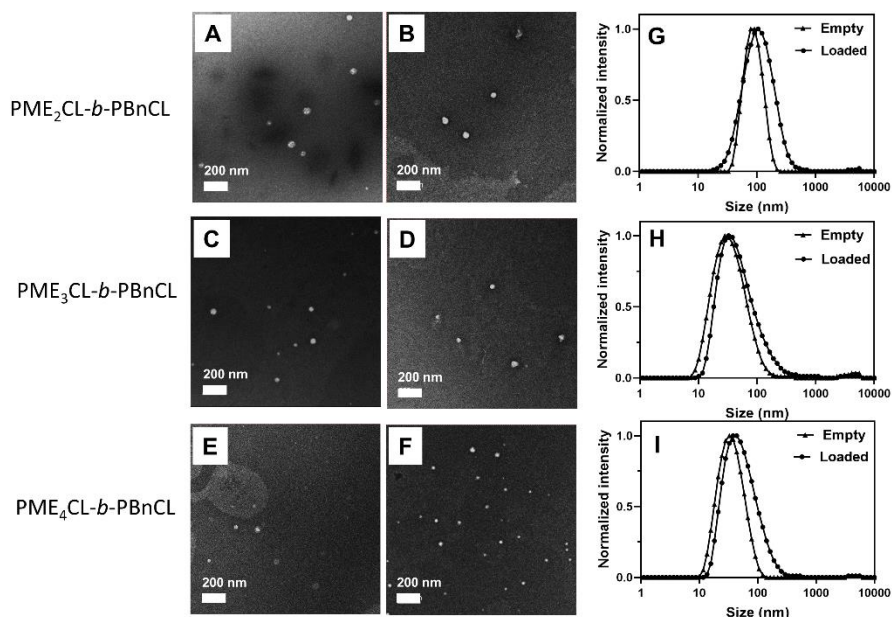
Figure 2.19. TEM and DLS images of empty and loaded micelles. The TEM images of empty (A,C, and E) and loaded (B, D, and F) micelles showed that the polymers self-assembled in spherical shaped micelles. Empty PME2CL-b-PBnCL, PME3CL-b-PBnCL and PME4CL-b-PBnCL blocks showed sizes of 81.5, 29.2 and 31.1 nm, respectively. In all synthesized polymers, a slight increase in the size of the micelles was observed after the loading. Sizes measured by TEM were in agreement with the sizes obtained from DLS for PME$_2$CL-b-PBnCL (G), PME$_3$CL-b-PBnCL (H), and PME$_4$CL-b-PBnCL (I) blocks.

2.4.4 Drug Loading Capability

The possibility of using micelles as drug carriers were examined by loading Dox only, Que only, and a combination of both at different variations. In the initial loading study, three loading ratios of polymer: Dox: Que were examined with variations in the amount of feeding of Que to find the optimal loading ratio that results in the highest encapsulation efficiency. The quantity of drug-loaded into micelles was determined using UV-Vis spectroscopy to compare the absorption of loaded drugs to a standard curve of the relevant molecule. The DLC and EE were calculated.

We varied the feeding amount of Que to determine whether this variation would affect the encapsulation of drugs through Dox-Que interactions. Table 2.2 demonstrates that increasing the

ratio of Dox:Que from 1:1 to 1:5 increased the amount of loaded Dox in PME$_2$CL-b-PBnCL from 4.0 to 8.2 %, in PME$_3$CL-b-PBnCL from 3.1 to 6.2%, and in PME$_4$CL-b-PBnCL from 2.0 to 5.7%. However, a further increase in the feeding ratio of Que in Dox: Que ratio of 1:10 resulted in a lower encapsulation of Dox. It was observed that there was a drop in Dox encapsulation efficiency (Figure 2.20) of about 30%, 10%, and 20% in PME$_2$CL-b-PBnCL, PME$_3$CL-b-PBnCL, and PME$_4$CL-b-PBnCL, respectively. With the best encapsulation efficiency and loading at the ratio of polymer:Dox: Que of 10:1:5, this ratio was chosen for further studies, *in vitro* drug release, and cell studies. Figure 2.21 gives the encapsulation efficiency of single-loaded Dox, and single loaded Que and co-loaded Dox and Que for each polymer. The DLC values are presented in Table 2.3. This study was performed to investigate the effect of the co-loading of drugs on enhancing the loading amount. The loading of Dox in PME$_2$CL-b-PBnCL micelles increased from 3.5 % in single loading to 8.2% in co-loaded micelles. PME$_3$CL-b-PBnCL and PME$_4$CL-b-PBnCL also demonstrated about 2.3 % and 2.7 % increased loading in co-loaded micelles. This can be attributed to the hydrogen bonding and π stacking interactions between Dox and Que, which have been observed in previous studies.[96]
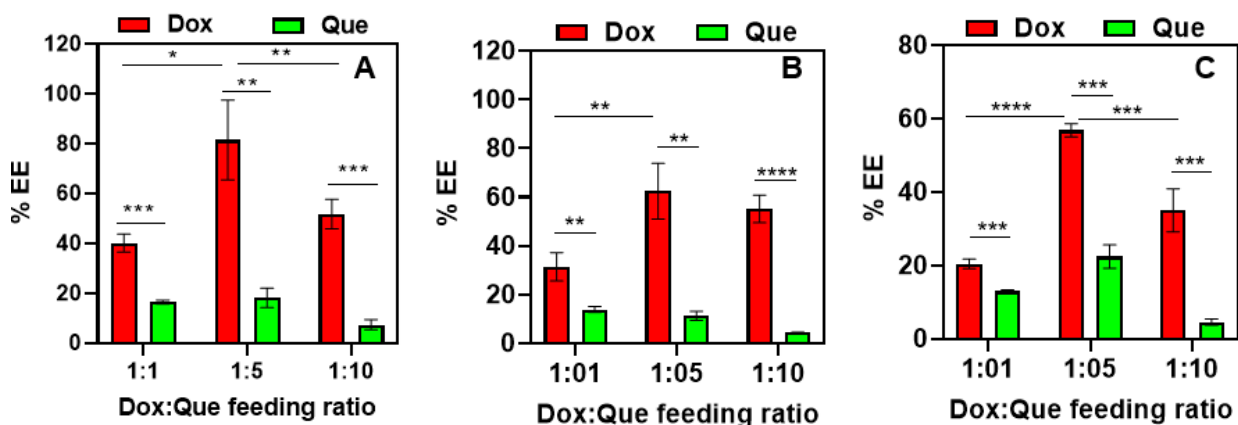
Figure 2.20. Encapsulation efficiencies with drug loading variations. The feeding ratio of [polymer]:[Dox]:[Que] was varied from 10:1:1 to 10:1:10. The drug-loaded samples were subjected to UV-Vis spectroscopy the quantify the drug-loaded. Loading variations of Dox and Que in (A) PME_2CL-b-PBnCL, (B) PME_3CL-b-PBnCL and (C) PME_4CL-b-PBnCL demonstrated that the higher encapsulation efficiency is observed in feeding ratio of [polymer]:[Dox]:[Que] of 10:1:5.

Table 2.2. DLC of combination loaded micelles

		Feed ratio (Dox : Que)		
		1 : 1	1: 5	1 : 10
PME_2CL-b-PBnCL	%DLC_{Dox}	4.0 ± 0.4	8.2 ± 1.6	5.2 ± 0.6
	%DLC_{Que}	1.6 ± 0.1	9.1 ± 2.0	7.4 ± 2.0
PME_3CL-b-PBnCL	%DLC_{Dox}	3.1 ± 0.6	6.2 ± 1.1	5.5 ± 0.6
	%DLC_{Que}	1.4 ± 0.1	5.6 ± 0.9	4.4 ± 0.1
PME_4CL-b-PBnCL	%DLC_{Dox}	2.0 ± 0.1	5.7 ± 0.2	3.5 ± 0.6
	%DLC_{Que}	1.3 ± 0.0	11.2 ± 1.6	4.6 ± 0.9

Table 2.3. Comparison of DLC values of combination loaded micelles versus single loaded micelles in feeding ratio of [polymer]:[Dox]:[Que] of 10:1:5

		Dox Single loading	Que Single loading	Co-loading
PME$_2$CL-*b*-PBnCL	%DLC$_{Dox}$	3.5 ± 0.6	N/A	8.2 ± 1.6
	%DLC$_{Que}$	N/A	2.9 ± 0.8	9.1 ± 2.0
PME$_3$CL-*b*-PBnCL	%DLC$_{Dox}$	3.9 ± 0.8	N/A	6.2 ± 1.1
	%DLC$_{Que}$	N/A	2.7 ± 0.8	5.6 ± 0.9
PME$_4$CL-*b*-PBnCL	%DLC$_{Dox}$	3.0 ± 0.1	N/A	5.7 ± 0.2
	%DLC$_{Que}$	N/A	2.8 ± 0.7	11.2 ± 1.6
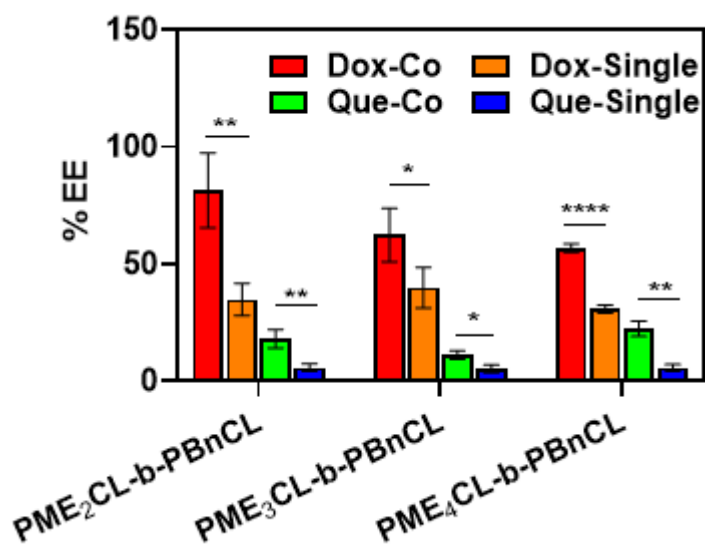
Figure 2.21. Encapsulation efficiencies of single and co-loaded micelles. Polymers were loaded with Dox only, Que only, and co-loaded with Dox and Que. The samples were subjected to UV-Vis spectroscopy, and the amounts of Dox and Que were quantified in both single and co-loaded samples. The encapsulation efficiencies for both Dox and Que were significantly higher in co-loaded samples compared to single-loaded, which is an indicator of favorable interactions between drugs.

2.4.5 *In Vitro* Release

In our study, the *in vitro* release of Dox from micelles was performed by dialysis of co-loaded micelle solutions in PBS (pH 7.4) at 37 ˚C and 42 ˚C for 48 hours. The release profile of Dox from the micelles is shown in Figure 2.22. At specific time points, aliquots of the release medium were removed and replenished with fresh PBS while measuring the drug content in samples using UV-Vis spectroscopy. As it is shown in Figure 2.22(A and C), there was no significant difference in the release of PME$_2$CL-*b*-PBnCL and PME$_4$CL-*b*-PBnCL micelles at 37 ˚C and 42 ˚C over 48 hours, with the maximum release of 94 % in PME$_2$CL-*b*-PBnCL and 67 % release in PME$_4$CL-*b*-PBnCL. This result can be explained with the low LCST of PME$_2$CL-*b*-PBnCL (15 ˚C) and high LCST of PME$_4$CL-*b*-PBnCL (59 ˚C). As a proof of concept, the release study was repeated for PME$_4$CL-*b*-PBnCL at 60 ˚C (temperature above LCST). The result indicates that there was a significant increase (about 32%) in the release of drug from these micelles at higher temperatures. The Dox release from PME$_3$CL-*b*-PBnCL polymer demonstrated an increase from 67% at 37 ˚C to 100% at 42 ˚C. This behavior is most likely due to the LCST value of this polymer, which leads to higher release at elevated temperatures.
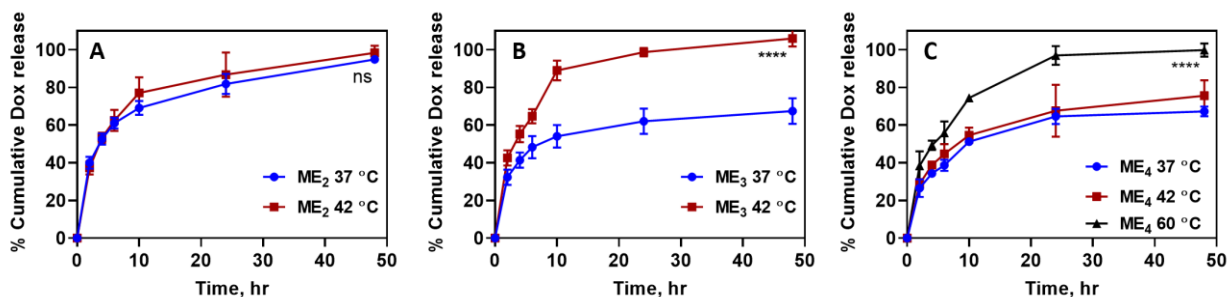
Figure 2.22. Dox release curve from micelles at different temperatures. In vitro Dox release from (A) PME2CL-b-PBnCL, (B) PME3CL-b-PBnCL and (C) PME4CL-b-PBnCL polymeric micelles are shown. The cumulative release profile was obtained by taking samples from the release medium of drug-loaded samples at specific time intervals. PME$_2$CL-*b*-PBnCL samples showed

similar release profiles in both temperatures. There was a significant increase in the release of Dox from PME$_3$CL-b-PBnCL samples at a higher temperature, which was above the LCST of this polymer. PME$_4$CL-b-PBnCL micelles also demonstrated similar release profiles at 37 ˚C and 42 ˚C; however, another release profile at 60 ˚C (above LCST) indicated an increase in the release.

2.4.6 Cytotoxicity Studies of Co-loaded Micelles

To investigate the cytotoxicity of empty micelles, the H9c2, and HepG2 cells were exposed to the micelles with concentrations ranging from 0.02 to 0.2 mg/mL. The viability values demonstrated in Figure 2.23 indicates that the micelles did not show any cytotoxicity to any of the cell lines. To perform the cytotoxicity experiments, H9c2 and HepG2 cells were treated with micelles loaded with Dox-only, Que-only, and Dox+Que with variation in polymer concentration from 0.02 to 0.25 mg/mL at 37 ˚C. Free Dox, free Que, and free Dox+Que treatments with concentrations calculated based on drug-loaded micelles were used for comparison. As it is shown in Figure 2.24, there was no significant difference in the viability of H9c2 cells when treated with free Dox and free Dox+Que, while in the case of HepG2 cells, there was a significant decrease in viability when the cells were treated with the combination of drugs. This can be due to the cardioprotective effect of polyphenols when used in combination with chemotherapy.[27,91] Also, combination therapy with polyphenols can lead to a chemosensitizing effect in cancer cells, which results in higher cytotoxicity.[37,106] However, this effect was not observed in similar treatment with micelles, which could be due to incomplete release of drugs from micelles in a way that may result in cardioprotection in heart cells and chemosensitizing effect in cancer cells. Therefore, in future studies, a more precise synergistic study is needed to determine the optimum dose that causes cardioprotection in heart cells and chemosensitizing effects in cancer cells at the same time.
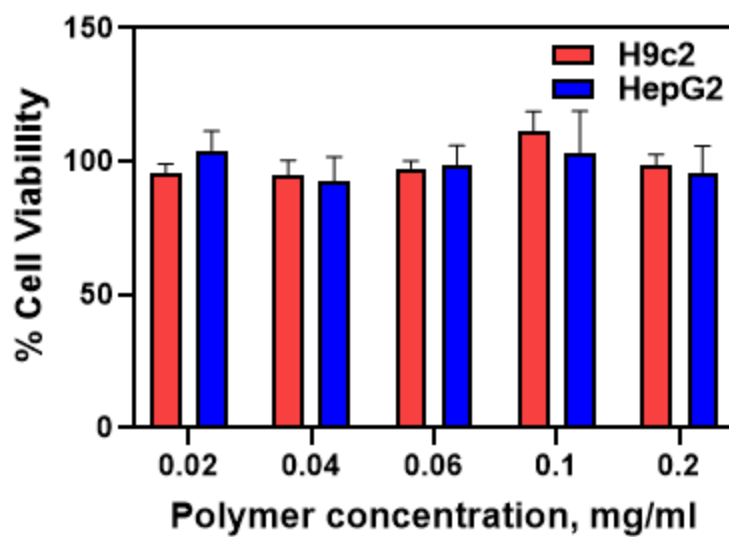
Figure 2.23. Cytotoxicity of PME3CL-b-PBnCL empty micelles. HepG2 and H9c2 cells were incubated with empty micelles at different concentrations of polymer for 24 hours. Cell viability evaluations demonstrate no significant cytotoxicity of polymer on HepG2 and H9c2 cells even at high concentrations.
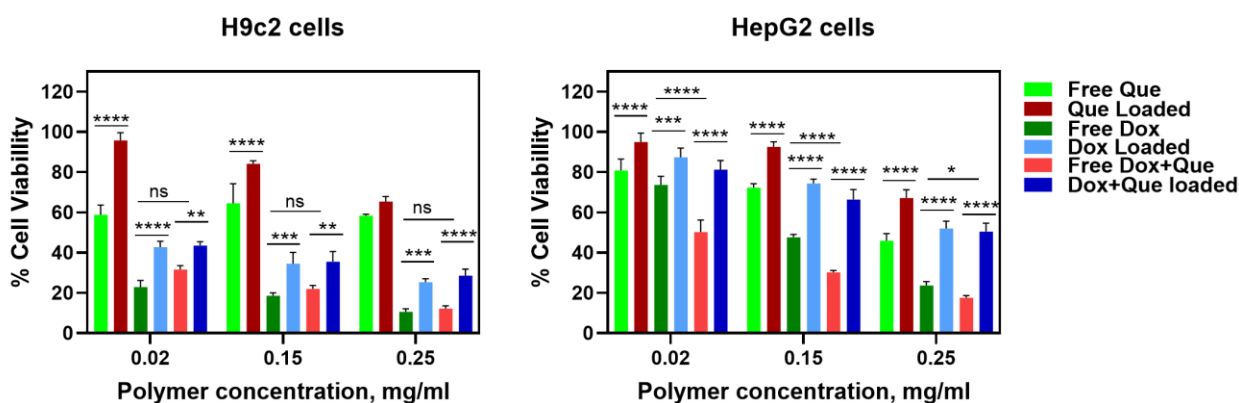
Figure 2.24. Cytotoxicity of Dox, Que, and a mixture of Dox and Que in free form and loaded in PME3CL-b¬-PBnCL micelles. After incubation of H9c2 and HepG2 cells with drug solutions for 24 hours, the cell viability was assessed using CellTiter-Blue. Cells were treated with free Dox, free Que, free Dox+Que, Dox loaded, Que loaded, and Dox+Que loaded micelles. After removing the drug solutions and adding the CellTiter-Blue reagent, the cells were incubated 3 hours before recording fluorescence (560Ex/590Em).

In almost all treatments, the viability of cells treated with micelles was significantly higher

than the viability of the cells that were treated with free drugs, which can be due to incomplete

release of drugs after 24 hours. Therefore, another study was performed to see the effect of higher drug release from micelles at more elevated temperatures on HepG2 cells. Figure 2.25 demonstrates the effect of temperature on the cytotoxicity of micelles on HepG2 cells. To consider the effect of temperature in cell death, the viability of the cells only (control) was considered in the determination of the cell viability of the treated cells. The result indicates that the micelles at 42 ˚C showed about 20% more cytotoxicity than the micelles at 37 ˚C with the highest administered dose. The considerable decrease in cytotoxicity was attributed to the accelerated release of Dox from micelles above their LCST. This unique temperature-responsive properties of micelles and its effect on cell viability of HepG2 cells have been observed by Shi's group previously.[107]
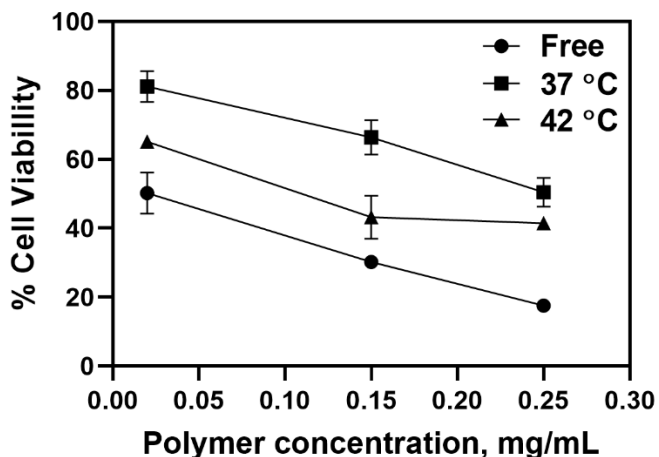
Figure 2.25. Viability of HepG2 cells after treatment at different temperatures. HepG2 cells were treated with free Dox+Que at 37 ˚C, and Dox+Que loaded PME3CL-b¬-PBnCL micelles at 37 ˚C and 42 ˚C. After 24 hours, the viability of cells was evaluated using CellTiter-Blue. The results indicate that the viability of cells after treatment with micelles is temperature-dependent, which is related to the LCST of the polymer.

2.4.7 Cellular Uptake Studies

The cellular uptake of drug-loaded PME$_3$CL-b-PBnCL micelles was performed on HepG2 cells at 37 ˚C (below LCST) and 42 ˚C (above LCST). Cells were incubated with micelles for 2

hours after fixating the cells and staining their nuclei with DAPI, and the images were obtained

using Cytation 3 fluorescent microscope. The images presented in Figure 2.26 demonstrate the

uptake of the drug into the cells. The results indicate that Dox preferentially accumulates in the

nucleus to interact with the DNA's double helix.[108,109] The images also show that the hyperthermia

could facilitate drug release and uptake, as more Dox and Que is visualized within the cells at a

higher temperature. This observation may be due to the enhanced interaction of micelles with the

cell membrane at higher temperatures or higher drug release in the extracellular microenvironment

of cells at elevated temperature and its uptake by the cells.[107,110] A more precise detection of drug

release location can be performed in future studies by attaching a fluorescent tag to the backbone

of the polymer, such as fluorescent dansyl.[111]
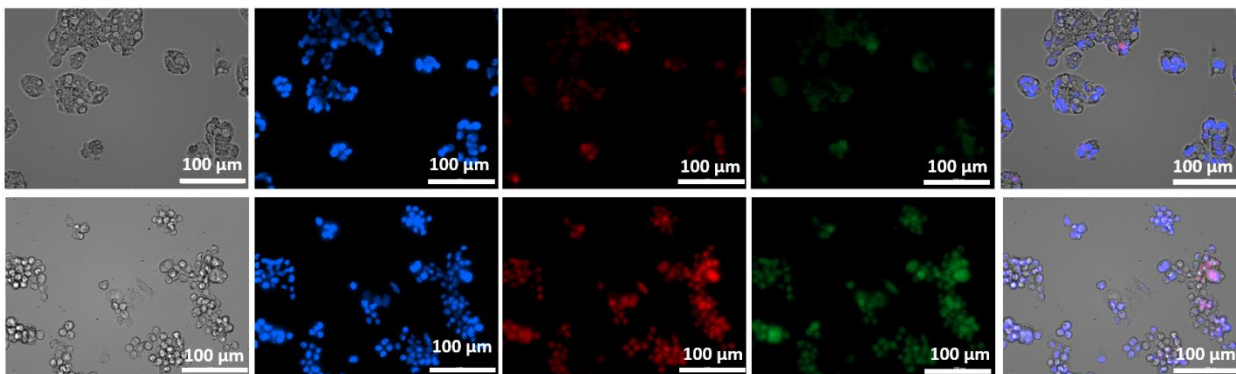
Figure 2.26. Cellular uptake of co-loaded PME3CL-b¬-PBnCL micelles into HepG2 at different temperatures. Fluorescent micrographs of HepG2 cells treated with below LCST (top row) and above LCST (bottom row) were recorded after 2 hours of incubation with co-loaded micelles. Images from left to right show bright field, cells with nuclei staining using DAPI, Dox visualized with RFP filter, Que visualized with GFP filter, and overlays of all images.

2.5 Conclusion

In this study, thermoresponsive poly(ε-caprolactone)-based amphiphilic block copolymers

were synthesized through the *living* ring-opening polymerization of functionalized ε-caprolactone

monomers, ME$_x$CL (x = 2,3,4) and BnCL. The polymers showed thermodynamic stability having CMC values in the order of 10^{-5} mg/mL. The polymers also exhibited thermoresponsive behaviors wherein varying OEG chains allowed tuning of the LCST values. These polymers were used as a micellar drug delivery system for Dox and Que. Combination loading was demonstrated as a successful approach to improve the drug loading efficiency of both drugs in all the polymers. Release studies in physiological conditions showed a temperature-dependent release of drug from the micelles. PME$_3$CL-b-PBnCL had an LCST value (41 ˚C) higher but close to physiological temperature; hence it was used for further biological studies. Twenty percent more cytotoxic effect on HepG2 cells was observed from the micelles at a higher temperature, which is attributed to a higher release of anticancer drugs. Future optimization of thermoresponsive drug delivery systems will be focused on performing synergistic studies on combination therapies to achieve the best therapeutic efficiency in cancer cells while protecting the healthy cells.

2.6 Author Contributions

E.L. Calubaquib and P. Soltantabar contributed equally to work. E.L Calubaquib synthesized the monomers and polymers and performed LCST and TEM measurements. P. Soltantabar performed the synthesis of micelles, characterization, and biological studies. E. Mostafavi contributed to analyzing the data and suggested additional experiments.

Notes

The authors declare no conflict of interest.

2.7 Acknowledgment

CHAPTER 3

HEART/LIVER-ON-A-CHIP AS A MODEL FOR THE EVALUATION OF

CARDIOTOXICITY INDUCED BY CHEMOTHERAPIES[1]

Authors- Pooneh Soltantabar, Erika L. Calubaquib, Ebrahim Mostafavi, Atefeh Ghazavi, and
Mihaela C. Stefan

The Department of Bioengineering, BSB 11

The University of Texas at Dallas

800 West Campbell Road

Richardson, Texas 75080-3021

Author contribution:

MCS conceived the idea, acquired funding, and supervised all the authors on this project. PS designed the microfluidic device and fabricated the device with inputs from AG. PS investigated the fluid dynamic of the system and assessed the functionality of cells in the device. Device assembly and cell culture were performed by PS. Cell viability assays and flow cytometry was conducted and analyzed by PS with inputs from EM. PS wrote the manuscript, and it was revised and edited by MSC, ELC, AG, and EM.

3.1 Abstract

Drug discovery is facing challenges due to the lack of proper preclinical tests, including conventional cell cultures and animal studies. Organ-on-a-chip devices can mimic the whole-body response to therapeutics by fluidically connecting microscale cell cultures and generating a realistic model of human organs of interest. Here, we describe a pumpless heart/liver-on-a-chip (HLC) using the HepG2 hepatocellular carcinoma cells and H9c2 rat cardiomyocytes to reproduce the cardiotoxicity induced by Doxorubicin (DOX) *in vitro*. Cell studies confirmed the high viability of both cells up to 5 days of culture in HLC. The developed device demonstrated more significant damage to heart cells within the HLC compared to conventional static 3D culture in case of DOX treatment, which is because of exposure of cells to both the parent drug and its cardiotoxic metabolite, Doxorubicinol (DOXOL). Our designed HLC device represents a unique approach to assess the off-target toxicity of drugs and their metabolites, which will eventually improve current preclinical studies.

3.2 Introduction

The pharmaceutical industry is in urgent need of enhanced drug discovery and development tools. It has been reported that it takes about 13.5 years and costs about $2.5 billion for a drug to get into the market. Besides the exorbitant cost and time-consuming process of drug development, 92% of the drugs fail in human clinical trials .[112] There are ethical and scientific arguments arising from the usage of animals as the currently most common preclinical testing method. Animal studies impose not only suffering to the animals but also stress for the researchers who are performing the experiments.[113] Moreover, discoveries from animal studies do not effectively translate into the clinic due to differences between the animal and human biology .[114]

To address some of the limitations of preclinical tests, a new class of microfluidic devices was developed to replicate *in vivo* functions of organs on a microchip. This new technology, called "organ-on-a-chip" (4, 5), has been extended to "body-on-a-chip" [116–118] to simulate multi-organ interactions. The organ-on-a-chip field is now progressing as a better tool for the replication of human physiology by the creation of *in vivo*-like 3D tissue architectures *in vitro*. Within these devices, tissue explants, iPSC-derived cells, and cell lines as human organ representatives are connected fluidically in a closed system to answer various scientific questions .[112] Using these devices, scientists can mimic a physiologically relevant 3D microenvironment while providing the dynamic supplement of nutrients and multi-organ interaction .[118]

When the number of organs increases, the complexity of the system increases, and consequently, several challenges in the design and interpretation of the results might appear; moreover, design complexity is related to determining appropriate organ sizes and media flow rate, which results in a physiologically realistic system that does not distort the nature of the interactions

between organs. The interpretation complexity arises when researchers need to translate the experimental outcomes from these devices to *in vivo* responses in humans. Therefore, to understand the multi-organ interaction dynamics, robust mathematical tools can be implemented. These mathematical approaches are developed from mathematical methods that have been used in biological and pharmacological sciences for a long time .[119]

Shuler et al. [120–122] designed a series of pioneering devices guided by the concept of a mathematical model known as a physiologically based pharmacokinetic-pharmacodynamic (PBPK–PD) model aimed at reproducing the multi-organ interactions within the body for drug toxicity testing. The term pharmacokinetics (PK) is used for the time-dependent concentration of a substance in a living system.[123] A PBPK model is built on physiological considerations where the human body is segregated into compartments with various cell lines representing different organs that are fluidically connected. Pharmacodynamics (PD) seeks to characterize the time course of drug effects through the application of mathematical modeling .[124] Integration of the PK of a drug with the subsequent *in vivo* pharmacological response (PK/PD modeling) has been extended to all phases of drug development .[125]

The Shuler group first examined the possibility of coupling the PK/PD modeling with a microfluidic device.[122] They applied residence-time scaling where the residence times of medium in each organ compartment were matched to blood residence times in the *in vivo* counterparts, letting the organs within the device be exposed to drugs for the same length of time as the human organs are exposed *in vivo*. Most of their early designs required external pumps, however pumpless devices which work based on gravity-induced flows are economical, operate with physiologically

realistic shear stress (less than two dynes cm^{-2}) on cells, and can prevent bubble formation or entrapment, which is a significant problem in microfluidic devices .[126]

One of their studies compared the PK profile of the doxorubicin (DOX) anticancer drug predicted from a multi-organ-on-a-chip to the data expected in the human body. This study illustrated an early integration of microfluidic devices and PK modeling.[127] They showed that a specific combination of drugs could inhibit the proliferation of a multidrug-resistant variant of uterine cancer. They were able to scale-up the result to calculate doses *in vivo*. In another study, the same group managed to link a three-organ micro-engineered cell culture device with computational PK/PD models. As a proof-of-concept study, they showed that a PBPK-PD could be used as a mathematical platform to model the toxicity of 5-fluorouracil (5FU) anticancer drug on hepatocyte, colon carcinoma, and myeloblast cell lines. In this analysis, an experimental cell death study was applied for numerically fitting the parameters of the computational model to generate the best estimates of cell death *in vivo*.

One of the main challenges in drug discovery for cancer therapy is the cardiotoxicity associated with anticancer drugs.[128] Moreover, in our previous study [129], we demonstrated that the cardiotoxicity induced by anticancer drug DOX could be alleviated by co-administration of DOX with natural antioxidants. DOX is an anthracycline anticancer drug that interferes with the synthesis of DNA and RNA by inhibiting the separation of DNA double helix, an essential step for cell proliferation [130]. Although DOX can effectively combat the rapid division of the cells and is known as one of the most potent chemotherapeutic drugs approved by the Food and Drug Administration (FDA) [131], it causes toxicity to the major organs, especially life-threatening cardiotoxicity .[130] While the mechanism of this cardiotoxicity induced by DOX is not fully

understood yet, some studies are showing that one of the means of this cardiotoxicity can be attributed to doxorubicinol (DOXOL), the primary metabolite of DOX. [79,132] Previous studies showed that DOXOL is significantly more potent than DOX at compromising both systolic and diastolic cardiac function.

Here we introduced a pumpless device named Heart/Liver-on-a-chip (HLC) that enables the culture of two different cell lines in a closed loop of gravity-induced flow. The cell lines used in this study were HepG2 hepatocellular carcinoma cells and H9c2 rat cardiomyocytes. As the representative of cardiomyocytes, we used this permanent cardiac cell line, which are characterized by several cardiomyocytelike properties .[133] H9c2 cells which are most often used as a cardiac cell model for routine cytotoxicity screening [134–136], has been extensively used in organ-on-a-chip devices as well.[137–139] Therefore, we decided to use them in our research for the sake of simplicity and proof of concept. As the HLC performs without any pumps, the width of the channels across the chambers was calculated to achieve the desired flow rates. The fluid dynamics of the system were characterized to confirm that the residence time of the media in each chamber matches the residence time of the blood in the associated organ within the body. We then thoroughly investigated the viability of the cells cultured in HLC compared to conventional cell culture platforms, including static 2D and 3D cultures. Drug testing was finally performed within the HLC to investigate whether this device can produce the metabolite of the interest and to indicate whether HLC can serve as a proof of concept tool for recreating the cardiotoxicity induced by anticancer and its metabolite *in vitro*. The integration of metabolizing components to *in vitro* models, which cannot be studied through conventional preclinical platforms, would improve the prediction of drug toxicity studies. These models have the potential to more realistically capture

both the efficacy and the side effects of newly developed drugs, leading to tremendous time and cost savings.

3.3 Materials and Methods

3.3.1   Overall device description and design

Our design was inspired by two pumpless layered designs reported by Shuler.[122,140] The HLC contains two polydimethylsiloxane (PDMS) layers, which separate the fluidic channel layer and cell culture chamber layer, that is inserted between two polycarbonate frames (Figure 3.1(A)). The whole device was secured and held together using two stainless steel screws. The culture chambers accommodate both liver cancer cells and heart cells in separate chambers, which are fluidically linked through the channel layer that is placed on top of them, so the circulating media is shared between two cell types.

Because there is no external pump in the system, the width of the channels was the controlling factor for the fluid dynamic of the system, which was designed in a way to mimic the residence time of the blood in each associated organ in the body. All HLC parts were selected from an autoclavable and transparent material to facilitate the operation and usage. A photograph of actual assembled HLC injected with dye for better visualization is shown in Figure 3.1(B).
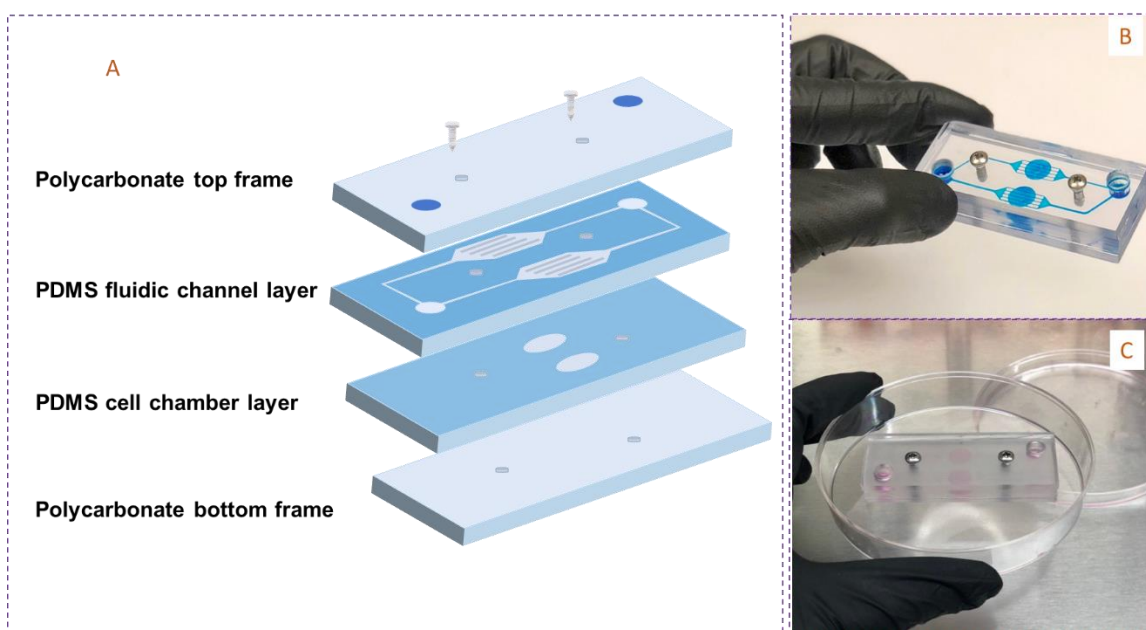
Figure 3.1. Design and actual photograph of the two-layered pumpless microfluidic device. **(A)** Schematic illustration of the two-chamber cell culture layer and the device microfluidic channel layer (with the channels facing down), both made from PDMS. The cell chamber layer and the channel layer are sandwiched between two polycarbonate frames, and the system is secured with two stainless steel screws. **(B)** Photograph of the HLC with the CellTiter Blue dye flowing through the channels and chambers for better illustration of the microchannels and the reservoir. **(C)** Picture of the actual HLC assembled with a hydrogel containing the cells. The reservoirs are filled with the media, and the HLC is placed on a programmable rocker platform to create gravity-induced flow.

3.3.2 Channel layer design

Designing an organ-on-a-chip that is physiologically realistic is essential as the flow between the chambers can influence the PK of the device.[140] To achieve this goal, we designed our HLC by scaling based on residence time.[140,141] In this method, the cells will be exposed to drugs with the same duration that the cells in native organs in the body are exposed.[140,141] First, the residence time of the blood in each organ in the body was calculated by dividing the organ size by the flow rate of the blood in each organ.[142] Based on the residence time scaling, the residence time of the blood in each organ of the body should be the same as the residence time of the media in an

associated organ within HLC; thus, the flow rate of the media to each chamber can be calculated. By substituting the flow rate of each chamber in Hagen–Poiseuille's equation (**equation 1**) for gravity-induced flow (and substituting Δh by L×Sine(α); α = tilting angle), the hydraulic radius, cross-section area of each channel and finally the width of each channel can be calculated. [143,144]

$$Q = \frac{\rho g \pi \, \Delta h \, R_H{}^4}{8 \, \mu L} \qquad\qquad (1)$$

where Q is the flow rate generated by the pressure difference, ρ is the density of the media (1009 g/m^3), g is the gravity constant (9.8 m/s^2), Δh is the height difference (m), R_H is the hydraulic radius of the channel (m), μ is the fluid viscosity (0.001011 Pa.s), and L is the channel length (m). By using this approach, the channel dimension for each chamber was calculated to achieve the desired flow rate. The residence time and expected volumetric flow rate for each organ were calculated and presented in Table 3.1.

Table 3.1. Physiological information and the performed calculation to estimate the flowrate of channels within the HLC

Organ	Volume in the body (mL) [142]	Flow rate in the body (mL/min) [142]	Residence time (s)	Volume in the device (µL)	Flow rate main channels in the device (µL/s)
Heart	360	730	29.6	25.13	0.85
Liver	1350	1566	51.72	25.13	0.48

3.3.3   Microfabrication of HLC

To develop the channel layer, PDMS prepolymer (Sylgard 184, Dow Corning) was mixed with a hardener with a ratio of 10:1 and was dispensed on a 4-inch silicon wafer master followed by curing at 70 °C for 30 min. The master for the channel layer was made by soft lithography. SU-8 2100 photo epoxy (Kayaku Advanced Materials, Inc., MA, USA) was selected as it is suitable for creating relatively thick features (250 µm in this case) on the silicon wafer. The photoresist was spin-coated on the silicon wafer with different spin speeds to obtain the desired thickness. The 250 µm thickness was obtained by spinning at 500 rpm spin speed with an acceleration of 100 rpm/s for 20 s followed by a 1380 rpm spin speed with 300 rpm/s acceleration for 30 s. Spin coating was followed by soft baking performed at 65 °C for 7 min and 95 °C for 60 min based on SU8 2100 datasheet. The spin-coated SU8 layer was patterned by UV-exposure at an exposure dose of 360 mJ/cm2 using the designed photomask. The photomask pattern was created using Autosketch software, and the mask was fabricated at The University of Texas at Dallas cleanroom facility. The post-exposure bake was performed at 65 °C for 5 minutes and 95 °C for 40 min. To develop the SU8 structure, the master was then immersed in the SU8 developer (Kayaku Advanced Materials, Inc., MA, USA) for 30 min. The frame of the device was milled out of a 5 mm thick polycarbonate sheet at a machine shop located at the University of Texas at Dallas. The cell culture chamber layer was made from a commercially available PDMS sheet with a thickness of 0.5 mm. The two cell chambers were created using a biopsy punch with a diameter of 8 mm, which were later filled with hydrogel-encapsulated cells.

3.3.4 Device degassing and assembly

The surface of the PDMS is hydrophobic, which limits its usage in applications involving aqueous solutions. Bubbles tend to stick to the surface of the PDMS, which results in their entrapment during the device assembly, causing problems for the cells by flow blockage. With some modifications to a previously developed method by Wang,[145], we were able to prevent bubble formation in the HLC through the combination of surface treatment and a vacuum filling method.

The PDMS layers were oxygen plasma-treated at 50 W for 120 s to make the parts hydrophilic. All HLC parts were immersed in 70% EtOH. The container, including device parts soaked in EtOH, was then transferred to a desiccator connected to a vacuum for 30 min. The device parts were rinsed with PBS solution and were transferred to another container filled with PBS + 5% fetal bovine serum (FBS), then the device parts were vacuumed for another 60 min. After vacuuming, the device parts were autoclaved for 30 min at 125 °C while still immersed in PBS and FBS solution. The device assembly was done from bottom to top. The cell chamber layer was placed on top of the bottom polycarbonate frame. The chambers were filled with PGmatrix encapsulated cells, followed by PGwork addition and incubation for 1 hour inside an incubator for effective crosslinking. The cell chamber layer was removed from the incubator and flooded with media to minimize air contact during assembly. Finally, the channel layer was placed on the top (with the channels facing down). The system was fixed and secured using the screws, and the reservoirs were filled with media. The device was placed in a sterile 100 mm petri dish and was placed on a tilting rocker inside an incubator.

3.3.5 Cell culture

HepG2 hepatocellular carcinoma cells and H9c2 rat cardiomyocytes were purchased from American Type Culture Collection. The cells were maintained in Dulbecco's modified Eagle medium supplemented with 10% (v/v) FBS and 1% (v/v) penicillin/streptomycin in an incubator at 37 °C and 5% CO_2. Cell culture media was changed every three days.

For further characterization of the HLC, the rocker was set on three different angles (5, 10, and 20 degrees), and the flow rate at each angle was measured in channels. Based on the Hagen–Poiseuille's **equation 1,** which was the basis of our design, the flow rate is supposed to be linearly proportional to Δh, which is the height difference, and consequently linearly proportional to Sine (α) as Δh is equal to L×Sine (α) (where α = tilting angle). The experimental data from this study is presented in Figure 3.2(A). The high R^2 value of the plot indicates that the claim is valid, and the observed flow rates are close to the theoretically calculated flow rate from Hagen–Poiseuille's **equation 1**.

To make 3D construct of cells, a suspension of cells in PGmatrix with a concentration of 10^7 cells/mL was prepared based on the manufacturer's guide. The cells were detached from the confluent flasks of cells using trypsin/ethylenediaminetetraacetic acid (EDTA). After adding media for neutralization of trypsin/EDTA, the cell pellet was obtained by centrifugation at 125 xg for 5 min. Cells were resuspended in media, followed by adding PGwork. After homogenizing the cell suspension, PGmatrix was added. Based on the manufacturer's protocol, the added PGwork was 4% of pure PGmatrix solution. 20 µL of each cell suspension were added to 96 well plate and device cell chambers for cell culture in static 3D and device, respectively. After 1 hour of incubation at 37 °C and 5% CO2, 100 µL of DMEM was added to each well for

static study. In the case of the device, the cell chamber layer was flooded with media, the channel layer was placed on top, and the system was closed using the screws.

3.3.6 Characterization of fluid dynamics in the system (flowrate and distribution)

To investigate the fluid dynamics, the device was assembled as described above. However, the cells were not encapsulated into the hydrogel for this study, and the reservoirs were filled with media. The flow rate of the media in each channel was measured by a video capturing method developed by Shuler et al. [144]. The assembled device was placed on the rocker at different angles (5,10, and 20 degrees). A dye was injected into the reservoir at a higher position, and the video was recorded while the dye was flowing into the channels. By measuring the time that dye traveled at a specific length in the channel, the linear flow rate was calculated and multiplied by the cross-section area of each channel to calculate the volumetric flow rate. The experiment was performed in triplicate, and the average linear flow rate was calculated. A video of dye injection into the HLC is included in the Supplementary Information.

The flow distribution study was performed to investigate whether the reservoirs will reach an equilibrium concentration after injecting an agent to the system with the selected rocker tilting pattern. For this study, the device was placed on the rocker with one reservoir at a higher position on the rocker with a tilting angle of 5 degrees, which was the base of our calculations. At t=0, 10 µL of media was removed and replaced with the same volume of the CellTiter Blue dye, and then the device started to tilt on the rocker. Two different tilting programs were tested on the device: (1) 30 splits, where one side is up for 30 s, then the other side is up for 30 s, and (2) 60 splits, where one side is up for 60 s, then the other side is up for 60 s. At specific time intervals, 5 µL of media sample was removed from each reservoir and was collected in a microcentrifuge tube. This

study was performed by setting multiple devices on the rocker. The samples were then subjected to UV-Vis spectroscopy to record the absorbance of samples at the wavelength of 600 nm to quantify the amount of dye in each sample. Due to the small sample size, regular UV-Vis spectroscopy was not possible, so a Nanodrop instrument was used to collect the absorbance data.

3.3.7 Cell viability in the device (2D vs. 3D & 3D vs. device)

Viabilities of both heart and liver cancer cells were studied and compared in 3 different platforms: conventional 2D culture, static 3D culture, and the device. For 2D culture, the cells were trypsinized and cultured in 96 well plates with a density of 10^4 cells per well. For static 3D and device, cells were incorporated into the hydrogel with the cell density of 4×10^6 cells/mL in the PGmatrix (crosslinking process described above). 20 µL of samples were added to 96 well plates for static 3D and to cell chambers within the device. The volume of cell chambers in the device was 25 µL. About 20% of this total volume of the chamber was left empty to provide some space for media flow over the cells.

On days 1, 3, and 5 after culture, the viability of the cells was assessed using a commercial live/dead assay kit (Molecular Probes). For this assay, the ethidium homodimer-1 red dye (2 µL/mL in PBS) for dead cells and calcein-AM green dye (0.2 µL/mL in PBS) for live cells were mixed. For 2D and static 3D, 96 well plates were used for imaging, however in the case of culture in the device, the device was disassembled, and the hydrogels were transferred to a 35 mm petri dish for subsequent staining and imaging. After incubating the cells with dyes for 15 mins, the cells were washed a few times with PBS, and the images were obtained using the Cytation 3 fluorescent microscope.

3.3.8 Cell functional evaluation through urea synthesis

To quantify the level of urea production by cell lines, in both static monocultures and device, a DIUR assay kit (BioAssay Systems, Hayward, CA) was used. For static monocultures, HepG2 and H9c2 cells were cultured separately in 96 well plates with a cell density of 4×10^6 cells/mL, and 150 µL of media was added to each well. For culture in the device, three different conditions were studied: HepG2 only, H9c2 only, and HepG2+H9c2 co-culture in the device (as described above). In the case of monocultures in the device, the other chamber was filled with hydrogel only (with no cells incorporated). At days 1, 3, and 5, with day 1 corresponding to 24 h after the culture in 96 well plates and device assembly, 50 µL culture media was collected in 96 well plates and were stored at -80 °C for later measurements. 100 µL of the chromogenic reagent was added to each well resulting in a stable colored complex with urea, which was incubated at room temperature for 20 min. Finally, the optical density was measured at 430 nm using a BioTek Cytation 3 fluorescent microscope. The concentrations were calculated and reported in mg/dl by comparing to a standard curve.

3.3.9 Investigation of *in Vitro* DOX metabolism by HepG2 cells

To investigate the ability of HepG2 cells to metabolize the DOX within *in vitro* 3D culture, the cells were cultured in 3D hydrogels in 96 well plates as it was described above. 24 h after the culture, media was replaced by DMEM containing 1µM (543.2 ng/mL) DOX. At specific time points (up to 72 h) the media was collected and was stored at -20 °C for further quantification of DOX and its cardiotoxic metabolite DOXOL.

3.3.10 Analytical liquid chromatography-mass spectrometry (LC-MS) condition

Compound levels for cellular stability were monitored by LC-MS/MS using an AB Sciex (Framingham, MA) 4000 QTRAP® mass spectrometer coupled to a Shimadzu (Columbia, MD) Prominence LC. Analytes were detected with the mass spectrometer in positive MRM (multiple reaction monitoring) modes by following the precursor to fragment ion transitions indicated here: **DOX**: 544.171 to 397.000; **DOXOL**: 546.198 to 399.100. An Agilent C18 XDB column (5 micron, 50 X 4.6 mm) was used for chromatography with the following conditions: Buffer A: dH20 + 0.1% formic acid, Buffer B: acetonitrile + 0.1% formic acid, 0 – 2 min 5% B, 2 – 3.5 min gradient to 60% B, 3.5 - 5 min 60% B, 5 – 5.1 min gradient to 5% B, 5.1 - 7.5 5% B. Daunorubicin (transition 528.147 to 321.000) was used as an internal standard (IS). All measurements were performed in triplicate, and average responses with associated error bars are presented in Figure 3.2(B).

3.3.11 Sample preparation for LC-MS/MS analysis

At varying times (0h, 3h, 6h, 12h, 24h, 48h, and 72h) post addition of 1uM doxorubicin to the HepG2 cultures, media was removed, and the lysate precleared of protein by the addition of a two-fold volume of acetonitrile containing 100 ng/mL of internal standard (daunorubicin) followed by vortexing and incubation at room temperature or 10 min. After two steps of centrifugation at 16,000 x g for 5 min. The supernatant was analyzed by LC-MS/MS for levels of doxorubicin and doxorubicinol. Compound levels were quantitated in reference to standard curves prepared by adding varying concentrations of doxorubicin and doxorubicinol to untreated blank cell media and processing, as described above. The concentrations of drug in each time-point sample were

quantified using Analyst software (Sciex). A value of 3-fold above the signal obtained from blank plasma or tissue homogenate was designated the limit of detection (LOD). The limit of quantitation (LOQ) was defined as the lowest concentration at which back-calculation yielded a concentration within 20% of theoretical.

3.3.12 Cell treatment in the device

For cell treatment, the device and static controls were set as described above. DOX was dissolved in DMSO to give a 10 µg/µL stock solution. The stock solution was then added to DMEM media to make the desired concentrations. The final DMSO concentration in media was set to be less than 0.1% (v/v) to avoid any toxic effect of the solvent. For controls, the cells were treated with a comparable amount of DMSO (without drug). 24 h after cell culture in the device and in 96 well plates (for static controls), media was changed with media containing the drug. During the cell treatment, the device was placed in a petri dish to minimize the media evaporation. All assembled devices and static controls were placed in a humidified incubator at 37 °C under 5% CO_2.

3.3.13 Flow cytometry analysis

After 24 h drug treatment, the hydrogels were harvested from the device chambers (after the disassembly) or static 3D cultures and were collected in a microtube. For flow cytometry analysis, the cells were needed to be recovered from the gel. For the cell recovery, the gel was mechanically disrupted thoroughly by pipetting. 100 µL PBS was added to the tube, and the mixture was pipetted thoroughly, followed by centrifugation at 400 xg for 5 min. The supernatant was then removed, and the cell pellet was used for the staining to discriminate the early stage of

apoptosis from necrosis. Alexa Fluor 488 annexin V/Dead Cell Apoptosis Kit (catalog no. V13241) were purchased from Invitrogen Life Technologies (Carlsbad, CA) and was used according to the manufacturer's instructions. This kit provides a rapid and convenient assay for apoptosis. Briefly, the cells were re-suspended in 100 µL of the kit's specific binding buffer. 5 µL Alexa Fluor 488 annexin V and 1 µL of 100 µL/mL PI working solution (in binding buffer) was added to the cell suspension. After 15 min of incubation at room temperature, the final volumes were adjusted to 500 µL, and the samples were transferred on ice for flow cytometry analysis measuring the fluorescence emission at 530 nm and 575 nm and the excitation of 488 nm (using the FITC and PE filters).

3.3.14 Statistical analysis

All data analyses were performed using GraphPad Prism Software version 8. A significant difference between 2 groups was evaluated using the F-test to compare variances followed by the student t-test. In contrast, for meaningful difference evaluation between 3 or more groups, one-way and two-way ANOVA was performed. A P-value of <0.05 was considered to be significantly different.

3.4 Results and discussion

3.4.1   The fluid dynamic of the device

The linear flow rate of media in each channel was measured by video recording after dye injection to one reservoir. Figure 3.2(B) shows the calculated volumetric flow rate versus the observed flow rate. The calculated flow rate for the heart and liver chambers were 0.85 and 0.48

µL/s, respectively. The experiment was performed in triplicate, and the average observed flow rate for heart and liver chambers was 1.04 ± 0.14 and 0.59 ± 0.05 µL/s, respectively. In general, the predicted and observed flow rate were comparable. The results indicated that the observed flow rate was slightly higher than the calculated flow rate for both chambers. Similar discrepancies were observed by Shuler et al.,[144] which was attributed to the high sensitivity of flow rate to small changes and imperfections in the device. As was demonstrated in **equation 1**, the hydraulic radius is correlated to the flow rate by the power of four; therefore, small changes in the radius results in significant deviations from the predicted flow rate.
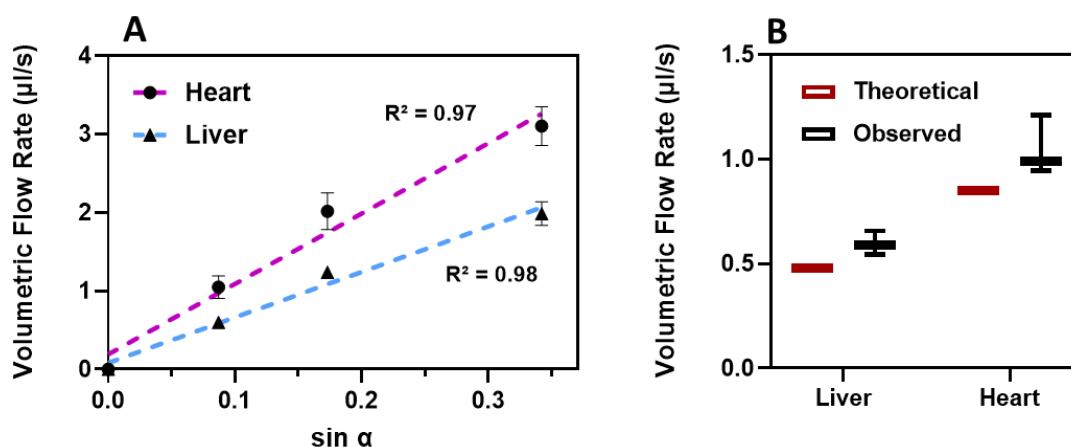
Figure 3.2. The fluid dynamic of the device. **(A)** The device was set on the 3 different angles (5, 10, and 20 degrees). The flowrate associated with each chamber was measured and plotted versus the tilting angle. A linear relationship between the volumetric flow rate and the height (tilting angle) was observed, which is in agreement with the Hagen–Poiseuille's equation 1. **(B)** Volumetric flow rate of the media for each chamber shows that the calculated flow rate is comparable with the observed flow rate in device. A slightly higher flow rate within the device compared to the theoretical one is due to the high sensitivity of the flow rate to imperfections of microfabricated channels.

The flow distribution studies were performed by injecting CellTiter Blue dye into one of the reservoirs, starting the rocker to tilt at two different programs, and taking samples from both reservoirs at specific time points. The samples were collected in microtubes, and the absorbance

was measured at 600 nm using a nanodrop device as the volume of the collected sample was very low. The results revealed that by setting the rocker at 30 s splits program (one side up for 30 s, then the other side up for 30 s), the reservoirs did not reach an expected equilibrium concentration after 1 h of rocking on the device. However, after injecting the dye to one of the reservoirs and applying the 60 s splits program (one side up for 60 s, then the other side up for 60 s), both reservoirs could reach an equilibrium concentration only after about 40 min of tilting on the rocker, which is an indicator of better dye distribution at this rocking program. Figure 3.3 shows the absorbance data versus time for both 30 s splits and 60 s splits programs.
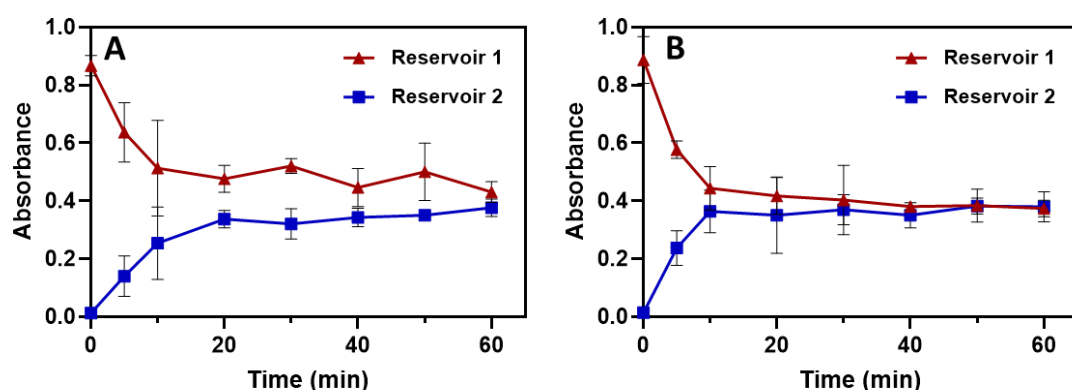
Figure 3.3. Dye distribution in the microfluidic device. The dye distribution within the device was investigated by injecting Cell TiterBlue dye into one of the reservoirs and setting the device in motion on a rocker, then taking samples of each reservoir at specific time points. The samples were then subjected to spectroscopy at a wavelength of 600 nm to quantify the amount of dye in each sample. **(A)** Overall dye distribution in device with 30 seconds splits. **(B)** Overall dye distribution in device with 60 seconds splits.

3.4.2   Cell viability

Figure 3.4 and Figure 3.5 represent the live/dead staining of H9c2 and HepG2 cells that were cultured in 2D, 3D, and device to investigate whether the device can keep the cells healthy and viable for five days post culture. The quantitative cell viability values are presented in Figure

3.6**.** As shown, there was no significant difference in the viability of H9c2 cells in 2D, 3D, and device cultures over a 5-day culture, where all three platforms showed the viability of more than 90%. A similar trend was observed for HepG2 cells on days 1 and 3; however, on day five, the viability in 2D culture was about 17% and 21% lower than 3D and device, respectively. This can be due to the clumping of HepG2 cells, which prevents the cells from receiving enough nutrients in 2D culture after five days. Additionally, the viability of HepG2 cells significantly increased in device compared to 2D and static 3D, which can be attributed to media circulation and better penetration of nutrients into the hydrogel. In general, this experiment demonstrated that the device could support high cell viability for both H9c2 and HepG2 cells over a 5-day culture.
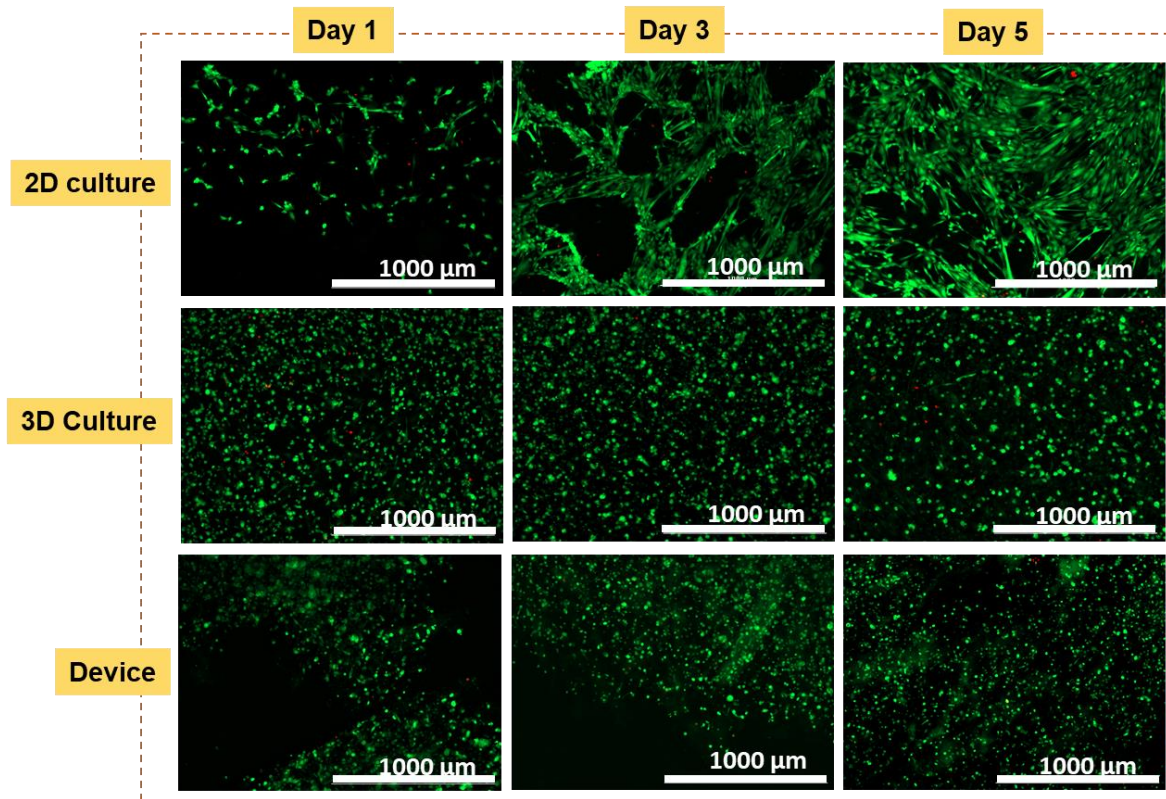
Figure 3.4. Fluorescent micrographs of H9c2 cells cultured in conventional 2D,3D, and device. Live/dead assay was performed to assess the cell viability of H9c2 cells in 3 different platforms: static 2D culture(top), static 3D culture by embedding the cells in hydrogel (middle), and 3D

culture within the device (bottom). For 3D culture, the cells were incorporated into the hydrogel and were pipetted into the 96 well plates. For device culture, the same hydrogel as static 3D was used. The cells were embedded in the hydrogel and were introduced to the device chambers. After 1 h, when the gelation was complete, the device was assembled, and the reservoirs were filled with media. On days 1, 3, and 5 post- culture, the cells were stained with live/dead assay kit to visualize the live cells (green) and dead cells (red) for further imaging.
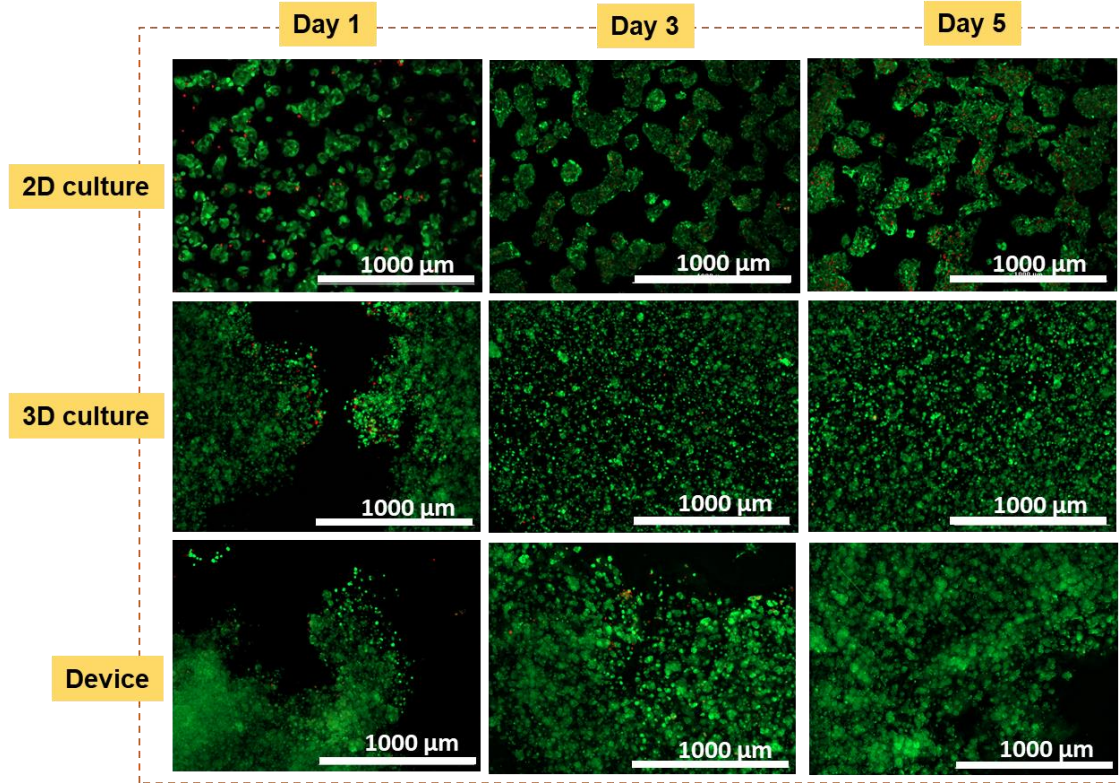
Figure 3.5. Fluorescent micrographs of HepG2 cells cultured in conventional 2D, 3D, and device. Live/dead assay was performed to assess the cell viability of HepG2 cells in static 2D culture (top), static 3D culture (middle), and 3D culture within the device (bottom). For 3D culture, the cells were incorporated into the hydrogel and were pipetted into the 96 well plates. For device culture, the gels containing the cells were introduced to the device chambers. After 1 h, when the gelation was complete, the device was assembled, and the reservoirs were filled with media. On days 1, 3, and 5 post culture, the cells were stained with live/dead assay kit to visualize the live cells (green) and dead cells (red) for further imaging.
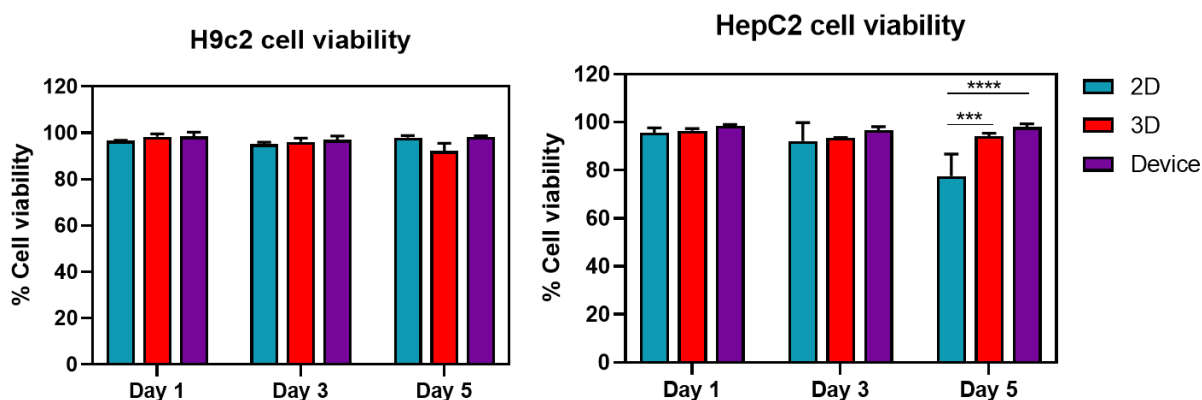
Figure 3.6. Viability of the H9c2 and HepG2 cells in device versus static 2D and 3D controls. Values are shown as the average percentage viable (n=3). H9c2 cells (left) demonstrated similar and very high (above 90%) cell viability in all three platforms throughout a 5-day culture. However, the HepG2 cells (right) demonstrated similar and very high (above 90%) cell viability in all three platforms only up to day 3 of the culture. On day 5 post culture, the viability of 2D culture dropped below 80%, which might be due to the tendency of these cells to grow in clumps, and some cells in lower layers were not exposed to enough nutrients from the culture media. Error bars indicate the standard error of the means, asterisks mark significance levels of $p < 0.001$ (***), $p < 0.0001$ (****), and n=3.

3.4.3 Urea quantification

The inability to produce urea in hepatocytes can be an indicator of hepatic damage. [146] Urea production by heart and liver cells were assessed throughout the culture period by analyzing the media removed from the device and the static culture on days 1, 3, and 5 post-culture. The devices (n=3) were assembled as described above, and the urea production was compared to static 3D culture for the monocultured and co-cultured cell lines. The results indicated that in the case of HepG2 cells, the hepatic function was improved in a 3D dynamic environment within the device. For instance, on day five post-culture, the urea production was $3 \pm 0.18\,\mu g$ in static culture while the urea was quantified as $4.3 \pm 0.44\,\mu g$ for the device on the same day. This observation could be due to significant induction of CYP1A1 and CYP3A4 enzymes, which have pivotal roles for drug metabolism, in dynamic culture within the device compared to static culture as reported by the

Shuler group. [144] However, a similar trend was not observed for heart cells, and there was not any significant difference between the urea production of heart cells in the device and static 3D culture. Moreover, the results of this experiment show that the co-culture of cells in the device does not seem to have any significant impact on the total urea production compared to monocultures, which was similarly observed by Oleaga et al. [80] Altogether, these results demonstrate the improvement in overall liver function within the device and its advantages over the conventional systems.
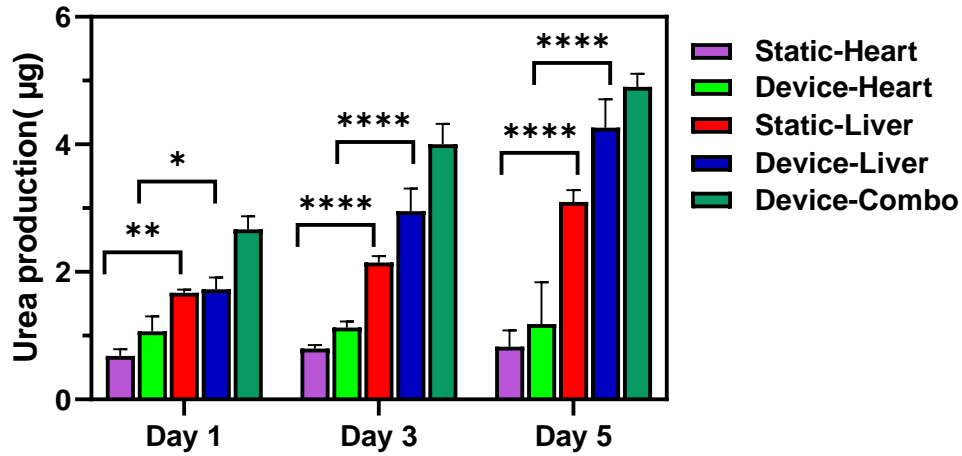
Figure 3.7. Characterization of the functionality of the cells through urea synthesis. Urea production of the rocked device versus the static 3D culture was quantified using a DIUR assay kit by taking samples of the culture media on days 1, 3, and 5 post culture. For the conventional static cultures, cells were embedded into the hydrogel and were added to the 96 well plates. For culture in the device, 3 different conditions were tested: H9c2 cells alone, HepG2 cells alone (where the other chamber within the device was filled with hydrogel only without any cells), and both cells cultured in the device in their specific chambers. The urea production was increased significantly in a dynamic environment of the device compared to static culture. Error bars indicate the standard error of the means, asterisks mark significance levels of $p < 0.05$ (*), $p < 0.01$ (**), $p < 0.0001$ (****), and n=3.

3.4.4 DOX metabolism

One of the proposed mechanisms for the cardiotoxic effect of DOX involves the formation of toxic metabolites, specifically DOXOL, [79,132]; therefore, we investigated the ability of HepG2 cells to produce this metabolite *in vitro*. The HepG2 cells were treated with 1 µM DOX, and the supernatant was harvested and analyzed using LC-MS for parent drug DOX and its metabolite DOXOL detection. The results (Figure 3.8(A)) indicate that more than 70% of the initial DOX was metabolized by the liver cells after 72 h. Moreover, the results showed the production of DOXOL over time (Figure 3.8(B)), which indicates that the liver cells can convert DOX to the cardiotoxic metabolite DOXOL *in vitro*. The rate and routes for the metabolism of DOX and four other anthracycline drugs have been investigated previously by Guillouzo et al.[147] using both rat and human adult hepatocytes. They could similarly demonstrate that both rat and human adult hepatocytes could metabolize the anthracycline drugs *in vitro;* however, the higher metabolic activity of human hepatocytes compared to rat emphasizes the differences between the species and the importance of developing a human *in vitro* model to fully capture the potential of these drugs in terms of both efficacy and adverse effects.
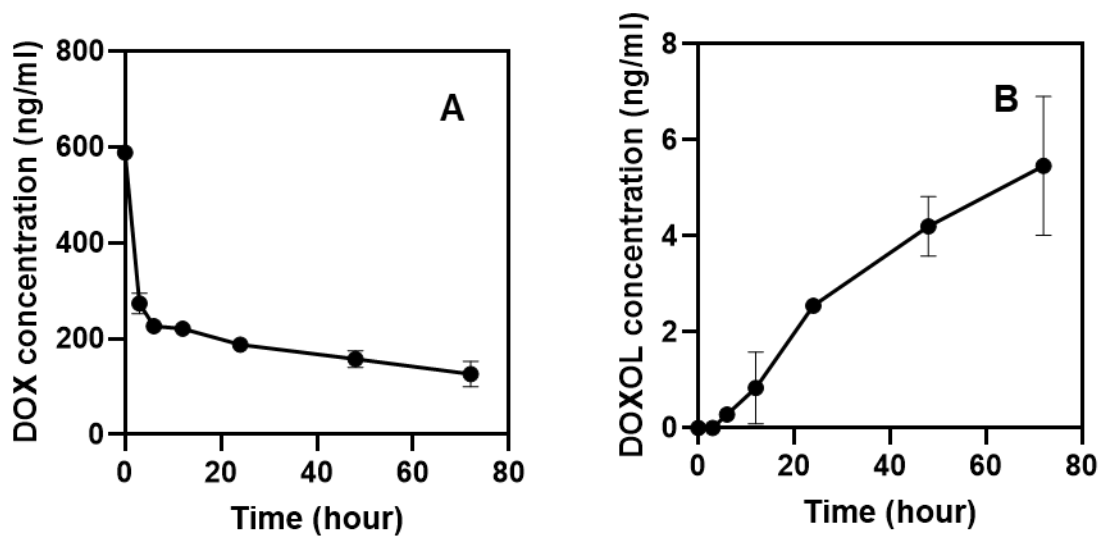
Figure 3.8. Measured DOX and DOXOL in the culture medium during the incubation of the HepG2 cells in 3D culture. The media was collected at specific time points, and after the protein precipitation, the samples were analyzed using LC-MS. (A) The amount of the DOX measured in the media indicated that more than 70% of initial DOX added to the culture medium was metabolized by HepG2 cells after 72 h of incubation. (**B**) The amount of DOXOL produced by the HepG2 cells in the media. The detection of DOXOL in the media indicates that the liver cells can effectively metabolize DOX and produce the cardiotoxic metabolite DOXOL *in vitro* setting.

3.4.5   Drug testing in device

In the next step, we performed drug testing on cells in the device to evaluate the toxicity of DOX and its metabolites on the liver and heart cells. As a control, a conventional 3D static culture was performed in 96 well plates. While the dynamic device is believed to recreate the interactions that generally exist between the organs (through media circulation within the device), no interactions can be observed in static controls. After drug treatments, cells were harvested, recovered from the gel, and were stained using the Alexa Fluor 488 annexin V/Dead Cell Apoptosis Kit. Phosphatidylserine (PS) within healthy cells is located in the inner surface of the cell membrane; however, in damaged apoptotic cells, PS is flipped from the inner to the outer

leaflet of the plasma membrane.[148] Annexin V labeled with Alexa Flour 488, can identify apoptotic cells by binding to PS exposed on the outer leaflet of the plasma membrane.[149]

Moreover, PI is a nucleic acid binding dye that can only penetrate the cells that are dead, not the live and apoptotic cells. Therefore, after staining using this kit, apoptotic cells are Annexin $V^+ PI^-$, and cell death is demonstrated in $V^+ PI^+$ populations. Figure 3.9 shows that DOX had anticancer activity on HepG2 cells as a large population of apoptotic cells ($V^+ PI^-$) and dead cells ($V^+ PI^+$) are observed compared to the control. Based on the flow results, we could not detect any significant differences between the two experimental setups (3D and device) in terms of cell damage meaning the metabolite might not affect the cancer cells. However, in the case of H9c2 heart cells (Figure 3.10), there was a significant difference between the apoptotic and dead cell populations in two setups. The results indicate an increase in the number of apoptotic cells ($V^+ PI^-$) within the device compared to static culture. Different cell damage pattern between the device and the static culture is attributed to the exposure of heart cells to not only the parent drug but also to the metabolite being release from the HepG2 cells which reached the heart cells through the media circulation. High cardiotoxicity of DOXOL was previously observed on human cardiomyocytes in a similar microfluidic platform. [79]
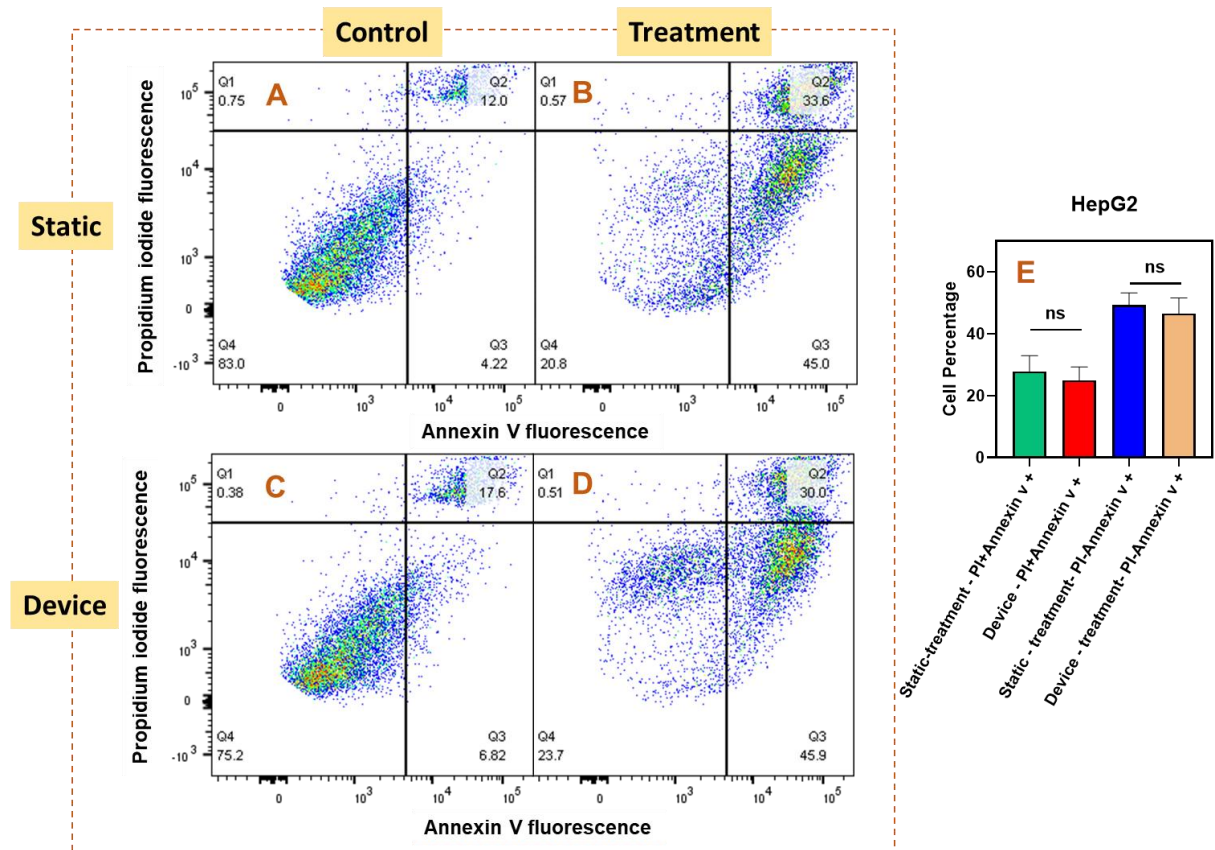
Figure 3.9. Representative flow cytometry analysis of Annexin V/PI staining in HepG2 cells in two experimental setups. Conventional static 3D culture (top) and culture in the device (bottom). (A) and (C) are the control samples with no drug introduced into the system for the 3D static and device cell culture, respectively. For these control samples, only the corresponding amount of DMSO that was used for drug dissolution in treatment groups was added to the culture medium. The high population of Annexin V^- PI^- in these two groups is an indicator of the high and the comparable number of healthy HepG2 cells in these two platforms. (B) and (D) are the treatment groups (with added DOX into the culture medium) for static 3D culture and the device, respectively. Similar populations of Annexin V^+ PI^- and Annexin V^+ PI^- in device compared to the static culture is an indicator of the same damage patterns in this cell line. (E) Quantitative analysis of flow cytometry. Results are expressed as the percentage of the total number of the cells counted. Values are mean $\pm$ SD. No significant difference ($0.05 < P$) was detected between the static culture and the culture within the device for the Annexin V^+ PI^- and Annexin V^+ PI^+ populations. Error bars indicate the standard error of the means, ns= non-significant, and n=3.
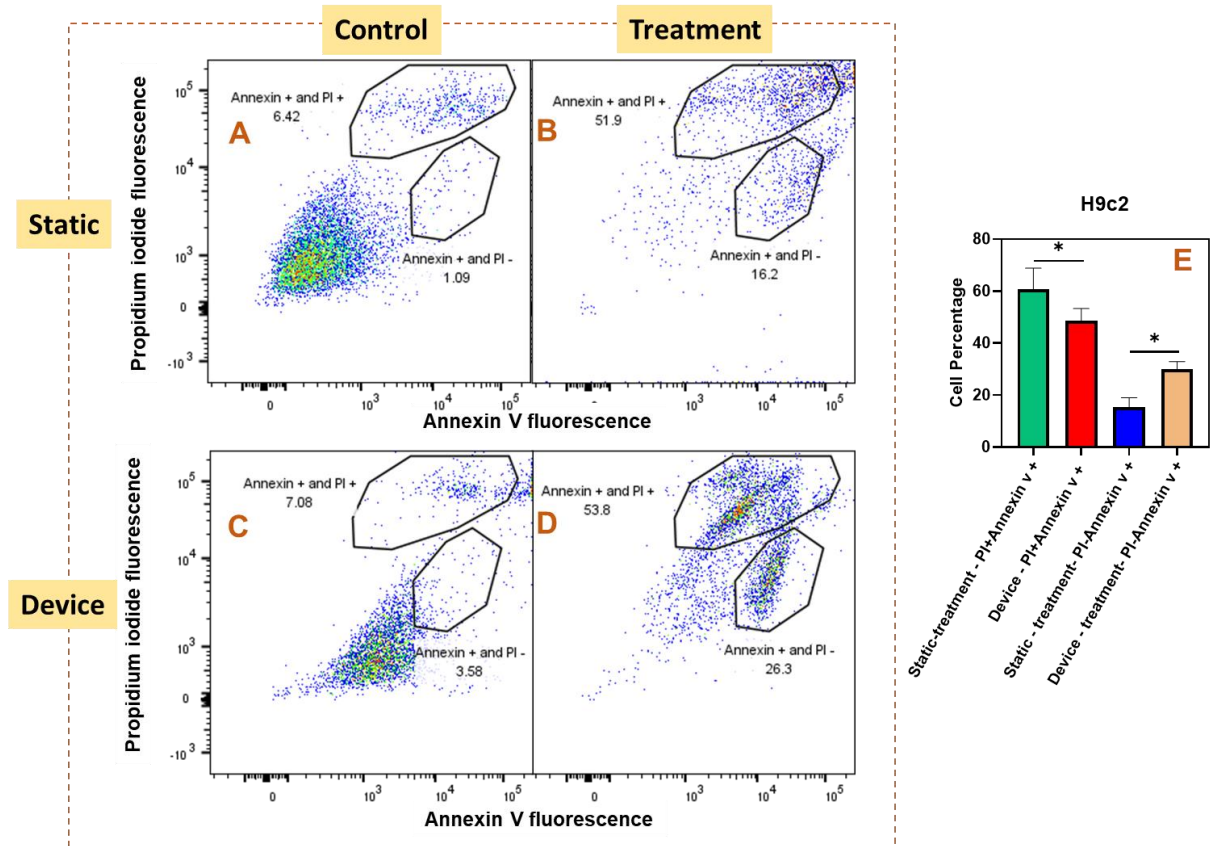
Figure 3.10. Representative flow cytometry analysis of Annexin V/PI staining in H9c2 cells in two experimental setups. Conventional static 3D culture (top) and culture in the rocked device (bottom). (A) and (C) are the control samples with no drug introduced into the system for the 3D static and device cell culture, respectively. For these control samples, only the corresponding amount of DMSO that was used for drug dissolution in treatment groups was added to the culture medium. The high population of Annexin V^- PI^- in these two groups is an indicator of the high and a comparable number of healthy H9c2 cells in these two platforms. (B) and (D) are the treatment groups (with added DOX into the culture medium) for static 3D culture and the device, respectively. Higher Annexin V^+ PI^- population in the device compared to the static culture is an indicator of the greater extent of damage in these cells, which can be due to the produced cardiotoxic DOXOL in the device by the metabolizing component (liver cells). (E) Quantitative analysis of flow cytometry. Results are expresses as the percentage of the total number of the cells counted. Values are mean ± SD. There is a significant difference (P-value < 0.05) between the static culture and the culture within the device for the Annexin V^+ PI^- and Annexin V^+ PI^+ populations. Error bars indicate the standard error of the means. Asterisks mark significance levels of $p < 0.05$ (*), and n=3.

3.5 Conclusions

One advantage of organ-on-a-chip devices is the possibility of toxicity evaluation of both parent drug and its metabolites. Here we described a heart/liver-on-a-chip device that could accommodate both HepG2 liver cells and H9c2 cardiomyocytes, which could successfully maintain both cell lines with more than 90% viability up to 5 days. Our device is pumpless, which is easy to operate based on gravity-induced flow and realistic shear stress. The fluid dynamics of the system was characterized, and the functionality of the cells in terms of urea production was evaluated. Moreover, the ability of 3D HepG2 culture to metabolize DOX *in vitro* and producing its primary metabolite (DOXOL) was investigated. Drug testing within the device demonstrated more significant damage to heart cells than the static culture, which is an indicator of the exposure of the cells to both parent drug and its cardiotoxic metabolite that cannot be reproduced in conventional cell cultures. This device can be implemented as a starting point to move toward a more complex human-on-a-chip device.

3.6 Acknowledgments

3.7 Disclosure

There are no conflicts to declare.

CHAPTER 4

SUMMARY AND FUTURE WORK

4.1 Summary of this work

Cancer, as the primary cause of death worldwide, puts the more efficient treatments in high demand. Conventional chemotherapy, as the most common cancer treatment, is facing severe challenges, including low water solubility of anti-cancer drugs and the cardiotoxicity induced by them. Moreover, the current chemotherapy drugs are not selective, so they have the potential to affect the normal tissues and cause an intense undesired adverse effect. Nanotechnology has made significant contributions to the development of drug delivery systems, especially for oncological applications, by reducing the toxicities, which leads to improvement in conventional chemotherapies. Polymer nanocarriers are used to increase the solubility of poorly soluble drugs; however, controlling the drug release from nanocarriers is still challenging. In this regard, thermoresponsive polymers may be the key to build controlled drug delivery systems. Polymeric micelles that demonstrate a dramatic change in their structure in response to temperature can be made by incorporating thermoresponsive polymer blocks in their core-shell structure. These systems can be exploited for selective drug release at the tumor site, which is possible through external temperature elevation at the site. Moreover, using these systems, the duration of the drug action at the target site can be controlled. Herein, we synthesized a micellar drug delivery system using γ-benzyloxy substituted poly(ε-caprolactone) as the hydrophobic block, and co-loaded anticancer doxorubicin (Dox) and antioxidant quercetin (Que). γ-Substituted oligo(ethylene) glycol (OEG) poly(ε-caprolactone)s were used as hydrophilic blocks to make the polymers

thermoresponsive. The polymers showed thermodynamic stability having CMC values in the order of 10-5 mg/mL. The polymers also exhibited thermoresponsive behaviors wherein varying OEG chains allowed tuning of the LCST values. These polymers were used as a micellar drug delivery system for Dox and Que. Combination loading was demonstrated as a successful approach to improve the drug loading efficiency of both drugs in all the polymers. Release studies in physiological conditions showed a temperature-dependent release of drug from the micelles. PME3CL-b-PBnCL had an LCST value (41 ˚C) higher but close to physiological temperature; hence it was used for further biological studies. Twenty percent more cytotoxic effect on HepG2 cells was observed from the micelles at a higher temperature, which is attributed to a higher release of anticancer drugs.

Although many therapeutics have been developed so far, the pharmaceutical industry is still facing challenges for drug discovery, which is mostly attributed to the lack of proper pre-clinical testing. Some of these challenges are high research and development costs and long development times. Animal studies are currently the most common preclinical testing method, but there are ethical and scientific arguments arising from the usage of animals for study purposes. Animal studies not only impose suffering on the animals, also stress for the researchers who are performing the experiments. Moreover, discoveries from animal studies do not effectively translate into the clinic due to differences between the animal and human biology, therefore besides the exorbitant cost and time-consuming process of drug development, 92% of the drugs fail in human clinical trials. To address some of the limitations of preclinical tests, "organ-on-a-chip" devices were developed to replicate in vivo functions of organs on a microchip. Here we described a heart/liver-on-a-chip device that could accommodate both HepG2 liver cells and H9c2

cardiomyocytes, which could successfully maintain both cell lines with more than 90% viability up to 5 days. Our device is pumpless, which is easy to operate based on gravity-induced flow and realistic shear stress. The fluid dynamics of the system was characterized, and the functionality of the cells in terms of urea production was evaluated. Moreover, the ability of 3D HepG2 culture to metabolize DOX in vitro and producing its primary metabolite (DOXOL) was investigated. Drug testing within the device demonstrated more significant damage to heart cells compared to the static culture, which is an indicator of the exposure of the cells to both parent drug and its cardiotoxic metabolite that cannot be reproduced in conventional cell cultures. This device can be implemented as a starting point to move toward a more complex human-on-a-chip device.

4.2 Future directions

In this work, we successfully designed and developed a thermoresponsive micellar system. Future optimization of thermoresponsive drug delivery systems will be focused on performing synergistic studies on combination therapies to achieve the best therapeutic efficiency in cancer cells while protecting the healthy cells. Currently, the translation of nanoparticles to industry and clinical is very slow. Organ-on-a-chip devices demonstrate a considerable promise in bridging the gaps between conventional static cell cultures, preclinical animal studies, and the human body for drug screening. Still, their effective utilization in assessing nanomedicine has been limited. Assessing the anti-cancer and cardioprotection activity of the drug delivery systems developed in Chapter 2 of the project through these tools would help better biological evaluations of the developed drug delivery systems. Overall, organ-on-a-chip platforms are complicated systems that mimic their human counterparts. However, they are also simple enough to decompose the *in vivo* biological environments, providing an opportunity for us to improve our fundamental

understanding of nanomedicine, which are likely to make an impact on the translation of nanomedicine in the future.

REFERENCES

1.   Bray, F. *et al.* Global cancer statistics 2018: GLOBOCAN estimates of incidence and mortality worldwide for 36 cancers in 185 countries. *CA A J. Clin.* **00**, 1–31 (2018).

2.   Senapati, S., Mahanta, A. K., Kumar, S. & Maiti, P. Controlled drug delivery vehicles for cancer treatment and their performance. *Signal Transduct. Target. Ther.* **3**, 7 (2018).

3.   Shi, J., Kantoff, P. W., Wooster, R. & Farokhzad, O. C. Cancer nanomedicine: Progress, challenges and opportunities. *Nat. Rev. Cancer* **17**, 20–37 (2017).

4.   Duncan, R. & Gaspar, R. Nanomedicine (s) under the Microscope. 2101–2141 (2011) doi:10.1021/mp200394t.

5.   Kakkar, A., Traverso, G., Farokhzad, O. C., Weissleder, R. & Langer, R. Evolution of macromolecular. *Nat. Publ. Gr.* **1**, 1–18 (2017).

6.   Parveen, S. & Sahoo, S. K. Polymeric nanoparticles for cancer therapy. **16**, 108–123 (2008).

7.   Hyung, J. *et al.* Polymeric nanomedicine for cancer therapy. **33**, 113–137 (2008).

8.   Zhou, Q., Zhang, L., Yang, T. & Wu, H. Stimuli-responsive polymeric micelles for drug delivery and cancer therapy. *Int. J. Nanomedicine* **13**, 2921–2942 (2018).

9.   Rainbolt, E. A., Washington, K. E., Biewer, M. C. & Stefan, M. C. Recent developments in micellar drug carriers featuring substituted poly(ε-caprolactone)s. *Polym. Chem.* **6**, 2369–2381 (2015).

10.   Katono, H. *et al.* Thermo-responsive swelling and drug release switching of interpenetrating polymer networks composed of poly(acrylamide-co-butyl methacrylate) and poly (acrylic acid). *J. Control. Release* (1991) doi:10.1016/0168-3659(91)90045-F.

11.   Aoshima, S. & Sugihara, S. Syntheses of stimuli-responsive block copolymers of vinyl ethers with side oxyethylene groups by living cationic polymerization and their thermosensitive physical gelation. *J. Polym. Sci. Part A Polym. Chem.* (2000) doi:10.1002/1099-0518(20001101)38:21<3962::AID-POLA130>3.0.CO;2-9.

12.   Gammas, S. *et al.* Thermo-responsive polymer nanoparticles with a core-shell micelle structure as site-specific drug carriers. *J. Control. Release* (1997) doi:10.1016/S0168-3659(97)00040-0.

13.   Ahmad, Z., Shah, A., Siddiq, M. & Kraatz, H. B. Polymeric micelles as drug delivery vehicles. *RSC Adv.* **4**, 17028–17038 (2014).

14. Tyrrell, Z. L., Shen, Y. & Radosz, M. Fabrication of micellar nanoparticles for drug delivery through the self-assembly of block copolymers. *Prog. Polym. Sci.* **35**, 1128–1143 (2010).

15. Kossmeh, G. S. and G. *Advances in Polymer Science*. *Adv. Polym. Sci.* (2011). doi:papers3://publication/uuid/871BA6C8-E6D0-4A90-A5AF-14CBFFA311D5.

16. Chang, L. *et al.* Poly(ethyleneglycol) - b - Poly(ε -caprolactone- co - γ -hydroxyl- ε - caprolactone) Bearing Pendant Hydroxyl Groups as Nanocarriers for Doxorubicin Delivery. (2012) doi:10.1021/bm301086c.

17. Peng, K. Y., Wang, S. W., Hua, M. Y. & Lee, R. S. Amphiphilic photocleavable block copolymers based on monomethyl poly(ethylene glycol) and poly(4-substituted-??-caprolactone): Synthesis, characterization, and cellular uptake. *RSC Adv.* **3**, 18453–18463 (2013).

18. Hao, J. *et al.* A combined experimental and computational study of the substituent effect on micellar behavior of γ-substituted thermoresponsive amphiphilic poly(ε-caprolactone)s. *Macromolecules* **46**, 4829–4838 (2013).

19. Ichikawa, Y. *et al.* Cardiotoxicity of doxorubicin is mediated through mitochondrial iron accumulation. *J. Clin. Invest.* **124**, 617–630 (2014).

20. Minotti, G. *et al.* Doxorubicin Cardiotoxicity and the Control of Iron Metabolism: Quinone-Dependent and Independent Mechanisms. *Methods Enzymol.* **378**, 340–361 (2004).

21. Minotti, G. Sources and Role of Iron in Lipid Peroxidation. *Chem. Res. Toxicol.* **6**, 134–146 (1993).

22. Gutteridge, J. M. C. Lipid peroxidation and possible hydroxyl radical formation stimulated by the self-reduction of a doxorubicin-iron (III) complex. *Biochem. Pharmacol.* **33**, 1725–1728 (1984).

23. Olson, R. D. *et al.* Doxorubicin cardiotoxicity may be caused by its metabolite, doxorubicinol. *Proc. Natl. Acad. Sci. U. S. A.* (1988) doi:10.1073/pnas.85.10.3585.

24. Mushlin, P. S. *et al.* Time-related increases in cardiac concentrations of doxorubicinol could interact with doxorubicin to depress myocardial contractile function. *Br. J. Pharmacol.* (1993) doi:10.1111/j.1476-5381.1993.tb13909.x.

25. Valko, M. *et al.* Free radicals and antioxidants in normal physiological functions and human disease. *Int. J. Biochem. Cell Biol.* **39**, 44–84 (2007).

26.   Wright, J. S., Johnson, E. R. & DiLabio, G. A. Predicting the activity of phenolic antioxidants: Theoretical method, analysis of substituent effects, and application to major families of antioxidants. *J. Am. Chem. Soc.* **123**, 1173–1183 (2001).

27.   Chem, F. Iron Chelation by the Powerful Antioxidant Flavonoid Quercetin. (2006).

28.   Gottesman, M. M. & Pastan, I. MULTIDRUG RESISTANCE MULTIDRUG TRANSPORTERl. *Annu. Rev. Biochem.* **62**, 385–427 (1993).

29.   Ambudkar, S. V *et al.* Biochemical, cellular, and pharmacological aspects of the multidrug transporter. *Ann.Rev.Pharmacol.Toxicol.* **39**, 361–398 (1999).

30.   Hospital, T., Sick, J. & Biophysics, M. A surface glycoprotein modulating drug in chinese hamster ovary cell mutants permeability. **455**, 152–162 (1976).

31.   Cotran, S., Cotran, S., Folkman, J., Growth, U. & Banda, J. Cell Surface P-Glycoprotein Associated with Multidrug Resistance in Mammalian Cell Lines. **1340**, (1983).

32.   Anuchapreeda, S., Leechanachai, P., Smith, M. M., Ambudkar, S. V. & Limtrakul, P. ngarm. Modulation of P-glycoprotein expression and function by curcumin in multidrug-resistant human KB cells. *Biochem. Pharmacol.* **64**, 573–582 (2002).

33.   Qian, F., Wei, D., Zhang, Q. & Yang, S. Modulation of P-glycoprotein function and reversal of multidrug resistance by (-)-epigallocatechin gallate in human cancer cells. *Biomed. Pharmacother.* **59**, 64–69 (2005).

34.   Mei, Y., Qian, F., Wei, D. & Liu, J. Reversal of cancer multidrug resistance by green tea polyphenols. 1307–1314 (2004) doi:10.1211/0022357044364.

35.   Angeles, L. Flavonoids : A class of modulators with bifunctional interactions at vicinal ATP- and steroid-binding sites on mouse P-glycoprotein. **95**, 9831–9836 (1998).

36.   Boumendjel, A., Di Pietro, A., Dumontet, C. & Barron, D. Recent advances in the discovery of flavonoids and analogs with high-affinity binding to P-glycoprotein responsible for cancer cell multidrug resistance. *Med. Res. Rev.* **22**, 512–529 (2002).

37.   Shapiro, A. B. & Ling, V. Extraction of Hoechst 33342 from the cytoplasmic leaflet of the plasma membrane by P-glycoprotein. **129**, 122–129 (1997).

38.   Pintha, P. L. K. K. Inhibition of P-Glycoprotein Function and Expression by Kaempferol and Quercetin. **1**, (2005).

39.   Lage, H. Review An overview of cancer multidrug resistance : a still unsolved problem. **65**, 3145–3167 (2008).

40.   Loo, T. W. & Clarke, D. M. Mutational analysis of ABC proteins. **476**, 51–64 (2008).

41.   Chen, C., Zhou, J. & Ji, C. Quercetin : A potential drug to reverse multidrug resistance. *Life Sci.* **87**, 333–338 (2010).

42.   Gu, L. & Mooney, D. J. Biomaterials and emerging anticancer therapeutics: Engineering the microenvironment. *Nat. Rev. Cancer* **16**, 56–66 (2016).

43.   Kamei, K. *et al.* Integrated heart/cancer on a chip to reproduce the side effects of anti-cancer drugs in vitro. *RSC Adv.* **7**, 36777–36786 (2017).

44.   Suggitt, M. & Bibby, M. C. 50 Years of Preclinical Anticancer Drug Screening : Empirical to Target-Driven Approaches 50 Years of Preclinical Anticancer Drug Screening : Empirical to Target-Driven Approaches. **11**, 971–981 (2005).

45.   Cook, D. *et al.* Lessons learned from the fate of AstraZeneca's drug pipeline: A five-dimensional framework. *Nat. Rev. Drug Discov.* **13**, 419–431 (2014).

46.   Greek, R. & Menache, A. Systematic reviews of animal models: Methodology versus epistemology. *Int. J. Med. Sci.* **10**, 206–221 (2013).

47.   Harrison, R. G. The outgrowth of the nerve fiber as a mode of protoplasmic movement. *J. Exp. Zool.* **9**, 787–846 (1910).

48.   Bhatia, S. N. & Ingber, D. E. Microfluidic organs-on-chips. *Nat. Biotechnol.* **32**, 760–772 (2014).

49.   Gill, B. J. & West, J. L. Modeling the tumor extracellular matrix: Tissue engineering tools repurposed towards new frontiers in cancer biology. *J. Biomech.* **47**, 1969–1978 (2014).

50.   Hanahan, D. & Weinberg, R. A. Hallmarks of cancer: The next generation. *Cell* **144**, 646–674 (2011).

51.   Computer, P. Integrin expression on colorectal tumor cells growing as monolayers, as multicellular tumor spheroids, or in nude mice. **5**, 133–165 (1990).

52.   Mammoto, T., Mammoto, A. & Ingber, D. E. Mechanobiology and Developmental Control. *Annu. Rev. Cell Dev. Biol.* **29**, 27–61 (2013).

53.   Sackmann, E. K., Fulton, A. L. & Beebe, D. J. The present and future role of microfluidics in biomedical research. *Nature* **507**, 181–189 (2014).

54.   Polini, A. *et al.* Organs-on-a-chip : a new tool for drug discovery. **10**, 1–18 (2014).

55. Dickey, C. A., Patterson, C., Dickson, D. & Petrucelli, L. Brain CHIP: removing the culprits in neurodegenerative disease. *Trends Mol. Med.* **13**, 32–38 (2007).

56. Guan, A. *et al.* Medical devices on chips. *Nat. Biomed. Eng.* **1**, (2017).

57. Misun, P. M., Rothe, J., Schmid, Y. R. F., Hierlemann, A. & Frey, O. Multi-analyte biosensor interface for real-time monitoring of 3D microtissue spheroids in hanging-drop networks. *Microsystems Nanoeng.* **2**, 16022 (2016).

58. Kusunose, J. *et al.* Microfluidic system for facilitated quantification of nanoparticle accumulation to cells under laminar flow. *Ann. Biomed. Eng.* **41**, 89–99 (2013).

59. Lin, W., Huang, Y. W., Zhou, X. D. & Ma, Y. Toxicity of cerium oxide nanoparticles in human lung cancer cells. *Int. J. Toxicol.* **25**, 451–457 (2006).

60. Esch, M. B., Mahler, G. J., Stokol, T. & Shuler, M. L. Body-on-a-chip simulation with gastrointestinal tract and liver tissues suggests that ingested nanoparticles have the potential to cause liver injury. *Lab Chip* **14**, 3081–3092 (2014).

61. Shin, K., Klosterhoff, B. S. & Han, B. Characterization of cell-type-specific drug transport and resistance of breast cancers using tumor-microenvironment-on-chip. *Mol. Pharm.* **13**, 2214–2223 (2016).

62. Shin, C. S., Kwak, B., Han, B. & Park, K. Development of an *in Vitro* 3D Tumor Model to Study Therapeutic Efficiency of an Anticancer Drug. *Mol. Pharm.* **10**, 2167–2175 (2013).

63. Yu, L., Chen, M. C. W. & Cheung, K. C. Droplet-based microfluidic system for multicellular tumor spheroid formation and anticancer drug testing. *Lab Chip* **10**, 2424–2432 (2010).

64. Zhang, Y. S., Zhang, Y. & Zhang, W. Cancer-on-a-chip systems at the frontier of nanomedicine. *Drug Discov. Today* **22**, 1392–1399 (2017).

65. Mathur, A. *et al.* Human iPSC-based Cardiac. 1–7 (2015) doi:10.1038/srep08883.

66. Bergström, G., Christoffersson, J., Schwanke, K., Zweigerdt, R. & Mandenius, C. Lab on a Chip bodies in a microfluidic device for toxicity testing. 3242–3249 (2015) doi:10.1039/c5lc00449g.

67. Ahn, S. *et al.* Mussel-inspired 3D fiber scaffolds for heart-on-a-chip toxicity studies of engineered nanomaterials. *Anal. Bioanal. Chem.* **410**, 6141–6154 (2018).

68. Khetani, S. R. & Bhatia, S. N. Microscale culture of human liver cells for drug development. *Nat. Biotechnol.* (2008) doi:10.1038/nbt1361.

69. Bhatia, S. N., Balis, U. J., Yarmush, M. L. & Toner, M. Effect of cell–cell interactions in preservation of cellular phenotype: cocultivation of hepatocytes and nonparenchymal cells. *FASEB J.* (1999) doi:10.1096/fasebj.13.14.1883.

70. LeCluyse, E. L., Witek, R. P., Andersen, M. E. & Powers, M. J. Organotypic liver culture models: Meeting current challenges in toxicity testing. *Critical Reviews in Toxicology* (2012) doi:10.3109/10408444.2012.682115.

71. Tsang, V. L. *et al.* Fabrication of 3D hepatic tissues by additive photopatterning of cellular hydrogels. *FASEB J.* (2007) doi:10.1096/fj.06-7117com.

72. He, J. *et al.* Fabrication of nature-inspired microfluidic network for perfusable tissue constructs. *Adv. Healthc. Mater.* (2013) doi:10.1002/adhm.201200404.

73. Slaughter, B. V., Khurshid, S. S., Fisher, O. Z., Khademhosseini, A. & Peppas, N. A. Hydrogels in regenerative medicine. *Advanced Materials* (2009) doi:10.1002/adma.200802106.

74. Mahto, S. K., Yoon, T. H. & Rhee, S. W. A new perspective on in vitro assessment method for evaluating quantum dot toxicity by using microfluidics technology. *Biomicrofluidics* (2010) doi:10.1063/1.3486610.

75. Liu, W. *et al.* Magnetically controllable 3D microtissues based on magnetic microcryogels. *Lab Chip* (2014) doi:10.1039/c4lc00081a.

76. Dittrich, P. S. & Manz, A. Lab-on-a-chip: Microfluidics in drug discovery. *Nature Reviews Drug Discovery* (2006) doi:10.1038/nrd1985.

77. E.F.A., B., C.D., R., I., M., J.H., B. & J.H.M., S. An update on in vitro test methods in human hepatic drug biotransformation research: Pros and cons. *Toxicol. Appl. Pharmacol.* (2003) doi:10.1016/S0041-008X(03)00128-5 LK

78. Albini, A. *et al.* Cardiotoxicity of anticancer drugs: The need for cardio-oncology and cardio-oncological prevention. *J. Natl. Cancer Inst.* **102**, 14–25 (2010).

79. Kamei, K. I. *et al.* Integrated heart/cancer on a chip to reproduce the side effects of anti-cancer drugs: In vitro. *RSC Adv.* **7**, 36777–36786 (2017).

80. Oleaga, C. *et al.* Investigation of the effect of hepatic metabolism on off-target cardiotoxicity in a multi-organ human-on-a-chip system. *Biomaterials* (2018) doi:10.1016/j.biomaterials.2018.07.062.

81. Oleaga, C. *et al.* Multi-Organ toxicity demonstration in a functional human in vitro system composed of four organs. *Sci. Rep.* **6**, 1–17 (2016).

82. Sarisozen, C., Joshi, U., Mendes, L. P. & Torchilin, V. P. Stimuli-responsive polymeric micelles for extracellular and intracellular drug delivery. in *Stimuli Responsive Polymeric Nanocarriers for Drug Delivery Applications* (2019). doi:10.1016/b978-0-08-101995-5.00012-x.

83. Tian, Y., Liu, Y., Ju, B., Ren, X. & Dai, M. Thermoresponsive 2-hydroxy-3-isopropoxypropyl hydroxyethyl cellulose with tunable LCST for drug delivery. *RSC Adv.* **9**, 2268–2276 (2019).

84. Akimoto, J., Nakayama, M. & Okano, T. Temperature-responsive polymeric micelles for optimizing drug targeting to solid tumors. *Journal of Controlled Release* (2014) doi:10.1016/j.jconrel.2014.06.062.

85. Washington, K. E. *et al.* Thermoresponsive star-like γ-substituted poly(caprolactone)s for micellar drug delivery. *J. Mater. Chem. B* **5**, 5632–5640 (2017).

86. Hao, J. *et al.* A Combined Experimental and Computational Study of the Substituent Effect on Micellar Behavior of Î³-Substituted Thermoresponsive Amphiphilic Poly(Îµ-caprolactone)s. *Macromolecules* **46**, 4829–4838.

87. Rainbolt, E. A., Washington, K. E., Biewer, M. C. & Stefan, M. C. Towards smart polymeric drug carriers: self-assembling [gamma]-substituted polycaprolactones with highly tunable thermoresponsive behavior. *J. Mater. Chem. B* **1**, 6532–6537.

88. Gutteridge, J. M. C. Lipid peroxidation and possible hydroxyl radical formation stimulated by the self-reduction of a doxorubicin-iron (III) complex. *Biochem. Pharmacol.* **33**, 1725–1728 (1984).

89. Minotti, G. Sources and Role of Iron in Lipid Peroxidation. *Chem. Res. Toxicol.* **6**, 134–146 (1993).

90. Valko, M. *et al.* Free radicals and antioxidants in normal physiological functions and human disease. *Int. J. Biochem. Cell Biol.* **39**, 44–84 (2007).

91. Wright, J. S., Johnson, E. R. & DiLabio, G. A. Predicting the activity of phenolic antioxidants: Theoretical method, analysis of substituent effects, and application to major families of antioxidants. *J. Am. Chem. Soc.* **123**, 1173–1183 (2001).

92. Gottesman, M. M. & Pastan, I. Biochemistry of multidrug resistance mediated by the multidrug transporter. *Annual Review of Biochemistry* (1993) doi:10.1146/annurev.bi.62.070193.002125.

93. Fatease, A. Al *et al.* Chemosensitization and mitigation of Adriamycin-induced cardiotoxicity using combinational polymeric micelles for co-delivery of quercetin/resveratrol and resveratrol/curcumin in ovarian cancer. *Nanomedicine Nanotechnology, Biol. Med.* (2019) doi:10.1016/j.nano.2019.03.011.

94. Zhang, J. *et al.* Co-delivery of doxorubicin and the traditional Chinese medicine quercetin using biotin-PEG2000-DSPE modified liposomes for the treatment of multidrug resistant breast cancer. *RSC Adv.* (2016) doi:10.1039/c6ra24173e.

95. Mu, Y. *et al.* pH-sensitive amphiphilic chitosan-quercetin conjugate for intracellular delivery of doxorubicin enhancement. *Carbohydr. Polym.* (2019) doi:10.1016/j.carbpol.2019.115072.

96. Washington, K. E., Kularatne, R. N., Biewer, M. C. & Stefan, M. C. Combination Loading of Doxorubicin and Resveratrol in Polymeric Micelles for Increased Loading Efficiency and Efficacy. *ACS Biomater. Sci. Eng.* **4**, 997–1004.

97. Hao, J. *et al.* A Combined Experimental and Computational Study of the Substituent E ff ect on Micellar Behavior of γ - Substituted Thermoresponsive Amphiphilic Poly(ε - caprolactone)s. *Macromolecules* **46**, 4829–4838 (2013).

98. Kularatne, R. N. *et al.* Histone Deacetylase Inhibitor (HDACi) Conjugated Polycaprolactone for Combination Cancer Therapy. *Biomacromolecules* **19**, 1082–1089.

99. Owen, S., P.Y. Chan, D. & S. Shoichet, M. *Polymeric micelle stability. Nano Today* doi:10.1016/j.nantod.2012.01.002.

100. Torchilin, V. P. Structure and design of polymeric surfactant-based drug delivery systems. **73**, 137–172 (2001).

101. Washington, K. E. *et al.* Synthesis of linear and star-like poly(ε-caprolactone)-b-poly{γ-2-[2-(2-methoxy-ethoxy)ethoxy]ethoxy-ε-caprolactone} amphiphilic block copolymers using zinc undecylenate. *J. Polym. Sci. Part A Polym. Chem.* (2016) doi:10.1002/pola.28246.

102. Kalyanasundaram, K. & Thomas, J. K. Solvent-dependent fluorescence of pyrene-3-carboxaldehyde and its applications in the estimation of polarity at micelle-water interfaces. *J. Phys. Chem.* **81**, 2176–2180 (1977).

103. Hoogenboom, R. Temperature-responsive polymers: Properties, synthesis and applications. in *Smart Polymers and their Applications* (2014). doi:10.1533/9780857097026.1.15.

104. Ishizone, T. *et al.* Anionic polymerizations of oligo(ethylene glycol) alkyl ether methacrylates: Effect of side chain length and ω-alkyl group of side chain on cloud point in water. *Macromolecules* (2008) doi:10.1021/ma702828n.

105. Kularatne, R. N. *et al.* Histone Deacetylase Inhibitor (HDACi) Conjugated Polycaprolactone for Combination Cancer Therapy. *Biomacromolecules* (2018) doi:10.1021/acs.biomac.8b00221.

106. Qian, F., Wei, D., Zhang, Q. & Yang, S. Modulation of P-glycoprotein function and reversal of multidrug resistance by (-)-epigallocatechin gallate in human cancer cells. *Biomed. Pharmacother.* **59**, 64–69 (2005).

107. Deng, L. *et al.* Magnetothermally responsive star-block copolymeric micelles for controlled drug delivery and enhanced thermo-chemotherapy. *Nanoscale* **7**, 9655–9663 (2015).

108. Hilmer, S. N., Cogger, V. C., Muller, M. & Couteur, D. G. Le. ABSTRACT : **32**, 794–799 (2004).

109. Tacar, O., Sriamornsak, P. & Dass, C. R. Doxorubicin: An update on anticancer molecular action, toxicity and novel drug delivery systems. *J. Pharm. Pharmacol.* **65**, 157–170 (2013).

110. Kim, S. H. *et al.* Thermoresponsive nanostructured polycarbonate block copolymers as biodegradable therapeutic delivery carriers. *Biomaterials* **32**, 5505–5514 (2011).

111. Cheng, Y. *et al.* Thermally Controlled Release of Anticancer Drug from Self-Assembled γ^3-Substituted Amphiphilic Poly(ε-caprolactone) Micellar Nanoparticles. *Biomacromolecules* **13**, 2163–2173.

112. Von Aulock, S. Is there an end in sight for animal testing? Can organ-on-a-chip replace animal use in safety testing with advanced human-focused approaches? *ALTEX* **36**, 142–144 (2019).

113. Bottini, A. A. & Hartung, T. Food for thought... on the economics of animal testing. *Altex* (2009) doi:10.14573/altex.2009.1.3.

114. Pistollato, F. *et al.* Alzheimer disease research in the 21st century: Past and current failures, new perspectives and funding priorities. *Oncotarget* **7**, 38999–39016 (2016).

115. Bhise, N. S. *et al.* Organ-on-a-chip platforms for studying drug delivery systems. *J. Control. Release* **190**, 82–93 (2014).

116. Misun, P. M., Rothe, J., Schmid, Y. R. F., Hierlemann, A. & Frey, O. Multi-analyte biosensor interface for real-time monitoring of 3D microtissue spheroids in hanging-drop networks. *Microsystems Nanoeng.* **2**, 16022 (2016).

117. Guan, A., Wang, Y., Guan, A. & Wang, Y. Medical devices on chips. (2017) doi:10.1038/s41551-017-0045.

118. Lee, S. H. & Sung, J. H. Organ-on-a-Chip Technology for Reproducing Multiorgan Physiology. *Adv. Healthc. Mater.* **7**, 1–17 (2018).

119. Sung, J. H., Wang, Y. & Shuler, M. L. Strategies for using mathematical modeling approaches to design and interpret multi-organ microphysiological systems (MPS). *APL Bioeng.* **3**, 021501 (2019).

120. Ghanem, A. & Shuler, M. L. Combining cell culture analogue reactor designs and PBPK models to probe mechanisms of naphthalene toxicity. *Biotechnol. Prog.* **16**, 334–345 (2000).

121. Sung, J. H. & Shuler, M. L. A micro cell culture analog (CCA) with 3-D hydrogel culture of multiple cell lines to assess metabolism-dependent cytotoxicity of anti-cancer drugs. *Lab Chip* **9**, 1385–1394 (2009).

122. Sung, J. H., Kam, C. & Shuler, M. L. A microfluidic device for a pharmacokinetic-pharmacodynamic (PK-PD) model on a chip. *Lab Chip* **10**, 446–455 (2010).

123. Gerlowski, L. E. & Jain, R. K. Physiologically based pharmacokinetic modeling: Principles and applications. *J. Pharm. Sci.* (1983) doi:10.1002/jps.2600721003.

124. Mager, D. E., Wyska, E. & Jusko, W. J. Diversity of mechanism-based pharmacodynamic models. *Drug Metab. Dispos.* **31**, 510–518 (2003).

125. Peck, C. C. *et al.* Opportunities for integration of pharmacokinetics, pharmacodynamics, and toxicokinetics in rational drug development. *Clin. Pharmacol. Ther.* **51**, 465–473 (1992).

126. Kim, L., Toh, Y. C., Voldman, J. & Yu, H. A practical guide to microfluidic perfusion culture of adherent mammalian cells. *Lab Chip* **7**, 681–694 (2007).

127. Tatosian, D. A. & Shuler, M. L. A novel system for evaluation of drug mixtures for potential efficacy in treating multidrug resistant cancers. *Biotechnol. Bioeng.* **103**, 187–198 (2009).

128. Albini, A. *et al.* Cardiotoxicity of anticancer drugs: The need for cardio-oncology and cardio-oncological prevention. *Journal of the National Cancer Institute* (2010) doi:10.1093/jnci/djp440.

129. Soltantabar, P., Calubaquib, E. L., Mostafavi, E., Biewer, M. C. & Stefan, M. C. Enhancement of Loading Efficiency by Coloading of Doxorubicin and Quercetin in Thermoresponsive Polymeric Micelles. *Biomacromolecules* **21**, 1427–1436 (2020).

130. Tacar, O., Sriamornsak, P. & Dass, C. R. Doxorubicin: An update on anticancer molecular action, toxicity and novel drug delivery systems. *Journal of Pharmacy and Pharmacology* (2013) doi:10.1111/j.2042-7158.2012.01567.x.

131. Carvalho, C. *et al.* Doxorubicin: The Good, the Bad and the Ugly Effect. *Curr. Med. Chem.* (2009) doi:10.2174/092986709788803312.

132. Hanna, A. D., Lam, A., Tham, S., Dulhunty, A. F. & Beard, N. A. Adverse effects of doxorubicin and its metabolic product on cardiac RyR2 and SERCA2A. *Mol. Pharmacol.* (2014) doi:10.1124/mol.114.093849.

133. Hescheler, J. *et al.* Morphological, biochemical, and electrophysiological characterization of a clonal cell (H9c2) line from rat heart. *Circ. Res.* **69**, 1476–1486 (1991).

134. Xue, J.-X., Zhang, X.-Q., Bian, W.-H. & Yao, C. Alleviation of doxorubicin-induced cardiotoxicity by Hong Huang decoction may involve a reduction in myocardial oxidative stress and activation of Akt/FoxO3a pathways. *Int. J. Clin. Exp. Med.* **11**, 10574–10584 (2018).

135. Chegaev, K. *et al.* Doxorubicin-antioxidant co-drugs. *Bioorg. Med. Chem. Lett.* **23**, 5307–5310 (2013).

136. Choi, E. H., Chang, H., Cho, J. Y. & Chun, H. S. Cytoprotective effect of anthocyanins against doxorubicin-induced toxicity in H9c2 cardiomyocytes in relation to their antioxidant activities. **45**, 1873–1881 (2007).

137. Giridharan, G. A. *et al.* Microfluidic Cardiac Cell Culture Model (μCCCM). *Anal. Chem.* (2010) doi:10.1021/ac1012893.

138. Hsiao, Y.-F., Pan, H.-J., Tung, Y.-C., Chen, C.-C. & Lee, C.-H. Effects of hydraulic pressure on cardiomyoblasts in a microfluidic device. *Biomicrofluidics* **9**, 24111 (2015).

139. Kobuszewska, A. *et al.* Heart-on-a-chip: an investigation of the influence of static and perfusion conditions on cardiac (H9C2) cell proliferation, morphology, and alignment. *SLAS Technol. Transl. Life Sci. Innov.* (2017).

140. Lee, H. *et al.* A pumpless multi-organ-on-a-chip (MOC) combined with a pharmacokinetic–pharmacodynamic (PK–PD) model. *Biotechnol. Bioeng.* (2017) doi:10.1002/bit.26087.

141. Sin, A. *et al.* The Design and Fabrication of Three-Chamber Microscale Cell Culture Analog Devices with Integrated Dissolved Oxygen Sensors. *Biotechnol. Prog.* (2004) doi:10.1021/bp034077d.

142. Price, P. S. *et al.* Modeling Interindividual Variation in Physiological Factors Used in PBPK Models of Humans. *Critical Reviews in Toxicology* (2003) doi:10.1080/10408440390242324.

143. Kirby, B. J. *Micro- and Nanoscale Fluid Mechanics: Transport in Microfluidic Devices*. *Brian* (2010). doi:10.1007/s13398-014-0173-7.2.

144. Miller, P. G. & Shuler, M. L. Design and demonstration of a pumpless 14 compartment microphysiological system. *Biotechnol. Bioeng.* **113**, 2213–2227 (2016).

145. Wang, Y. *et al.* Systematic prevention of bubble formation and accumulation for long-term culture of pancreatic islet cells in microfluidic device. *Biomed. Microdevices* (2012) doi:10.1007/s10544-011-9618-3.

146. Bolleyn, J., Rogiers, V. & Vanhaecke, T. Functionality testing of primary hepatocytes in culture by measuring urea synthesis. in *Methods in Molecular Biology* (2015). doi:10.1007/978-1-4939-2074-7_24.

147. Le Bot, M. A. *et al.* Different cytotoxicity and metabolism of doxorubicin, daunorubicin, epirubicin, esorubicin and idarubicin in cultured human and rat hepatocytes. *Biochem. Pharmacol.* **37**, 3877–3887 (1988).

148. Van Engeland, M., Nieland, L. J. W., Ramaekers, F. C. S., Schutte, B. & Reutelingsperger, C. P. M. Annexin V-affinity assay: A review on an apoptosis detection system based on phosphatidylserine exposure. *Cytometry* (1998) doi:10.1002/(SICI)1097-0320(19980101)31:1<1::AID-CYTO1>3.0.CO;2-R.

149. Koopman, G. *et al.* Annexin V for flow cytometric detection of phosphatidylserine expression on B cells undergoing apoptosis. *Blood* (1994) doi:10.1182/blood.v84.5.1415.1415.

BIOGRAPHICAL SKETCH

Pooneh Soltantabar grew up in Mazandaran, Iran. Prior to joining UTD, she graduated with her BS in Chemical Engineering from Semnan University(2013), and with her MS in Biomedical Engineering from Tarbiat Modares University(2016). She moved to Dallas, Texas, in 2016 to pursue her PhD in the Bioengineering graduate program at UTD under the supervision of Dr. Mihaela C. Stefan. Her project was focused on the design and development of drug delivery systems for cancer therapy and microfabrication of organ-on-a-chip devices for biological evaluations. In her free time, she enjoys cooking and spending time with her husband, Ebi.

CURRICULUM VITAE

Pooneh Soltantabar

EDUCATION

PhD in Bioengineering	Nov 2020
The University of Texas at Dallas, Richardson, Texas	**GPA: 3.9/4**
MSc in Biomedical Engineering	Sep 2013
Tarbiat Modares University, Tehran, Iran	**GPA: 17.34/20**
BSc in Chemical Engineering *1st Honors*	Sep 2009
Semnan University, Semnan, Iran	**GPA: 16.83/20**

SELECTED RESEARCH EXPERIENCE

Pfizer

Clinical pharmacology scientist (contract)   Sep 20-present

- Clinical data analysis on oncology drug, Avelumab using R
- Literature review on various Immuno-Oncology (IO) agents
- PK/PD modelling using NONMEM
- Familiarity with regulatory review process

The University of Texas at Dallas   Sep 16- Sep 20

Research Assistant

- PK/PD modelling using organ-on-a-chip devices for nanomedicine biological evaluation
- Design and development of drug delivery systems for cancer therapy
- *In vitro* biological evaluations of drug delivery systems through conventional cell cultures and microfluidic devices
- Gained interdisciplinary skills by working in environments including chemistry lab, cell culture lab and microfabrication clean room

Tarbiat Modares University   Sep 13 – March 16

Research Assistant

- Design and development of pH responsive drug delivery systems for cancer therapy

TECHNICAL SKILLS

- Clinical data analysis using R software
- Design and development of organ-on-a-chip PK/PD models
- Perform cell culture and bioassays
- Design and microfabrication of microfluidic devices
- Organic chemistry knowledge to do synthesis and polymerization reactions

- Operational skills with laboratory instruments including: Nuclear Magnetic Resonance (NMR), Dynamic Light Scattering (DLS), Transmission Electron Microscopy (TEM), UV-Vis Spectroscopy
- Software skills: R, MATLAB, NONMEM, Graphpad prism, COMPUSYN, Autosketch, ChemDraw, Image J, Topspin

PROFESSIONAL EXPERIENCES

Research Assistant, The University of Texas at Dallas, Dallas, Texas   Jan 18 – Sep 20

Research Topic: Microfabrication of an organ-on-a-chip device to model cardiotoxicity induced by chemotherapies for cancer nanomedicine evaluation

Teaching Assistant, The University of Texas at Dallas, Dallas, Texas   Sep 16-Dec 17

Courses: Biomaterials and Medical Devices, Fluid Mechanics and Transport Processes in Biomedical Engineering, Engineering Physiology Laboratory, Thermodynamics and Physical Chemistry in Biomedical Engineering,

PUBLICATIONS

- **P. Soltantabar,** E. L. Calubaquib, E. Mostafavi, A. Ghazavi, and M. C. Stefan. "Heart/Liver-on-a-chip as pharmacokinetic–pharmacodynamic (PK–PD) model for cardiotoxicity induced by chemotherapies", *Lab-On-a-Chip*, Submitted
- **P. Soltantabar,** E. L. Calubaquib, E. Mostafavi, M. C. Biewer, and M. C. Stefan. "Enhancement of Loading Efficiency by Co-loading of Doxorubicin and Quercetin in Thermoresponsive Polymeric Micelles", *Biomacromolecules*
- E. Mostafavi, **P. Soltantabar**, and T. J. Webster. "Nanotechnology and picotechnology: A new arena for translational medicine." *Biomaterials in Translational Medicine*
- K. E. Washington, J. Du, R. N. Kularatne, E. L Calubaquib, P. Soltantabar, , M. C. Biewer, M. C. Stefan. "Diketopyrrolopyrrole and benzodithiophene based near infrared-emitting small molecule for imaging applications", *Synthetic Metal*

VOLUNTEER EXPERIENCE

Member of volunteer program at Methodist Hospital, Dallas, Texas   Nov 19 – Sep 20